Self-Interacting Dark Matter in Cosmological Simulations

Alexander Bastidas Fry

A dissertation
submitted in partial fulfillment of the
requirements for the degree of

Doctor of Philosophy

University of Washington

2015

Reading Committee:

Fabio Governato, Chair

Matt McQuinn

Tom Quinn

Program Authorized to Offer Degree:
UW Astronomy

University of Washington

Abstract

Self-Interacting Dark Matter in Cosmological Simulations

Alexander Bastidas Fry

Chair of the Supervisory Committee:
Research Professor Fabio Governato
Astronomy

Self-Interacting Dark Matter is a cosmologically consistent alternative theory to Cold Dark Matter that solves problems of the Cold Dark Matter model on small scales. Our N-body simulations demonstrate that Self-Interacting Dark Matter creates constant density cores that are consistent with observations of Local Group dwarf galaxies. However, the apparent problems of Cold Dark Matter have natural astrophysical contributions from baryonic supernovae feedback. The evidence for Self-Interacting Dark Matter taken together with the evidence for the need for better feedback models presents a challenging environment in which to place constraints on either. We use high resolution cosmological simulations to compare the detailed properties of galaxies at a range of masses with a focus on dwarf galaxies which are the most dark matter dominated galaxies in the universe. We conclude that it is possible that velocity dependent Self-Interacting Dark Matter could explain the common mass scale of dark matter on small scales, the too big to fail problem, and the core versus cusp problem even in the absence of strong stellar feedback; however, baryonic processes offer solutions to these same problems. We find that once baryon physics and outflows are introduced, cores are created in both Self-Interacting Dark Matter and Cold Dark Matter cosmologies.

TABLE OF CONTENTS

Page

LIST OF FIGURES

LIST OF TABLES

ACKNOWLEDGMENTS

The author wishes to express appreciation to Miguel Morales. The author also wishes to thank those who have offered inputs and valuable discussions: Ferah Munshi, Jim Davenport, Sean Tulin, Hai-bo Yu, Alyson Brooks, and Andrew Pontzen.

This work funded by the Washington NASA Space Grant Consortium, Grant #NNX10AK64H. Some results were obtained using the analysis software pynbody, (Pontzen et al. 2013). ChaNGa was developed with support from National Science Foundation ITR grant PHY-0205413 to the University of Washington, and NSF ITR grant NSF-0205611 to the University of Illinois. This work was typeset from a TEX file with a custom thesis class file created by Jim Fox.

Chapter 1

INTRODUCTION

1.1 Overview

Dark matter is the simplest solution to a complicated problem. Dark matter is the most common and elusive physical thing in our Universe. It does not interact strongly with itself or with the regular matter found in stars, planets, or anything made of Standard Model (SM) particles. Its presence is inferred purely through its gravitational effects, and gravity, vexingly for theorists, is the weakest of the fundamental forces. But gravity is the only significant long-range force, and thus dark matter dominates the universe's architecture at the largest scales. In our standard cosmological model dark matter is the architect. Structure formation is hierarchical wherein small structures form first as dark matter aggregates to locations of space which have primordial over densities generated during the epoch of inflation. These dark matter halo structures host gas and stars and merge over time to create larger galaxies and clusters. A myriad of complex observations lead us to the conclusion that dark matter is a necessary component of our model of the Universe. Alternative theories to dark matter such as Modified Gravity are valid intellectual curiosities, but are strained to match observations of dark matter at all observed scales. By the logic of Occam's Razor, a model that includes dark matter is simpler than a model that does not, but how simple does dark matter have to be?

The past success of standard paradigms in theoretical physics leads us to hunt for a single generic dark matter particle — *the dark matter*. Arguably, though, we have little justification for supposing that there is anything to be found at all; as the physicist John D. Barrow said, "There is no reason that the universe should be designed for our convenience." With that caveat in mind, it appears the possibilities are as follows. Either dark matter exists or it doesn't. If it exists, then either we can detect it or we can't. If it doesn't exist, either we can show that it doesn't exist or we can't. The observations that led

astronomers to posit dark matter in the first place seem too robust to dismiss, so the most common argument against dark matter is to say there must be something wrong with our understanding of gravity — that it must not behave as Einstein predicted. That would be a drastic change in our understanding of physics, and it would make our model of the Universe more complicated so we reject that hypothesis. On the other hand, if dark matter exists and we can not detect it (through a force other than gravity), that would put us in a very inconvenient position.

If we can't detect dark matter in the laboratory it will not be for lack of trying, but from an astrophysical perspective there is a need to quantitatively constrain what we should expect to see in the laboratory. Standard cosmology successfully predicts or is consistent with a vast range of observations. This cosmology calls for 26% of the mass energy of the universe to be dark matter (or if we exclude dark energy and only measure the mass budget of the universe then dark matter composes 86% of the universe). We don't know what dark matter is, but we do have constraints on what it is (or rather what it is not):

- It interacts weakly with matter (not luminous).
- It is something other than baryons (not baryons).
- It is stable (not short lived).
- It is cold (not hot).

With these constraints in hand we endeavor to test whether dark matter, hereafter DM, could have self interactions that have physical consequences which are in better agreement with observations as compared to Cold Dark Matter (CDM). Self-Interacting Dark Matter (SIDM) is a cosmologically consistent alternative theory to CDM where dark matter particles collide and scatter. SIDM is motivated to solve problems of CDM in cosmological simulations on small scales. In this work we use high resolution SPH+N-Body cosmological simulations to identify differences between CDM and SIDM by focusing on predictions for the structural and observable properties of dwarf galaxies. Simulations of SIDM have been

examined for more than a decade (Moore et al., 2000; Spergel & Steinhardt, 2000; Burkert, 2000; Davé et al., 2001) and observations that constrain the cross section of SIDM are available, however many of this simulations do not include baryonic feedback. A DM interaction with a mean free path between ∼1 kpc and ∼1 Mpc (depending upon local density and the velocity dispersion of local DM particles) would only alter the evolution of cold (non-relativistic) dark matter in high density galaxy environments and large scale power spectrum measurements would be insensitive to the this modification of DM (see figure 1.1 that compares the large scale DM distribution of CDM and SIDM).

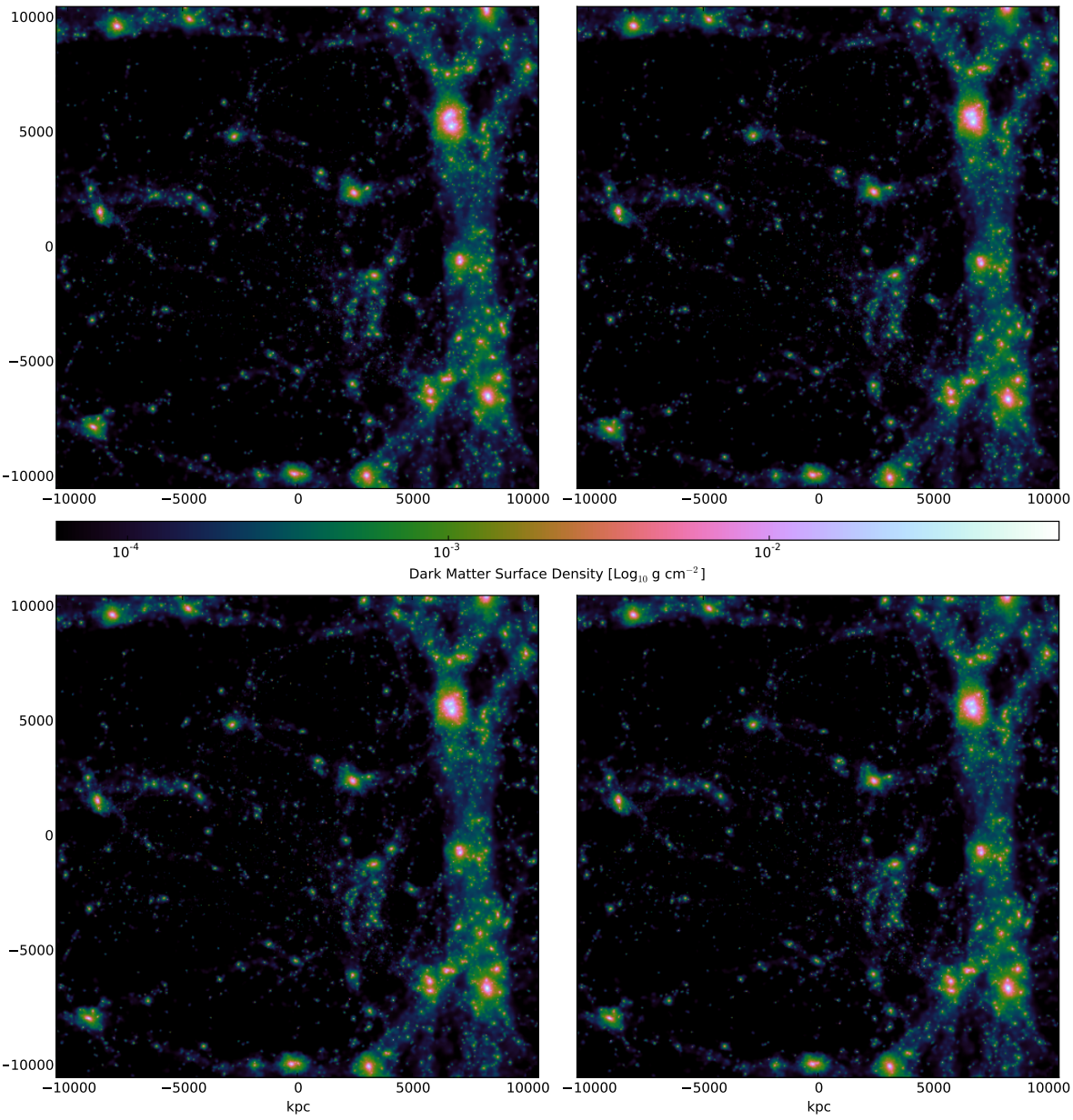

Figure 1.1: The large scale structure of CDM and several SIDM models at $z = 0$ for the 40 thieves simulation. Upper left: CDM, upper right: constant cross section SIDM model ($\sigma_{dm} = 2\ cm^2\ g^{-1}$), lower left: SIDM model with variable cross section ($\sigma_0 = 16\ v_{max} = 18$ km s^{-1}), lower right: SIDM model with variable cross section ($\sigma_0 = 35\ v_{max} = 10$ km s^{-1}). The figures are nearly identical at this large scale. This satisfies cosmological constraints and is exactly what we except for these regimes of DM interaction cross section.

The dominant form of mass in the standard dark energy and CDM (ΛCDM) cosmological model is consistent with a collisionless CDM. Simulations and observations on cosmological scales (>>1 Mpc) are in strong agreement (Eisenstein et al., 2005) with ΛCDM and it is not our intention, nor apparently the intention of anyone who examines SIDM models to challenge the large scale success of ΛCDM. However the distribution of DM is poorly understood on galactic scales ($\leq$ few Mpc) and there may in fact be a lack concordance between CDM predictions and observations. Some of the most pressing problems are: 1) The inner density profile of galaxies inside the scale radius is much shallower than expected (Walker et al., 2010). A density ρ that scales as a power law $\rho \propto r^{\alpha}$ for small radius, $r \to 0$, is predicted to go as $\alpha = -1$ or steeper by CDM simulations(Navarro et al., 1996b,a), but observations show the slope can be much closer to $\alpha = -0.5$ or even flat $\alpha = 0$ (Navarro et al., 2010). Additionally the central density of DM halos is observed to be constant (with intrinsic scatter) nearly independent of halo mass (Strigari et al., 2008a). This is the so called core versus cusp problem. 2) The number of observed satellite galaxies in the Local Group (Mateo, 1998) is an order of magnitude lower than that predicted by CDM simulations (Klypin et al., 1999; Moore et al., 1999). This is the so called missing satellite problem. 3) The most massive satellites around Milky Way analog hosts predicted by CDM simulations are too dense to host the brightest observed Milky Way companions, despite the fact that abundance matching would strongly predict them to be the most luminous companions that should be observed (Boylan-Kolchin et al., 2012, 2011). This is the so called too big to fail problem. 4) Dwarf galaxies display a common mass scale of dark matter on small scales (Strigari et al., 2008a; Gilmore et al., 2007; Hayashi & Chiba, 2015). Small galaxies in the local group that span a factor of 10,000 in luminosity all have a characteristic density of $\sim 10^8\ M_{\odot}\ \mathrm{kpc}^{-3}$ at their center.

The problems of CDM at small scales are ameliorated by mechanisms which lower the central density of galaxies and or raise the phase space density of DM. Mechanisms which are relevant include baryonic feedback and collisional DM. Evidence is mounting that including the effects of baryons in high resolution numerical simulations (such as gas cooling, star formation, and gas outflows driven by supernovae) is absolutely necessary to match the observations such as flatter cores in dwarf galaxies and realistic star formation rates and

histories. SIDM creates cored dark matter profiles and exponential stellar surface density profiles without abundant star formation. We argue that the inclusion of realistic baryons simultaneously with SIDM is necessary for reasonable predictions and to discover degeneracies in the theory; disentangling DM and SIDM without the context of baryons is simple, but not accurate. In Kaplinghat et al. (2014) for example it is demonstrated that the inclusion of baryons even while ignoring feedback effects results in SIDM cores that are tied to the scale of the baryonic potential (this holds true in the limit of 'significant interactions'). And for example we find that in SIDM simulations of DM only there are twice as many interactions in the inner 1 kpc compared to SIDM+baryon simulations, however the total density profile is very similar. In SIDM only simulations the core sizes are smaller and core densities are higher than compared to a SIDM and baryons simulation. Cores will form in regions which get hotter because the higher kinetic energy particles have larger apocenters. DM matter particle collisions isotropize the cores of galaxies and transfer mass outward from the dense central regions of DM halos over cosmic time scales. This process creates large cores, more spherical halos, and a flatter radial profile of the DM velocity dispersion.

The organization of this work is as follows: in this first chapter a background of DM with an overview of the current state of the field in observational and theoretical terms is discussed. In the second chapter an overview of the implementation and calibration of the code is given with a brief discussion of the simulations. In the third chapter a brief theoretical discussion is begun. And in the fourth chapter results are presented. In the fifth chapter an outlook discussion is presented along with conclusions.

1.2 Background

There exists a preponderance of observational evidence that supports this standard model of cosmology that includes the dark energy term Λ which is responsible for the accelerating expansion of the Universe. Dark energy and DM are not related in any way in most theories except in name. This work is within the framework of standard cosmology, but we focus on observations that may indicate deviations from CDM, however we do not mean to imply that the CDM model is untenable. Cosmology as a whole has placed exquisite constraints on DM's properties as mentioned in section 1.1. The ΛCDM cosmological model has just a few

main parameters which are constrained by a joint combination of observations from Type Ia supernova, the cosmic microwave background, galaxy correlations, galaxy cluster lensing, and other observational schemes. This model is constructed starting with the Einstein equation, making assumptions about the symmetries (and homogeneity and isotropy) of the universe, and then specifying an equation of state which specifies the relation between matter and energy density. The solution of these problems leads to the first Friedman Equation.

$$\left(\frac{\dot{a}}{a}\right)^2 = \frac{8\pi G\rho(t)}{3} - \frac{kc^2}{a(t)^2} \tag{1.1}$$

where $a(t)$ is the size scale factor of the universe at a time t, k is the spatial curvature of the universe (from the isotopic and homogeneous FriedmannLemaitreRobertsonWalker metric such that $k = -1$, 0, or 1), ρ is the density of the universe, and G is the gravitational constant. We can define the scale parameter in terms of the Hubble parameter

$$H = \frac{\dot{a}(t)}{a(t)} \tag{1.2}$$

The age of the universe within a given cosmology is defined precisely by the expansion factor a related to the redshift z by:

$$a = \frac{1}{1+z} \tag{1.3}$$

The Hubble parameter determines the current expansion trajectory of the universe:

$$\frac{\dot{a}}{a} = \begin{cases} > 0 & \text{expanding} \\ 0 & \text{stopped} \\ < 0 & \text{collapsing} \end{cases} \tag{1.4}$$

The Friedman equation demonstrates that the expansion trajectory of the universe depends on the density of the universe which may change as a function of time (in general relativity, in cosmology, energy is not necessarily conserved). The density of the universe has been dominated by different forms of matter or energy as the universe has evolved.

Let us examine how the expansion of universe scales with the various matter or energy constituents by defining a critical density of the universe:

$$\rho_c = \frac{3H^2}{8\pi G} \tag{1.5}$$

If Ω is the density of a given constituent of the Universe divided by the Universe's critical density then we have

$$H(z) = H_0\sqrt{\Omega_m[1+z]^3 + \Omega_\Lambda + \Omega_r[1+z]^4 + \Omega_k[1+z]^2} \tag{1.6}$$

where constituents of the universe are Ω_m matter, Ω_Λ dark energy, Ω_r radiation, Ω_k curvature. The values of these parameters have been tightly constrained by cosmological measurements. The recent best fit values are Ω_m = .309, Ω_b = .049, Ω_λ=.73, H_0 = 67.7 km s^{-1} Mpc^{-1} constrained from CMB data, galaxy gravitational lensing, Supernovae, and BAO data Komatsu et al. (2011); Planck Collaboration et al. (2014). It is within this cosmological context that this work is carried out, however, the exact parameters we use are slightly different from these current best fit values in order to facilitate comparison to our previous work (see chapter 2).

This work retains almost all of the theoretical, mathematical, and observations underpinnings of the standard cosmological model beginning with the Big Bang and the Cosmic Microwave Background(CMB). The temperature anisotropies in the CMB at the largest scales represent primordial ripples from quantum fluctuations of the inflation and at the smaller scales the process of structure formation; the power spectrum measurement of the CMB shows us in the first peak the curvature of the Universe, the second peak normalizes the baryon density, and the third peak is related to the dark matter density. The third and higher order acoustic peaks are sensitive to the ratio of the DM to radiation density and because the total amount of radiation is well constrained by the total amplitude of the temperature of the CMB (2.725 K) then with some assumptions then these higher order peaks tells us directly about the density of DM in the universe. These power spectrum variations of the dark matter are Baryonic Acoustic Oscillations (BAO) which can also be measured by optical surveys that track the clustering of galaxies (Anderson et al., 2014,

2012). BAO is one of the robust methods for measuring the growth of structure in the universe as it provides a standard ruler throughout the expansion of the universe. The variations in the CMB power spectrum or the peak in the galaxy correlation function originate from the coupling of baryons and photons in the early universe before recombination: photon pressure carried baryonic matter out of primordial over densities until the mean free path of photons became larger than the horizon size (recombination), but DM did not have significant interactions with the photons and remained in the gravitational potential of the primordial over densities and generated a restoring force to the outflow of baryons. The distance that sound waves traveled before decoupling is the acoustic scale ($\sim$ 150 Mpc). These observations indicate the ubiquitous presence of dark matter in the Universe from scales all the way down to the characteristic BAO scale size of $\sim$ 150 Mpc in the present epoch. At smaller scales the lensing of background galaxies indicates the presence of dark matter at the scale of a few Mpc. Finally, at even smaller scales down to a few pc the rotation curves of galaxies indicates the presence of DM. However, the exact shape of these rotation curves does not dictate what kind of DM is present, it could be SIDM.

1.3 Motivation

The existence of DM was not theoretically predicted. Yet given the ample evidence for the existence of DM from astrophysics it is not obvious that the dark sector should be minimal (that is only interacting via gravity). The standard model displays rich intricacies, and so why not the dark sector? From an astronomical perspective if CDM is adequate to explain the observations then we should favor it for consistency and simplicity. A body of well-confirmed theory governs the assortment of fundamental particles that physicists have already observed. The same theory allows the existence of other hitherto undetected particles (presumably anything that is not proscribed as unphysical could be physical). Theorists have posted many potential particles in the last century including neutrinos, top quarks, and the Higgs boson. Some of these particle predictions were considered all but certain to exist, and others were speculative, but today we know they all represent successful predictions of the Standard Model. Well motivated particle physics theories predict particles that have not yet been observed including sterile neutrinos, axions, and weakly interacting

massive particles.

Sterile neutrinos of order KeV would acquire non-negligible thermal velocities in the early universe and generate a small-scale cutoff in the linear density power spectrum which scales approximately inversely with the particle mass; this is a warm dark matter (WDM) model. Paradoxically, if WDM solves the missing satellites problem, then it cannot simultaneously create cores in those satellites — those galaxies would have been prevented from forming in the first place (Macciò et al., 2012a; Nierenberg et al., 2013). The addition of self interactions to sterile neutrino WDM models can modulate DM thermalization in the early universe to further make the theory compatible with precision cosmological observations of structure formation (Hannestad et al., 2014).

Another enticing DM candiate is the axion. The axion is theoretically motivated to solve the strong CP problem in quantum chromodynamics. Axions could exist and not be the dark matter or they could exist with just the right properties to be dark matter. The properties of axionic dark matter would include no electric charge, small mass (few eV to $\sim 10^{-6}$ eV), and oscillating to and from photons in the presence of large magnetic fields.

Finally, the Weakly Interacting Massive Particle (WIMP) is another particle candidate that predicted was predicted several decades ago. This generic DM particle would have all the right characteristics to be DM, and it would be able to hide right under our noses, yet be observable with observational effort (perhaps, that it is detectable at all is what makes the WIMP more popular than say an undetectable particle). If dark matter is indeed a WIMP, it would interact so feebly with regular matter that we would have been able to detect it only with the generation of dark matter experiments that are just now coming on-line such as: Large Underground Xenon (LUX), Alpha Magnetic Spectrometer, CDMS, or XENON100. The first results from these high profile current generation experiments that are sensitive to dark matter are not always consistent with know-background-only signals, but they make no confident confirmed detection (Aguilar et al., 2014; Agnese et al., 2013).

Although the exact choice and nature of the DM particle are beyond the scope of this work it is relevant to review suitable candidates. Candidates for DM are constrained by analysis of the formation of structure in the Universe. The large scale BAO observations or cosmic microwave background studies lack any deviation from a purely CDM model

(Anderson et al., 2012; Komatsu et al., 2011). Thus the DM candidate particles should be cold meaning that that the particles were non-relativistic during the onset of structure or galaxy formation (corresponding to the time when the object which would eventually collapse was entirely inside the casual horizon). A DM candidate particle must be stable over cosmological time scales. If DM interacts at all with standard particles such as baryons or leptons then that interaction must be exceedingly weakly through electromagnetic radiation. A DM particle must have a relic density that is equal to $\Omega_m = .26$ today. Particle candidates include primordial black holes, axions, WIMPs, gravitinos, or hidden dark matter to name a few (Feng, 2010). The WIMP particle, though not exclusively selected by observations gets the majority of attention and citations currently.

A theoretically natural WIMP is the lightest super symmetric particle, however, no observational evidence for such a particle exists and the general properties of a WIMP particle are independent of the exact particle type. WIMPs are particles with an interaction cross section on the order of the weak strength and a mass of a few GeV to a few TeV. The WIMP model posits that in the dense early universe just after inflation the WIMP particles were interacting with Standard Model particles in a dynamic equilibrium mediated by a weak scale cross section; the reaction changed Standard Model particles into WIMPs and vice versa. The WIMPs dropped out of this thermal equilibrium at a point when they were non-relativistic. It turns out that a particle interacting with this weak scale cross section and a mass of ∼100 GeV has the just right current abundance relative to the rest of matter to be DM. The rate of this reaction is proportional to the product of the WIMP number density and the WIMP pair annihilation cross section into Standard Model Particles, σ_A, times the relative velocity between the two WIMPs v. The density of WIMPs became Boltzmann suppressed at a temperature $T < M_\chi$ depending on the mass of DM particle M_χ (the DM particle is denoted χ) and they they dropped out of thermal equilibrium, that is the rate of interactions became smaller than the Hubble expansion rate of the Universe and WIMPs underwent freeze-out. The cosmologically averaged co-moving WIMP density remains constant and scales with the current CMB temperature $\Omega_\chi h^2 \propto T_0^3 \langle \sigma_A v \rangle$ where h is the dimensionless Hubble Constant and $\langle ... \rangle$ denotes thermal averaging. The freeze-out temperature of such a WIMP (approximately $T_F = M_\chi/25$) is nearly independent of the

WIMP model and thus WIMPs are non-relativistic by the time of plasma decoupling. A non-relativistic particle interacting with this weak scale cross section σ_A (and mass $M_\chi \approx 100$ GeV) has the just right current abundance relative to the rest of matter to be DM. This is the so called WIMP miracle (Feng, 2010).

SIDM is not necessarily a WIMP or any other kind of particle that physicists are looking for. SIDM relies upon the introduction of the hidden sector. Thus SIDM can be completely independent of any WIMP model of DM. At this point there in fact no evidence that DM interacts in any way with the standard model other than gravity. If DM only interacts with standard model via gravity then humans will spend an eternity placing upper limits on an interaction cross section with SM particles; to understand how dark matter behaves the only recourse would be looking at the resultant behavior of astrophysical objects. SIDM is weakly collisional in that the mean free time between particle collisions is much longer than the dynamical time of the system itself. Our simplest SIDM model is governed only by a single additional free parameter which is the cross section per unit mass σ_{DM}. Small cross sections of order 0.1 cm^2 g^{-1} can easily match observations and simulations, but the observable effects of such small cross sections will be unseen at most scales. The introduction of an interaction with a mediator in general produces a velocity dependent cross section. A velocity dependent SIDM model is interesting in that it forms less concentrated cores and flattens inner density profile for subhalos compatible with dwarf galaxies, but has a negligible effect on the density profile of larger mass galaxies and clusters. In the absence of a positive DM direct-detection experiment result (and as prospect of hitting the cosmic neutrino background are on the horizon) SIDM will remain to be viable and indeed certain models may only be constrained with astrophysical simulations and observations. Finally, we note that the cross section region of interest is a value close the cross section of hadrons in neutron neutron (100 microbarns at 40 MeV, Riddle et al. (1965)) self scattering or hadronic annihilation (e^+ e^- to hadrons) of about 10^{-31} cm^2 GeV^{-1}.

1.4 Observational Constraints

On small scales observations have uncovered discrepancies of the expected behavior of dark matter at the center of luminous galaxies at a range of mass scales from dwarf galaxies to

galaxy clusters. The resolution of this problem may be found in 1) the modification of DM scenario or 2) the coevolution of the DM and baryons in a galaxy through feedback 3) better observations that explain discrepancies through secular processes.

Fascinatingly there are very few actual constraints on what dark matter is or how significant its interactions could be. For example if DM was coupled to dark radiation or formed dark atoms (as in double disk dark matter) it would give rise to dark matter acoustic oscillations and imprint the characteristic sound horizon scale of DM at decoupling onto the matter power spectrum of the universe; CMB observation constraints allow that at most 5% of the DM is interacting in any dark atom and dark photon model (Cyr-Racine et al., 2014).

It is is reasonable to consider if DM could be ordinary baryonic matter such as failed stars or primordial black holes. These ordinary matter explanations for DM are Compact Halo Objects (MACHOs). Searches for such objects have shown that they are not present or that at least they cannot account for all of the DM mass. Theory and observations have shown that primordial black hole MACHOs in mass range from $10^{-18}\ M_{\odot}$ (Hawking's black hole mass evaporation limit) to $10^{16}\ M_{\odot}$ can not account for all of the DM mass. However, a recent analysis of microlensing events from the Kepler field finds that there remains some parameter space from $3 \times 10^{-13}\ M_{\odot}$ to $3 \times 10^{-9}\ M_{\odot}$ where MACHO DM could potentially make up the entirety of DM (Griest et al., 2013). MACHOs composed of aggregates of leptons and baryons in any reasonable intermediate mass range of failed stars (consider Jupiter as a failed star at $10^{-3}\ M_{\odot}$) are ruled out by numerous microlensing surveys. In fact MACHOs composed of any baryons would leave observational signatures in the CMB and in the BAO scale because of their coupling with radiation. DM cannot be very small rocks, ducks, or failed stellar objects because while these forms of matter lack strong coupling to radiation during the present epoch they would leave observational signatures during the radiation to matter dominated transition epoch. The only way around this constraint is if DM formed dense objects well before the radiation matter decoupling which is not plausible for ordinary baryonic matter.

We must be cautious with our ambition for DM models. A large fraction of the astrophysically driven support for non-standard DM models has come from simplified simulations

that lack the complexities of baryon physics and follow only the the assembly of the DM component. There is ample evidence through photometric and spectroscopic observations that outflows generated by bursty SF are a common phase in galaxy evolution (Martin et al., 2012; Kauffmann, 2014; Domínguez et al., 2014). We also know that it is necessary to couple DM models with baryon physics in order to remove low angular momentum gas from galaxies through feedback processes (Brook et al., 2011) to explain the observed bulgeless galaxies (Binney et al., 2001; van den Bosch et al., 2001; Governato et al., 2010). Further motivation for including baryon physics includes the necessity to quench SF in galaxy satellites (Klypin et al., 1999; Moore et al., 1999). Weakly Self-Interacting dark matter models (like those explored here and in most cosmologically consistent models) can produce cores, but can not significantly reduce the absolute number of satellite halos we would expect in the Local Group (D'Onghia & Burkert, 2003) because the SIDM power spectrum is similar to CDM at small scales and subhalos survive evaporation (Zavala et al., 2013). Analytical and numerical work shows that feedback lowers the central DM density in galaxies by creating gas outflows and repeated fluctuations in the gravitational potential (Mashchenko et al., 2008; Del Popolo, 2009; Teyssier et al., 2013; Di Cintio et al., 2014b). This results in irreversible energy transfer to the DM (Pontzen & Governato, 2012). The ability of feedback to dynamically heat the DM can potentially remove the need for SIDM at galactic scales. Further, because only the largest (> 10 cm^2 g^{-1}) constant cross section SIDM models have been shown to reduce the absolute number of halos we must likely rely upon baryon physics or more intricate galaxy formation models to resolve the missing satellite problem. Thus we must question the motivation for a more complicated DM model.

There is limited sample of satellites of the Milky Way that we can study in detail and from which most of the observational constraints of this work are drawn from. To date there are at least 35 known luminous galaxies that are within 380 kpc of the Milky Way. Two of these objects have been known since prehistory: the Large and Small Magellanic clouds. Nine satellites were discovered more recently by the Sloan Digital Sky Survey and ten more were discovered within the last few months by the Dark Energy Survey (Koposov et al., 2015; The DES Collaboration et al., 2015; Strigari et al., 2007b). These surveys identify new dwarf galaxies by finding statistically significant over-densities of individual

stars consistent with the expected isochrone and luminosity function of an old and metal-poor stellar population. It is not clear if all of the galaxies recently discovered by the Dark Energy Survey should be considered subhalos of the Milky Way because they cluster around the Large and Small Magellenic Clouds. Including these objects, there are at least 30 luminous objects considered to be in subhalos of the Milky Way and of these 28 are dwarf spheroidals. Each of these galaxies has unique properties (for example Sagittarius is undergoing tidal stripping) that make them suitable or unsuitable for direct comparison so simulations. The only direct kinematic measurements available for these galaxies is the line-of-sight velocity measurements their stars and sometimes the number of stars used to constrain the objects is less than ~ 100. As telescopes become more powerful, we will be able to sample more stars, examine lower luminosity galaxies, and accurately probe dwarfs around our neighbor M31. It is the observational constraint from an ensemble of dwarf galaxy observations that will truly constrain SIDM.

1.4.1 Dissociative Galaxy Clusters

It has been proposed that the DM self interaction cross section is as large as 100s of cm^2 g^{-1} for small dwarf galaxies, but this conclusion does not hold for larger systems. Observations of dissociative galaxy cluster mergers place upper limits on the cross section of SIDM. These are mergers between two clusters of galaxies of comparable mass which have a small impact parameter and are observed during the short period when the cluster gas is significantly offset from the galaxies and DM. These merging clusters must be observed in multiple wavelengths to make the tightest constraints: X-ray to map the intracluster hot gas, multi-wavelength optical to reconstruct the DM mass distribution from background lensed objects, and high resolution spectra to identify the redshift of cluster members. To be identifiable they must occur transverse to the line-of-sight such that the apparent angular separation of gas and galaxy is maximized. To date at least seven such systems have been observed with detailed observations at all these wavelengths: 1E 0657-56 (Clowe et al., 2006), MACS J0025.4-1222 (Bradač et al., 2008), A520 (Okabe & Umetsu, 2008), A2744 (Merten et al., 2011), A2163 (Okabe et al., 2011), A1758 (Ragozzine et al., 2012), and

DLSCL J0916.2+2951 (Dawson et al., 2012). The gas interacts, shocks, and stalls between the clusters. The individual galaxies and stars do not interact and are collisonless. The cluster's dark matter halos interact weakly, if at all, and pass through each other. These studies and previous simulation work (Koda & Shapiro, 2011; Davé et al., 2001) report upper limits on the SIDM cross section as low as 0.5 cm^2 g^{-1} or up to 7 cm^2 g^{-1} (and in other units 10^{-24} cm^2 GeV^{-1}). Around this cross section range DM particles will have less than 10 interactions over a Hubble time in an environment ~ 200 times over the mean critical density of the universe (this is the virial density of a typical halo). In much denser galaxy environments like in galactic disks where the density over the mean is a factor of 10^6 the DM will begin to behave more collisionally. This increases the local phase space density, increases the entropy of the DM, and creates shallower density profiles. Thus these constraints would leave observational signals that would be weakly observable in individual Milky Way like luminosity, $L_\star$, galaxies and smaller, but the effects would be subtle and difficult to disentangle from secular and baryonic effects. The much larger interaction cross sections proposed for smaller galaxies can be reconciled with the upper limits found from dissociative galaxy clusters by invoking velocity dependent models of SIDM.

Some literature argues that constraints from dissociative galaxy clusters may actually favor the existence of SIDM. In the dissociative cluster DLSCL J0916.2+2951 (Musket Ball Cluster) the offsets of the DM, gas, and stars actually favor a dark matter cross section and that cross section could be as large as .2 cm^2 g^{-1} with a $\sim 85\%$ confidence (Dawson et al., 2013).

1.4.2 Inner Density Profiles Or Core versus Cusp

The cores versus cusps problem apparent in dwarf irregular galaxies is a question of whether or not the inner dark matter density profile of dwarf galaxies is increasing as a power law in a cuspy manner or whether it is flat in density in a cored manner. The density profile of dark matter halos is a difficult measurement. The observations available are the surface brightness and the line-of-sight velocity dispersions of stars. The most common analysis of observational data applies the spherical Poisson and Jeans equations under the assumption

a particular stellar anisotropy. In the case of dwarf spheroidals this leads to generic solutions that is close to an isothermal sphere ($\rho \propto r^{-2}$) at large radii. Alternatively one can apply an axisymmetric Schwarzschild model to the data which requires no assumptions to be made about the orbital anisotropy of the stars and similar results that favor cores is still obtained (Jardel & Gebhardt, 2012). With limited observations identifying whether a dwarf galaxy has a core or cusp at the center with certainty is not always possible. Even if spherical symmetry is assumed the line-of-sight velocity dispersion does not produce a unique radial and tangential velocity dispersion, for example the density profile could in reality be triaxial and the velocity dispersion may not be isotropic (Evans & Bridle, 2009). Even under the assumption of a particular profile a degeneracy between the characteristic density and characteristic radius can emerge. This degeneracy persists into the determining the V_{max} and the radius where V_{max} occurs. Presently the majority of the literature presents analysis of dwarf data that favors a core while acknowledging that their data is in some cases consistent with cusps (Amorisco & Evans, 2012). Some analysis does in fact favor cuspy halos (Adams et al., 2014). Baryons affect the dark matter density profiles of galaxies (Teyssier et al., 2013; Governato et al., 2012; Zolotov et al., 2012; Macciò et al., 2012b) in particular this has been shown with supernova feedback in simulations such that high integrated star formation efficiency correlates with cores (Di Cintio et al., 2014b; Brooks & Zolotov, 2014). Regardless of the true shape of the center of these galaxies it is accepted that stellar feedback has the potential to drastically alter the DM distribution of galaxies. The mechanism of dark matter core formation with baryons relies upon bursty star formation which occurs at a time scale smaller than the DM dynamical timescale (Pontzen & Governato, 2012). It is not conclusive whether physical star formation feedback energy is sufficient to create cores in the smallest galaxies where cores are observed.

Dwarf galaxies often reside in galactic environments within the substructure of larger galaxies. The closest and most readily observable dwarf galaxies populate the dark matter halo around the Milky Way. The distribution of mass or equivalently the shape of the potential determines the orbits of the visible stars and gas of the galaxy. The dark matter, stars, and gas of a galaxy collectively determine the potential of a galaxy. In some galaxies the stars and gas are a tiny fraction of the total mass of the galaxy and can be thought

of as tracers of the dark matter, for example ultra faint dwarf spheroidals are the most dark matter dominated objects known (Strigari et al., 2008b). Precise measurements of line-of-sight velocities for stars or gas is possible using spectra and large telescopes, but for dispersion supported galaxies these limited measurements make the true 3D velocity dispersion unknown. Precision astrometry with interferometry instruments in space or deep Hubble or James Web Space Telescope observations over baselines of several decades would be the only way determine transverse velocities for individual stars. These fundamental observational challenges mean the true potential shape of halos is unknown. The spherical Jeans equation provides the total gravitational potential $\Phi(r)$ of a spherically symmetric, dispersion supported, collisionless system to the radial velocity dispersion $\sigma_r(r)$ and number density n_* of tracer particles, which are in effect stars.

$$-n_* \frac{d\Phi(r)}{dr} = 2\frac{\beta n_* \sigma_r^2}{r} + \frac{d(n_* \sigma_r^2)}{dr} \tag{1.7}$$

Here the tangential velocity dispersion is σ_t and also $\sigma_t = \sigma_\phi = \sigma_\theta$. The difference between the radial σ_r and tangential velocity dispersion is quantified by the stellar velocity dispersion antisotropy parameter β

$$\beta = 1 - \frac{\sigma_t^2}{\sigma_r^2} \tag{1.8}$$

The galaxy potential shape problem is solved by making assumptions about the full dispersion of particles based on line-of-sight velocity measurements and then mass profile solutions are evaluated. For example if the velocity dispersion profile remains flat out to half-light radius R_c then the half mass enclosed is $M_{1/2} = 3G^{-1}\langle\sigma^2\rangle r_{1/2} = 4G^{-1}\langle\sigma_{los}^2\rangle R_c$ (Wolf et al., 2010) for a galaxy with line of site velocity dispersion σ_{los}. This analysis makes assumptions that can be invalid for individual tracers, but should be valid for the ensemble; however, there are known and unknown unknown systematics in halo potential estimation such as the binary fraction of stars which if higher than estimated could inflate velocity dispersion measurements by up to 20% (Minor et al., 2010). For this reason and many others the mass assembly, stellar history, gas fraction, and the *astronomy* of the galaxy can not be taken for granted when determining the *astrophyics*. General solutions to the spherical Poisson and Jeans equations find a dark halo density that depends upon β (Evans

et al., 2009). Maximum likelihood mass profile solutions based on line-of-sight velocity measurements (Walker et al., 2010) for many dwarf spheroidals favor cores, but are still consistent with cusps.

The exact form of the effect of baryons (stellar feedback) is a known unknown in galaxy formation. Baryonic feedback creates a dependence of the inner slope of dark matter density profile as ρ^{α} depending on the value of the stellar-to-halo mass ratio M_*/M_{halo}. For M_*/M_{halo} below $\sim 10^{-4}$ the energy feedback is weak enough that different simulation schemes (variations of supernova feedback model ie. blastwave or other, massive young stars, UV reionization, initial mass function, and the density threshold for star formation) return different results as whether the stellar feedback is sufficient to change $\alpha > -0.5$ or create a core. At M_*/M_{halo} greater than 5×10^{-3} stellar feedback is overwhelmed by the stellar plus DM gravitational potential and cuspier ($\alpha \approx -1$) profiles form. Summarily α ranges from -2 to 0, increasing from $M_*/M_{halo} \sim 10^{-4}$ to $M_*/M_{halo} \sim 5 \times 10^{-3}$ where it peaks and then declines. Oh et al. (2011) shows a comparison of simulated dark matter distributions and observed galaxies from the THINGS HI survey. The observed THINGS galaxy sample has a logarithmic inner density slope $\alpha = -.29 \pm .07$ and the simulated sample galaxies have an inner slope of $-0.4 \pm .1$. In some simulations (Di Cintio et al., 2014b)(from the MaGICC project) cusps remain even when $M_*/M_{halo} \leq 10^{-4}$ because stellar feedback is insufficient to significantly alter the inner dark matter density. For these simulated galaxies at $M_*/M_{halo} = 5 \times 10^{-3}$ cores are flattest; thus the most cored galaxies are have a maximum circular velocity $\sim V_{max}$= 50 km s^{-1}. Including baryonic physics in CDM models naturally explains the observed low DM densities in the Milkly Way's intermediate mass (formed as least 10^6 $M_{\odot}$ in stars or near V_{max}= 50 km s^{-1}) dwarf spheroidal population (Brooks & Zolotov, 2014).

1.4.3 Missing Satellites

DM only simulations predict many more small halos around $L_{\star}$ type galaxies than are observed (Mateo, 1998). The lack of easily identifiable dwarf spherodial galaxies around the Milky Way is known as the missing satellite problem (Moore et al., 1999; Kazantzidis

et al., 2004b; Klypin et al., 1999); the resolution of this problem may be due to several equally important factors 1) dwarf spheroidals have extremely low M/L ratios and are hard to identify (Willman et al., 2005) 2) only certain volumes of the Milky Way can be probed due to obscuration and statistical variance could lead to an underestimation of the number of spheroidals in the total volume 3) the actual amount of small scale DM structure may be overestimated by traditional DM-only simulations. Factors 1 and 3 of the missing satellite problem could be explored in my research. The reason for the low M/L ratio of dwarf spheroidals is partially intrinsic - that is they are expected to have low star formation in proportion to their expected dark matter mass. The second factor which reduces the M/L ratio is tidal stripping and tidal shocking. These affects depend upon the potential of the host halo, the potential of the satellite, the orbit of the satellite, and the orbit of the stars within satellite (Read & Gilmore, 2005; Peñarrubia et al., 2010). Dwarf galaxies which have shallow density profiles (cores) will be easily stripped of gas and stars if they make plunging orbits deep into the potential well of a larger halo.

The number of observed satellite galaxies ($\sim$ 3 dozen today) around the Milky Way is vastly fewer than the number of predicted satellites from ΛCDM N-body simulations. This is expected because DM only N-body simulations create DM halos which will not be populated by observationally significant amounts luminous baryonic matter; DM halo substructure is nearly unobservable (though such clumping can amplify the expected signal seen in DM indirect detection annihilation experiments). The predicted number of satellites brighter than the faintest known dwarfs within 400 kpc is still very large: from 500 to 1000. The observed dozens compared to the predicted hundreds is the discrepancy that is the missing satellite problem. Fundamentally this is a problem of the faint end of the luminosity function for dwarfs. Nature has many ways to suppress the luminosity of dwarfs while simultaneously suppressing our ability to observe them. After corrections for luminosity bias and survey sky coverage, the literature often finds that the ΛCDM dwarf satellite predictions are consistent with observations (Tollerud et al., 2008).

Even if the MW displays unusual features there is always the chance that we are a statistical outlier. For example, on the bright end of the satellite spectrum there may be the opposite problem – to many bright satellites. The Milky Way has the Large Magel-

lanic Cloud. Searches through Sloan Digital Sky Survey (SDSS) imaging to find galaxies with LMC like partners find them in 10% of MW like galaxies, thus it is not statistically unlikely that we would have such a companion (Tollerud et al., 2011). However, the LMC is exceptionally blue which may be explained by tidal interaction from first infall initiating star formation.

Surveys of the faintest dwarfs are possible around our neighbor galaxy Andromeda just ∼750 kpc away. M31 has a similar population of dSphs as the Milky Way. The dSphs observed around M31 are too low density to be consistent with mass profiles derived from ΛCDM simulation abundance matching, however the total mass profile is consistent with the ΛCDM subhalos (Tollerud et al., 2014).

Recent imaging with data from the Dark Energy Survey finds at least 9 new ultra-faint satellites around the Milky Way (The DES Collaboration et al., 2015; Koposov et al., 2015) which were statistically predicted to exist (Koposov et al., 2009). Most of these new objects can not be classified as dSphs without follow up observations. They do seem to cluster around the LMC and SMC which would not be expected unless they were associated with the Magellanic Clouds in some way.

1.4.4 Halo shape

ΛCDM predicts that DM halos will be aspherical while warmer or interacting DM halos will be more spherical. Canonical CDM models form triaxially shaped halos which are high density in phase space. SIDM models should form more spherical and lower density phase space in the center of galaxies. The ellipticity of galaxy clusters argues for very tight constraints on the dark matter cross section (near .1 cm^2 g^{-1} from Miralda-Escudé (2002)), but these arguments are weakened by the observational uncertainties and parameter space open in velocity dependent SIDM models.

DM interactions thermalize the DM velocity distribution towards a Maxwell-Boltzmann distribution. The velocity distribution of SIDM differs from that of CDM to a greater extent in the inner cores of a halo. At large radii the decreased overall DM density leads to less interactions and SIDM and CDM velocity distributions converge. A large constant cross

section SIDM model will have an isotropic Maxwellian distribution even at very far radii (out to $\sim$ 10 kpc for a 10 cm^2 g^{-1} model); CDM does not have a Maxwellian velocity distribution.

SIDM is more spherical especially for large constant cross sections. SIDM interactions make the light distribution shape, the mass distribution shape, and the velocity distribution shapes more spherical. DM scattering isotropizes the DM orbits. There is more anisotropy in the velocity distribution ellipsoids in the inner regions of halos and in the outer regions. The velocity distribution of DM f_v along the principal components of the velocity dispersion tensor will be nearly identical for the inner regions of halos with significant DM interactions. For example, the ratio of f_v along the semi-major axis versus the semi minor axis will be nearly unity for a large constant cross section of greater than 1 cm^2 g^{-1} at a radius of 1 kpc. This is important for the prospects of DM detection in laboratory experiments.

Halo shapes are difficult to measure, observe, and interpret. It may be necessary to look at halo shape as a function of time to rule out periods of large distortion, utilize different kinds of halo shape algorithms of the inertia tensor, and consider the confounding effect of baryons particularly in the center of galaxies. For example, in earlier dark matter only studies (Cole & Lacey, 1996) it was found that halos are generally triaxial, more spherical towards the center, and show no significant trend with mass. In the modern literate only the first conclusion is still valid. Robust conclusions about halo shape include 1) more massive halos are more round 2) halos are increasingly rounder at larger radii 3) halos of a given mass are more triaxial at earlier times 4) dissipation processes such as radiative cooling, star formation, and feedback processes makes dark halos substantially rounder at small radii compared to adiabatic systems (Springel et al., 2004). The outer halo shape is unaffected by the presence of a disk, yet the inner halo is aligned such that the minor axis aligns with the disk axis (Bailin et al., 2005) during DM only mergers the final shape depends only on the orbital angular momentum, but with the inclusion of stellar disks substantial changes to shape may occur (Kazantzidis et al., 2004a).

1.5 State of the Field

There are many experimental programs attempting to identify the particle nature of dark matter (Hooper & Baltz, 2008). There is no single smoking gun of dark matter. There are several. It is common to categorize the DM detection schemes as follows:

- Indirect detection of DM by its annihilation into photons and or standard model particles that decay into photons. This would result in gamma ray photons from dense DM halos.

- Direct detection of DM by its interaction within a laboratory experiment. For a weakly interacting dark matter model, the sought out signal is the interaction of DM particles with the nucleus of laboratory detector material. For an axionic like DM model a several tesla magnetic field could convert axions into photons that could be observed in a microwave cavity. There is no single approach to direct detection.

- Creation of DM by a particle accelerator. DM could be created from Standard Model particles interacting, the DM particles would leave the detector without interacting, and the missing energy would signal something.

It is important to keep in mind that all of these detection methods rely upon hypothetical interactions of DM and further that they techniques are not necessarily exclusionary. The intersection of my work with these search techniques is primarily that the phase space distribution of dark matter affects the expected signal in indirect and direct detection techniques (the creation of DD in particle accelerators is beyond this scope and will not be discussed).

1.5.1 Indirect Detection

Emission of gamma ray photons or other particles may be evidence of annihilating dark matter. The source spectrum of conjugate annihilating particles is $\Phi_s(E)$ which is a function of secondary particle energy E:

$$\Phi_s(E) = \frac{\langle \sigma_A v \rangle}{8\pi M_\chi^2} \sum_f \frac{dN_f}{dE} B_{f,s} dE \tag{1.9}$$

where v is the relative velocity of the DM particles and σ_A is annihilation into all possible standard model particles (this is not the same cross section we use later), where the sum is over all final annihilation states f for branching fraction B_f. M_χ is the mass of the DM particle. $\frac{dN_f}{dE}$ is the production rate per given annihilation species f. The source spectrum applies to each standard model particle s that DM could annihilate to including photons, positrons, electrons, quarks, leptons, or gauge bosons (Porter et al., 2011; Feng, 2010). Many of these particles would decay rapidly and the observable particles would be gamma ray photons, protons, electrons, antiprotons, and positrons.

Gamma rays are a particularly clean signal of DM in the local universe because they would not be deflected by magnetic field and contaminating sources could potentially be identified. Equation 1.9 for the case of $s \rightarrow \gamma$ becomes $\Phi_\gamma(E)$ and the DM gamma ray source spectrum $\phi_\gamma(E, \psi)$ is the observable we seek that depends upon the distribution of matter in an astrophysical system and the energy spectrum so that:

$$\phi_\gamma(E, \psi) = J(\psi) \times \Phi_\gamma(E) \tag{1.10}$$

The *astrophysical factor* is J which depends upon the integral of the density ρ squared along the line of sight in the direction ψ over the solid angle $\Delta\Omega$

$$J = \int_{\Delta\Omega(\psi)} \int_\ell \rho^2(\ell, \psi) dl d\Omega(\psi) \tag{1.11}$$

It is the job of astronomers to constrain the astrophysical factor J. SIDM is of relevance here because the momentum mixing that SIDM adds to the centers of galaxies would lessen the central density and make a DM annihilation signal more diffuse. Recent observations and analysis of Milky Way center and the local dwarf galaxies by the Fermi Gamma-Ray Space Telescope, PAMELA (satellite payload), the Alpha Magnetic Spectrometer (on the International Space Station), ATIC (high atmosphere balloon-borne), and other various experiments (Geringer-Sameth & Koushiappas, 2011; Feng et al., 2010) have attempted to exclude certain particle annihilation channels and mass ranges of WIMPs (although not always WIMPs the interpretation of the data is dependent upon a given theoretical model). The weak-scale cross section of WIMPS is lower bounded by freeze-out in the canonical

WIMP model whereas the upper bound on the cross section is unbounded but may be constrained if self annihilation process are observed. Claims of DM annihilation signals from the center of the MW are confounded by astrophysical sources. Fermi collaboration observations and conservative analysis of the center of the MW find no significant signal from DM and they can only report upper limits (Ackermann et al., 2012; Buckley et al., 2015). Less conservative analysis of the same Fermi data has found a DM signal, but given that the excess signal spectrum attributable to DM is very nearly consistent with a population of unresolved millisecond pulsars the conclusion must be that no significant signal of DM has been found in the MW. Nearby dwarf galaxies are an excellent laboratory for such study due to several reasons 1) their close proximity 2) they are DM dominated objects 3) their dearth of astrophysical backgrounds (hot gas, X-ray binaries, or pulsars) (Charbonnier et al., 2011).

These searches look for cosmic ray particles as well as γ-rays. These high energy cosmic ray studies usually look for an excess of e^+ or e^- fluxes (or their ratio). These studies are inconclusive. Indeed an excess of these particles has been observed, but it is actually too large an excess to be attributed to a standard WIMP and more careful considerations of the background sources has made the excess interpretation ambiguous.

Astrophysical γ-ray sources are an obstacle for dark matter detection experiments. Analysis conclude that there is likely a large population of unidentified millisecond pulsars that is responsible for a portion of the observed signal in the galactic center, however, there may be remaining signal even after the pulsars are accounted for. Additionally it is surprising, or at least theoretically disturbing, that millisecond pulsars have such a similar energy spectrum to that expected of DM. Gamma ray photons may come from cosmic rays which produce a background of γ-rays in several ways. Cosmic rays, their secondary electrons, and positrons produce gamma rays via bremsstrahlung type interaction with interstellar gas and by inverse Compton scattering off of the interstellar radiation field. Cosmic ray nuclei produce γ-rays via scattering with the interstellar gas which produce secondary particles which then decay to gamma rays. Another confirmation that these processes are at work is the distributed microwave and radio spectrum they produce via synchrotron radiation included by the galactic magnetic field. Understanding the galactic astrophysical background is a

huge challenge: space based experiments have low angular resolution and low sensitivity. Below ∼100 GeV typical sources have fluxes large enough to be detected by balloon borne or satellite experiments. Above ∼100 GeV primary γ-rays produce air showers that can be detected by ground-based instruments used to determine the energy and direction. The Fermi Telescope receives ∼90% of its photons from a diffuse origin. The diffuse γ-ray emission is dominated by γ-rays produced by cosmic rays interacting in the galactic interstellar gas and radiation field. The extragalactic background is likely a superposition of contributions from unresolved extragalactic sources including: Blazars/AGN, starburst galaxies, γ-ray bursts (which contribute less than 1%), and true diffuse processes. Determining the origin of the extragalactic background is an unsolved problem in astrophysics

Critically for this work, as seen in equation 1.11, the shape and density profile of the DM halos enters these studies because the annihilation signal is dependent upon the line of site density of the DM. Measurements of dwarf's stellar velocity dispersion in attempts to reconstruct the density profile of the DM distribution (Strigari et al., 2008b; Martinez et al., 2009) remain the largest systematic error in attempts to constrain DM annihilation cross sections and rates. Precision simulations of dwarfs with the correct baryonic physics included will improve the mass reconstruction at the center of galaxies where densities and annihilation signals are both highest.

1.5.2 Direct Detection

Direct detection of DM is the scenario in which DM displays an observable signal within a laboratory experiment. The direct detection signal depends upon the ambient passage of galactic dark matter through the detector. Theoretically direct detection experiments of DM particles with SM particles in the laboratory could reveal the velocity distribution of DM, a velocity distribution which would be altered by SIDM. The velocity distribution of SIDM differs from that of CDM to a greater extent in the inner cores of a halo. At large radii the decreased overall DM density leads to less interactions and SIDM and CDM velocity distributions converge. A large constant cross section SIDM model will have an isotropic Maxwellian distribution even at very far radii (out to $\sim$ 10 kpc for a 2 cm^2 g^{-1} or

greater model). For a typical galaxy there is more anisotropy in the velocity distribution ellipsoids in the inner regions of halos than in the outer regions. The velocity distribution of DM f_v along the principal components of the velocity dispersion tensor will be nearly identical for the inner regions of halos with significant DM interactions. For example, the ratio of f_v along the semi-major axis versus the semi minor axis will be nearly unity for a large constant cross section of greater than 1 cm^2 g^{-1} at a radius of 1kpc. The rate of DM particles passing through the detector depends upon the local DM velocity phase space with respect to the motion of the solar system and the Earth; it is expected that there will be an annual modulation of the signal due to the Earth's orbit. SIDM with reasonable cross sections of .1 to 35 cm^2 g^{-1} can lead to a reduction in the interaction rate at the 10% level or an amplification of the annual modulation signal of 25% (Vogelsberger & Zavala, 2013). Ultimately the shape, mass, and tidal history of the Milky Way's dark matter halo are not known with precision greater than a factor of a few and so even if we had precision models of DM halo phase space we would still need precision observations of the Milky Way to solve this problem.

The detection schemes discussed here for DM are not necessarily signals confirming or negating the existence of SIDM (or even DM itself). Constraining the DM candidate particle's properties through astrophysical observations is an ongoing task. The WIMP model has some desirable features, but a hidden dark matter particle that interacts via hidden dark sector physics (small cross section of elastically scattering) beyond the standard model is the focus of this work.

Chapter 2

NUMERICAL SIMULATIONS

ChaNGa[1] (Charm N-body Gravity) is a parallel hydrodynamics self-gravity astrophysical simulation N-body code using smoothed particle hydrodynamics (Jetley et al., 2008, 2010; Menon et al., 2015). It is an update of the GASOLINE code with similar star formation and supernova feedback (Wadsley et al., 2004; Stinson et al., 2006; Wadsley et al., 2008). Our most detailed simulations include physics modules for: metal line cooling, self shielding, cosmic UV background, star formation, blastwave supernovae feedback, young star thermal feedback, and molecular hydrogen (H_2). Our star formation recipe is limited to dense gas regions and this concentrates feedback energy realistically. We use a Kroupa IMF (Kroupa, 2001). The cosmic UV background turns on at $z = 9$ and modifies the ionization and excitation state of the gas, following the model of (Haardt & Madau, 1996). The feedback and star formation parameters are the same as those adopted in Governato et al. (2012); one hundred percent of the supernovae energy is coupled to the surrounding gas. We include thermal diffusion (Shen et al., 2010) and we have addressed the artificial viscosity contact discontinuity issues that are common in smoothed particle hydrodynamic (SPH) simulations by using the geometric mean density in the SPH force solution. This means that, for example, Kelvin-Helmoltz (KH) instabilities generated from shearing flows are much better modeled than in previous versions of the code where spurious surface tension acts to suppress the growth of the KH instability. This updated SPH method captures mixing in multiphase gas (an important feature for galaxy simulations) much more accurately.

We use the ΛCDM cosmological parameters discussed in chapter 1. The particular values are $\Omega_0 = .26$ $\Omega_\Lambda = .76$ $\sigma_8 = 0.77$ (density perturbation amplitude normalized at 8 Mpc), and $n = 0.96$ (the running of the spectral index of perturbations). We use gravitational force spline softening lengths in the range of 64 to 144 pc. The smoothing length for gas

[1] http://hpcc.astro.washington.edu/tools/changa.html and https://github.com/N-bodyShop/changa

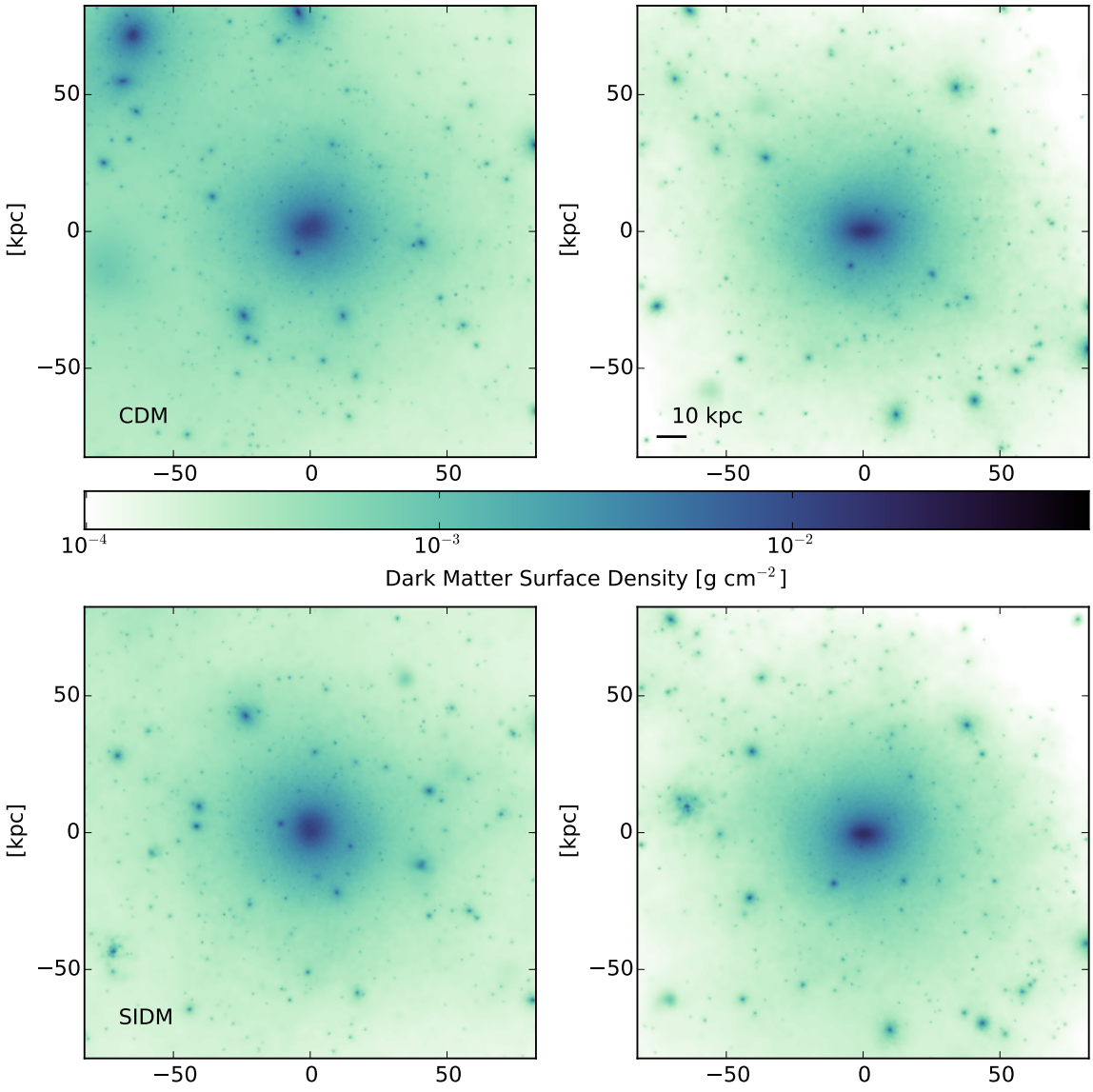

Figure 2.1: The dark matter distribution of halo h516 at 13.5 Gyr. The top two figures show CDM and the bottom show SIDM (constant cross section $\sigma_{dm} = 2$ cm^2 g^{-1}). The left figures are the face-on view and the right are edge-on, however such differentiation is hard to discern when viewing the nearly spherical DM distribution.

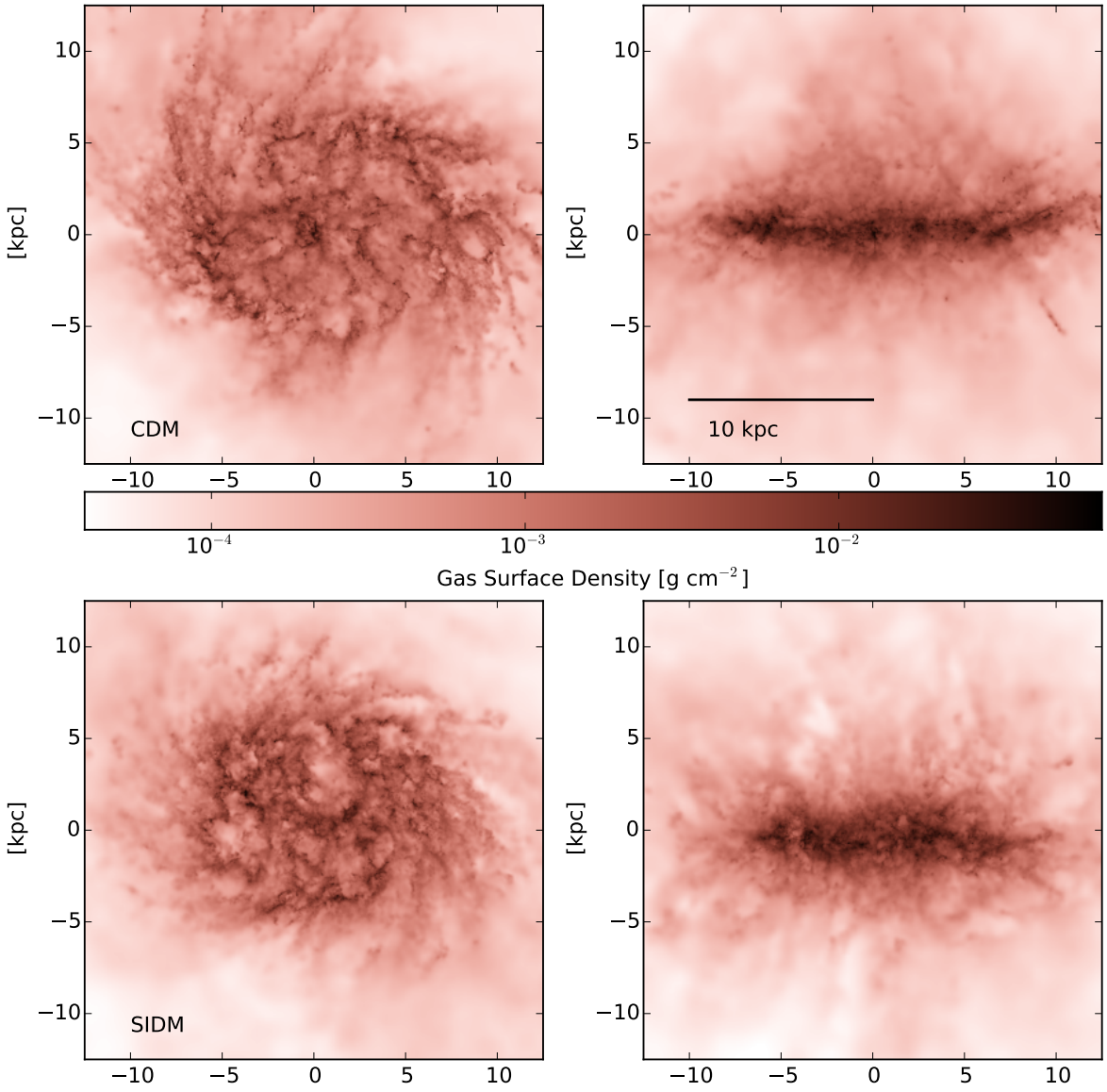

Figure 2.2: The projected gas distribution of halo h516 at 13.5 Gyr top is CDM bottom is SIDM (constant cross section $\sigma_{dm} = 2$ cm^2 g^{-1}). The top two figures show CDM and the bottom show SIDM. The left figures are the face-on view and the right are edge-on.

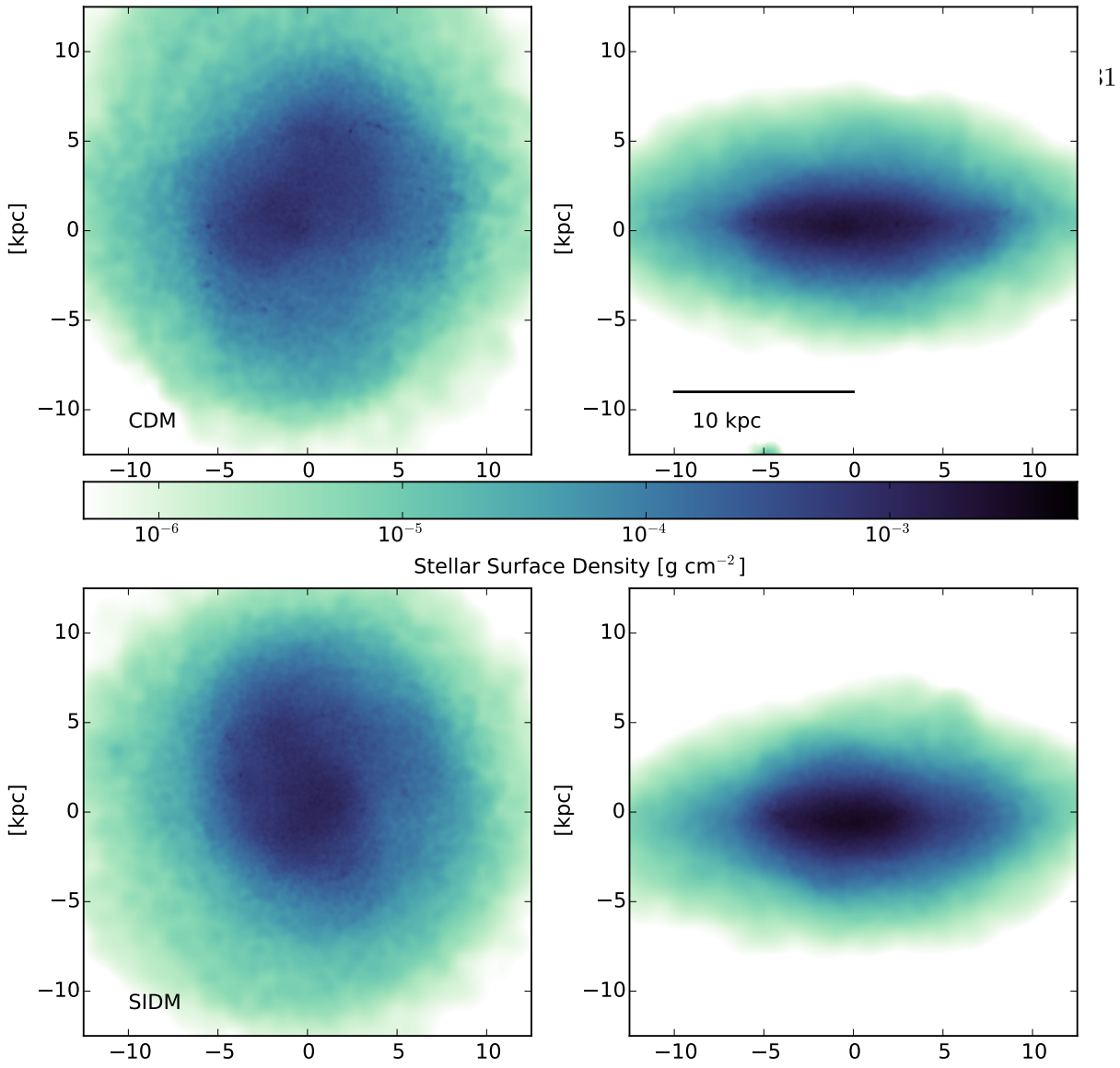

Figure 2.3: The projected stellar distribution of halo h516 at 13.5 Gyr top is CDM bottom is SIDM (constant cross section $\sigma_{dm} = 2$ cm^2 g^{-1}). The top two figures show CDM and the bottom show SIDM. The left figures are the face-on view and the right are edge-on. The orientations are defined by the sum of the particles in the halos particles net angular momentum such that in the face-on view the disk lies in the x-y plane and the angular momentum vector is in the z plane.

particles is allowed to be .1 the force softening. Simulations start at z$\sim$120. We want to compare our simulations to nearby small galaxies at the present time so our simulations are run to $z = 0$. Additionally we use the zoom-in technique to achieve high resolution in the regions of interest. The first three figures figures 2.1, 2.2, and 2.3 in this chapter show the surface density of DM, gas, and stars with the complete suite of physics including star formation, feedback recipes, metal line cooling, UV background, and thermal diffusion.

We have implemented a Monte Carlo scattering scheme into the code similar to previous works (Vogelsberger et al., 2012; Davé et al., 2001). This implementation assumes SIDM scattering is elastic, velocity independent or dependent, and isotropic in the center of mass frame. These assumptions simplify the problem as does the assumption that a Monte Carlo scheme to determine if a DM particle interacts discretely with any of its nearby neighbors is sufficient to model the problem. Previous work has shown that a Monte Carlo scheme reduces to the exact solution of the spatially homogeneous Boltzmann equation and the Navier-Stokes equation solution (Bird, 1994; Nanbu, 1983). The key to this scheme is determining the probability of two DM particles to interact and exchange momentum at any given time-step. The probability, P that an N-body DM particle denoted with a subscript 0 collides with another particle denoted with a subscript j is a function of the particle's relative velocity Δv, the time interval Δt, the local density ρ, and the cross section per unit mass of DM interaction σ_{dm} (and $\sigma/m_\chi = \sigma_{dm}$) thus we have

$$P = \rho\sigma_{dm}\Delta v\Delta t \tag{2.1}$$

An examination of the units here reveals that the resultant quantity is dimensionless and that is could be interpreted as the number of interactions (N) that occur. The probability for an interaction to occur and the number of interactions which occur are the same equation. The interpretation depends on the different regimes that are being probed, for example, if P is greater than one it cannot be strictly interpreted as probability and if N is less than one it can't be strictly interpreted as a count of a discrete event: equation 2.1 is only valid in the limit that the value is very small. In practice then we need to choose Δt (or control some other parameter) such that multiple collisions per DM particle are avoided

at a given time-step. In practice the cross section and other parameters are chosen to be adequate given characteristic conditions. The time step is not actively controlled to avoid multiple collisions per time step, but it is confirmed that $\rho\sigma_{dm}\sigma_{vel}\Delta t \leq .01$ for characteristic conditions (where σ_{vel} is the local velocity dispersion). The numbers work out such that the probability (P = density ($10^6 \times 10^{-29}$ g cm^{-3}) $\times$ cross section (2 cm^2 g^{-1}) $\times$ characteristic relative velocity (100 km/s) $\times$ time-step (10^{14} seconds)) is of order $\sim$0.02 for a characteristic halo that is at the extreme limit of what we expect (approach velocities of 100 km/s, halo that is a million times the critical density). For more typical values that are expected the probability is $\sim$.0002 at most. Multiple collisions are a concern when we move to larger cross sections and the velocity dependent cross section gets orders of magnitude larger, but only for low velocity dispersion systems. See figure 2.4 which shows a sample of probability values pulled from a velocity dependent simulation.

The particle by particle scattering of DM is simulated in our simulations by DM. DM is neither a fluid nor is it collisionless in this regime. It is treated as hard-sphere interaction. It can be shown that the fine grain Boltzmann function is approximated by the coarse grained Boltzmann function of numerical simulations (Rocha et al., 2013)

2.1 Implementation

The DM interactions are implemented in the smooth particle hydrodynamics code in a discrete manner corresponding to the discrete nature of tree code + SPH numerical simulations. The DM interaction scattering probability is calculated for each particle (denoted subscript 0) at each time-step with its k neighbors where k may be chosen such that a certain volume is probed or is simply cut off at a particle number. The value of k is chosen to be sufficient to be statistical and can be increased as necessary. We used a value of $k = 32$. We explored larger values of k ($k = 64$ and $k = 128$), and found no effect for high resolution simulations; $k = 32$ has been sufficient for previous work as well (Koda & Shapiro, 2011). The k neighbors characterize the density in the region of the given DM particle. The effective density depends on the mass of the DM particle m_0 times the cubic spline kernel in 3D. The cubic spline kernel $W(q)$ is a function of particle separation (Δx_{0k}) and the smoothing length h such that if $q = \Delta x_{0k}/h$ then

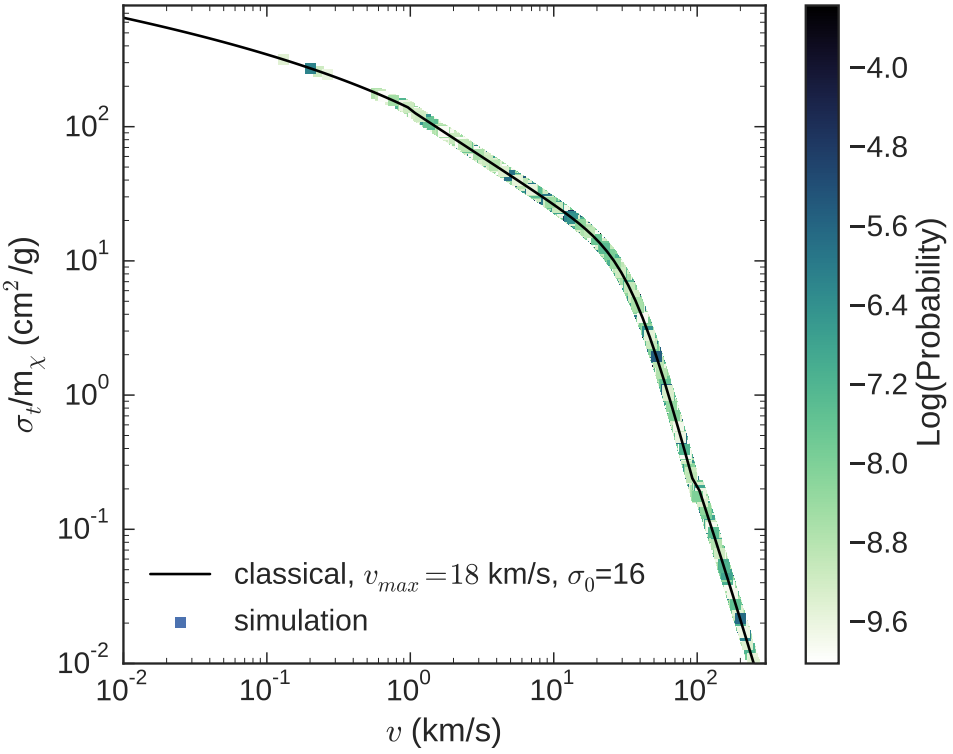

Figure 2.4: The velocity dependent classical cross section interaction curve compared to the values pulled directly from the output of halo h516 with a classical cross section with a v_{max} = 18 km/s and a normalization of σ_0=16. The probability values were pulled from the simulation with a random draw chance of 1/million because there are millions of interaction opportunities in a simulation but this sparse polling creates a statistical sample. This resulted in 10000 values and then those probability values are clipped showing only values greater than $1\times\ 10^{-10}$. Most of the interaction probabilities are sufficiently much smaller than this. This demonstrates that 1) the units input into the simulation code are correct and 2) that the probability for multiple interactions is very small 3) there are very few interactions (and interaction opportunities) that occur with approach velocities less than 1 km/s.

$$W(q) = \begin{cases} \frac{8}{\pi}(1 - 6q^2 + 6q^3) & 0 \leq q \leq 1/2 \\ \frac{16}{\pi}(1 - q) & 1/2 \leq q \leq 1 \\ 0 & 1 \leq q \end{cases} \tag{2.2}$$

The probability for particle 0 to interact with the kth particle is calculated in the code as

$$P_{0k} = m_0 W(\Delta x_{0k}) \sigma_{dm}(\Delta v_{0k}) \Delta v_{0k} \Delta t \tag{2.3}$$

where $\Delta v_{0k} = |v_0 - v_k|$, here we have made the cross section a function of the particle's relative velocities. This value of P_{0k} is calculated for each particle at each step then a random n number is generated and compared to $P/2$ and if $n < P/2$ then a particle collision occurs and the particles are re-orientated randomly in velocity. The comparison is to the probability over two because the kth particle later becomes particle 0 and checks for its own interactions with nearby neighbors. This Monte Carlo approach works because N-body particles are samples drawn from a smooth underlying distribution function.

We scatter dark matter particles with conservation of energy and momentum during an interaction. This is easily accomplished in the center of momentum frame. Here we will demonstrate how this is accomplished in theory and then within the ChaNGa code. We may begin by treating the first particle as if it were at rest which will be necessary later as we implement the interaction in ChaNGa where the variables we have access to are limited. Let us take particles p and q with velocities $\mathbf{v}_p$ and $\mathbf{v}_q$ and masses m_p and m_q. The quantities in bold are vectors with x, y, and z spatial components. We first define a frame denoted with a zero subscript where particle p is at rest

$$\mathbf{v}_{p,0} = \mathbf{v}_p - \mathbf{v}_p = 0 \tag{2.4}$$

$$\mathbf{v}_{q,0} = \mathbf{v}_q - \mathbf{v}_p = \mathbf{dv} \tag{2.5}$$

Thus we have defined $\mathbf{dv}$ as the difference of particle velocities. To translate to a center of mass frame we need to subtract the center of momentum frame velocity from the velocity of

the particle. In the center of mass frame the sum of the momentum is $m_p\mathbf{v}_{p,cm}+m_q\mathbf{v}_{q,cm}=0$ where particle p has a momentum in the center of momentum frame defined as $\mathbf{p}_{p,cm}$. We may immediately find that p has a momentum in the center of momentum frame $\mathbf{p}_{p,0,cm}$ of

$$\mathbf{p}_{p,0,cm}=\mu(\mathbf{v}_p-\mathbf{v}_q)=-\mu\mathbf{dv} \tag{2.6}$$

Where $\mu=\frac{m_pm_q}{m_q+m_p}$ is the reduced mass. It is true that $\mathbf{p}_{p,0,cm}=-\mathbf{p}_{q,0,cm}$ also. The velocity of the center of mass itself will later be used and is defined as.

$$\mathbf{v}_{0,cm}=-\mathbf{p}_{p,0,cm}/m_p \tag{2.7}$$

During a scattering event we add a momentum to p and simultaneously subtract that momentum from q such that the total momentum of the system $\mathbf{p}=\mathbf{p}_p+\mathbf{p}_q$ remains constant during the interaction. The new momentum directions are chosen randomly and isotropically by some unit vector $\mathbf{n}$ in three dimensions with components n_x, n_y, n_z such that $1=\sqrt{n_x^2+n_y^2+n_z^2}$ and this unit vector is truly chosen randomly (Marsaglia 1972) (to pick a random point on the surface of sphere it is not adequate to choose a point in $\theta\in[0,2\pi)$ and $\phi\in[0,\pi)$ because the area element $d\Omega$ has singularities at the poles which leads to over sampling at the poles). Then the total momentum in the center of mass frame is

$$P_{cm} \quad = \quad \sqrt{p_{x,cm}^2+p_{y,cm}^2+p_{z,cm}^2} \tag{2.8}$$

The momentum after the interaction is found by multiplying by the unit vector. We denote the state of the particle after an interaction by an apostrophe

$$\mathbf{p}'_{p,0,cm}=P_{cm}\ \mathbf{n} \tag{2.9}$$

The total momentum is conserved through this interaction as demonstrated below by expanding

$$P'_{cm} = \sqrt{P_{cm}^2 n_x^2 + P_{cm}^2 n_y^2 + P_{cm}^2 n_z^2} \quad (2.10)$$

$$P'_{cm} = P_{cm}\sqrt{n_x^2 + n_y^2 + n_z^2} = P_{cm} \quad (2.11)$$

Thus momentum and energy are equal before and afterwards in all frames. Finally, we must transform back to the non-center of mass frame and where particle p is not at rest. For p then

$$\mathbf{v}'_p = \mathbf{v}_p + \mathbf{p}'_{0,cm}/m_p + \mathbf{v}_{0,cm} \quad (2.12)$$

$$\mathbf{v}'_p = \mathbf{v}_p + \mathbf{v}'_{0,cm} + \mathbf{v}_{0,cm} \quad (2.13)$$

$$\mathbf{v}'_p = \mathbf{v}_p + \mathbf{v}'_0 \quad (2.14)$$

This series of transformations are undoing the transformations from equation 2.5 and equation 2.6. So then for q:

$$\mathbf{v}'_q = \mathbf{v}_q - \mathbf{v}'_{0,cm} + \mathbf{v}_{0,cm} - \mathbf{v}_{q,0} \quad (2.15)$$

$$\mathbf{v}'_q = \mathbf{v}_q - \mathbf{v}'_0 - \mathbf{v}_{q,0} \quad (2.16)$$

$$\mathbf{v}'_q = \mathbf{v}_q - \mathbf{v}'_0 - \mathbf{dv} \quad (2.17)$$

The analysis so far has not taken into account the expansion of space. The proper distance is the physical distance between objects at a particular expansion factor $a(t)$ at a time t. The relation between proper coordinates $\mathbf{r}$ and comoving coordinate $\mathbf{x}$ is $\mathbf{r} = a(t)\mathbf{x}$. Differentiating with respect to time gives us the proper velocity. The true physical velocity of a particle is the change in position of the particle in time is $d\mathbf{r}/dt = \dot{a}\mathbf{x} + \dot{\mathbf{x}}a$ where the first term is associated with the Hubble flow or expansion of the universe and the second term is associated with the peculiar motion of the particle.

The necessary quantities for each particle in the simulation are then position, velocity, and mass. However, the absolute position is not readily available in the ChaNGa code, but instead the relative position between any to particles is calculated on the fly to avoid

errors on periodic boundary conditions. In order to calculate dynamics ChaNGa uses the canonical momentum, that is $\mathbf{v}_{can} = a^2\dot{\mathbf{x}}$. Thus with the variable we have available the physical velocity relevant to interactions is

$$\frac{d\mathbf{r}}{dt} = \frac{\mathbf{v}_{can}}{a} + \dot{a}\mathbf{x} \tag{2.18}$$

For two particles p and q which may potentially interact we then calculate their relative velocities and continue work in this relative velocity space for example in the x direction the relative velocity is dvx.

$$dvx = \frac{v_{q,can} - v_{p,can}}{a} - \dot{a}dx \tag{2.19}$$

where $dx = x_q - x_p$ is a function returned by the code. And similarly for dy and dz such that the total relative velocity between particles p and q is

$$dv = \sqrt{dvx^2 + dvy^2 + dvz^2} \tag{2.20}$$

Then the center of mass momentum in the x direction (and similarly for y and z directions through this discussion) is readily calculable now

$$p_{x,cm} = \mu(v_{p,x} - v_{q,x}) \tag{2.21}$$

$$p_{x,cm} = -\mu dvx \tag{2.22}$$

And the velocity in the x direction the center of mass frame for this particle is then

$$v_{x,cm} = \frac{-p_{x,cm}}{m_p} \tag{2.23}$$

the momentum in the center of momentum frame is

$$P_{cm} = \sqrt{p_{x,cm}^2 + p_{y,cm}^2 + p_{z,cm}^2} \tag{2.24}$$

after generating new random orientation unit vector ($\mathbf{u}$) we would have, for example in the the x dimension that

$$p'_{x,cm} = P_{cm} u_x \tag{2.25}$$

We boost back to the simulation frame while noting our system of units and that we have

$$v'_{p,x} = v_{p,x} + a(p'_{x,cm}/m_p + v_{x,cm}) \tag{2.26}$$

and similarily, yet different, for q

$$v'_{q,x} = v_{q,x} + a(-p'_{x,cm}/m_q + v_{x,cm} - dvx) \tag{2.27}$$

These equations are equivalent to equations 2.14 and 2.17 where dv is the change in velocity. In the code these equations are implemented just as above (and for the y and z dimensions similarly). The comoving velocities of the particles has now been updated and a DM interaction has occurred.

2.2 Calibration and Testing of the Implementation

We verify our implementation of SIDM by comparing analytical predictions of the number of dark matter interactions to simulations of dark matter halos with a Hernquist density profile (Hernquist, 1990). We then demonstrate the formation of a flat core and the signature flat SIDM velocity dispersion profile, starting from an NFW profile with a cuspy density profile and a rising velocity dispersion (Navarro et al., 1996b). This analysis has been carried out for the constant cross section and velocity dependent SIDM models in scaled units and natural units. Our implementation code closely replicates published results of the predicted number of SIDM collisions as a function of halo mass and local density and the evolution of the central density profile (Rocha et al., 2013).

The number of dark matter interactions per unit time is an important cosmological value for SIDM theory and more practically here it is a diagnostic of the functioning of the numerical simulation code. The number of interactions that occur for a given halo determine whether the rate of interactions is sufficient over the lifetime of a halo to create cores. We have implemented a counter for the number of DM interactions per particle in the code which is output when the code runs so the theoretical and simulated number of interactions can be directly compared. The expected number of interactions can be calculated directly in simple cases. The total number of interactions, Γ, that occur per unit time is an integration of the velocity weighted cross sections in the volume V.

$$\Gamma = \int \frac{\rho^2(x)}{2m_\chi^2} \langle \sigma v_r \rangle(x) dV \tag{2.28}$$

Where m_χ is the mass of the dark matter particles in the simulation, σ is the dark matter cross section, and $\langle \sigma v_r \rangle(x)$ is the local thermal average of the cross section weighted by the particles relative velocity as a function of the position x. The local thermal average of the cross section is calculated by integrating over the relative velocity, $v_r = |\mathbf{v}_1 - \mathbf{v}_2|$ for the distribution functions $f(v_1)$ and $f(v_2)$ of the particles. A combined distribution function $F(v_r)$ can be found by changing variables from the individual velocities to the center of mass, $\mathbf{v}_c$ and relative velocity.

$$\langle \sigma v \rangle(x) = \int_0^\infty (\sigma v_r) F(v_r) dv_r \tag{2.29}$$

$$\langle \sigma v \rangle(x) = \int_0^\infty \sigma v_r f(v_1) f(v_2) d\mathbf{v}_1 d\mathbf{v}_2 \tag{2.30}$$

This quantity combined with the particle number density, n_χ leads to the thermal averaged reaction rate $\langle R \rangle = n_\chi^2 \langle \sigma v_r \rangle$ which when integrated over volume yields the total number of interactions Γ. In the most general case the distribution function can be a function of position (as for a galactic dark matter halo) and the cross section can be a function of relative velocity (for velocity dependent SIDM). In the simplest case for single value initial velocity particles and uniform density, the distribution the function $f(v)$ becomes a delta function at that given velocity where $f(v_r) = \frac{\delta(|v| - v_0)}{4\pi v_0^2}$ and interaction rate simplifies

to $\Gamma = \sqrt{2}/2N\rho\sigma_{dm}v$ where N is the total number of dark matter particles in the simulation. For a standard Maxwell-Boltzmann distribution $f(v) = \frac{1}{(2\pi)^{3/2}a^3}\exp\left[\frac{-v^2}{2a^2}\right]$ where a is the standard deviation of the velocity vector and has units of velocity. The average velocity of particles in a distribution is found by integrating over the first moment of velocity: $\langle v\rangle = \int_0^\infty vf(v)dv$. Of course we are actually interested in the relative speed of the dark matter particles. If we assume that two dark matter particles have speeds equal to this average speed then by also averaging over all angles of collision we conclude $\langle v_r\rangle = \sqrt{2}\langle v\rangle$. Then similarly the local thermal average of the cross section is calculated as $\langle\sigma_{dm}v_r\rangle = \sqrt{2}\langle\sigma_{dm}v\rangle$. For Maxwell-Boltzmann distribution of velocities the result is

$$\langle\sigma_{dm}v_r\rangle(x) \quad = \quad \sqrt{2}\sigma_{dm}\sqrt{\frac{8a^2}{\pi}}. \tag{2.31}$$

Under the assumptions of a Maxwell-Boltzmann distribution, constant density, and velocity independent interactions (perhaps an approximation of the center of a constant density core of a galaxy) Γ becomes

$$\Gamma = \frac{\sqrt{2}N\rho\sigma_{dm}}{2}\sqrt{\frac{8a^2}{\pi}}. \tag{2.32}$$

We would like to have an analytic calculation for the number of interactions that would occur in any given dark matter halo; however, in general the integrals of dark matter halos are not well behaved and further the interaction of dark matter particles themselves will modify the density and velocity distributions. One well behaved halo profile is the Hernquist profile which has a dark matter density profile of

$$\rho(r) = \frac{Ma}{2\pi r}\frac{1}{(r+a)^3} \tag{2.33}$$

where M is the mass of the halo, r is the radius of the halo, and a is the scale radius. Under the assumption of an isotropic velocity distribution, the velocity dispersion profile of the Hernquist profile is known analytically (Hernquist, 1990)

$$\sigma_v^2 = \frac{GM}{12a}\left[\frac{12r(r+a)^3}{a^4}\mathrm{Log}\left(\frac{r+a}{r}\right) - \frac{r}{r+a}\left(25 + 52\frac{r}{a} + 42\left(\frac{r}{a}\right)^2 + 12\left(\frac{r}{a}\right)^3\right)\right] \quad (2.34)$$

and the average of $< \sigma v > (x)$ is then

$$\langle \sigma v \rangle(x) = \frac{1}{2\sqrt{\pi}\sigma_v^3(x)} \int_0^\infty (\sigma v) v^2 \mathrm{exp}[\frac{-v^2}{4\sigma_v^2(x)}] dv \quad (2.35)$$

The total number of interactions per unit time is then

$$\Gamma = \int_0^\infty \frac{\rho(r)^2}{2m_\chi} \langle \sigma v \rangle(r) 4\pi r^2 dr \quad (2.36)$$

We calibrate our implementation of SIDM by comparing a simulation of a Hernquist profile and an analytic predictions of the density profile, interaction rate, and dispersion. We use the spherIC program to generate isolated spherical DM halos of millions of particles with tuneable density distributions (with parameters α, β, and γ that together determine the outer, inner, and transition logarithimic slope of the DM density). The particles are Monte Carlo sampled self-consistently from distribution functions of the given model. This results in stable equilibrium models; the velocities have an isotropic velocity tensor. The SphereIC program (created by Miguel Rocha[2]) is itself based upon the HALOGEN4MUSE program by Marcel Zemp.

In figure 2.5 we see the density profiles of a several SIDM only simulations at masses of 10^{10}, 10^9, 10^8 $M_\odot$ with $\sigma = 10$ and one SIDM simulation with $\sigma = 0$ after just .05 Gyr of evolution. In 2.2 we see the velocity dispersion of the halos in scaled units after .8 Gyr of evolution. Notice that the 10^{10} $M_\odot$ halo is moving away from the density profile of the other halos. We interpret this as that it has gone through less dynamical time than the other halos. These plots are in scale units and are comparable to the work in (Vogelsberger et al., 2012). Then in figure 2.7 we see the number of interactions that occur for this same halo as a function of radius as calculated with the equations described in this section. The analytic predictions here are only valid in the ideal case of a Hernquist profile. In a real halo, such

[2]https://bitbucket.org/migroch/spheric

as in this simulation, the interactions cause the halo to evolve away from a true Hernquist distribution, thus for the comparison of the number of interactions in figure 2.7 the halo was evolved for a short time step such that evolution of the halo density and velocity distribution is insignificant. The noise in the outer regions of the halos occurs because of the lack of particles in these bins. The evolution of these halos can be understood by considering how the elastic interactions transport heat to and within the DM as discussed in chapter 3.

2.2.1 Convergence

In Figure 2.8 we show a resolution test using the most massive halo of simulation 'h516' The halo (of final mass 4×10^{10} $M_{\odot}$was simulated lowering the mass resolution by a factor of 64 in mass and 4 in force resolution. The ratio of the spherically averaged local density as a function of radius show that the SIDM simulation converges at about 2 softening lengths, similar to the CDM run (Power et al., 2003). The 'central' density decreases by a factor of ~ 6 between the CDM and SIDM case. These results agree with previous works. To verify the convergence of the SIDM density profiles at the previously poorly explored regime of $\mathrm{M}_{vir} < 10^9$ $M_{\odot}$we also simulated the '40 Thieves' volume first with particle mass 8000 $M_{\odot}$and then again 2400 $M_{\odot}$, and a force resolution of 65pc in both cases. Combining these runs with the h148 volume we are able to cover four orders of magnitude in halo mass, from small halos with peak velocities smaller than 10 km s^{-1} to massive galaxies with a large system of satellites. We have simulated h148 at lower resolution with hydrodynamics and SF, finding that it hosts a large disc galaxy.

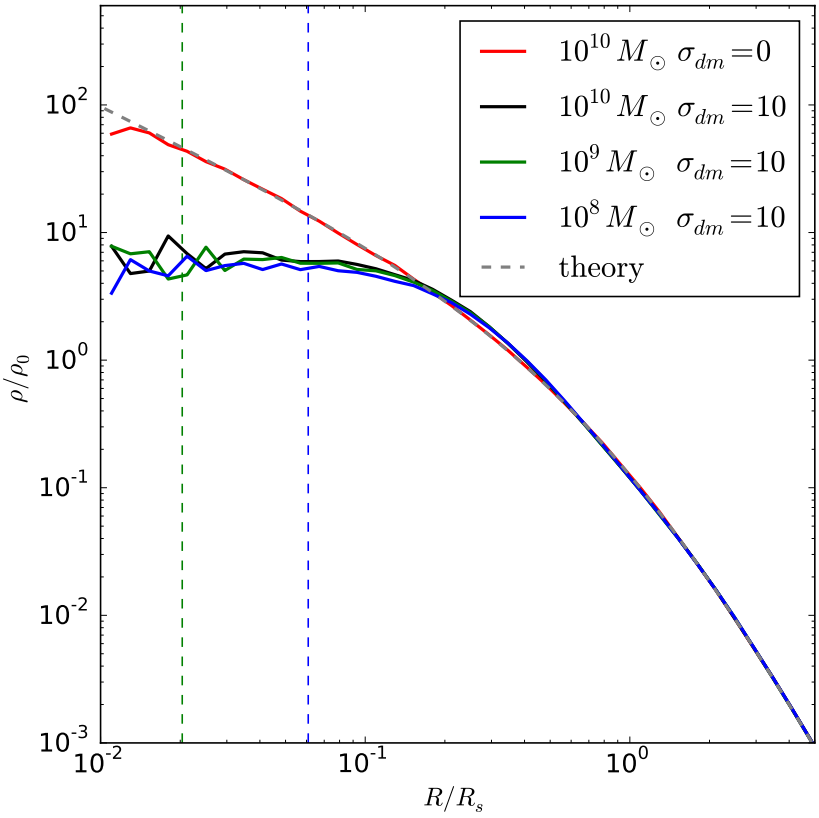

Figure 2.5: The density in scaled units of R/R_s for Hernquist halos of 10^{10} black, 10^9 green, and 10^8 $M_\odot$ blue which have scale radii of 1.099, .37, and .12 Kpc respectively based on the mass concentration ratio relation from Neto et al. (2007). Each halo has been evolved for about 25 scaled dynamical times which corresponds to 91, 44, and 20 million years respectively. The halos demonstrate self similar evolution in these scaled distance and time units. The density ρ has been scaled by the central density. The vertical dashed lines indicate the softening length of 7.5 pc that is scaled for each halo (the dashed line for the 10^{10} $M_\odot$ halo is off the plot further to the left). The dashed grey dashed line is the theoretical Hernquist density profile which matches extremely well to the evolved Hernquist profile with no dark matter interactions shown in red. Each halo was described with about 2 million particles.

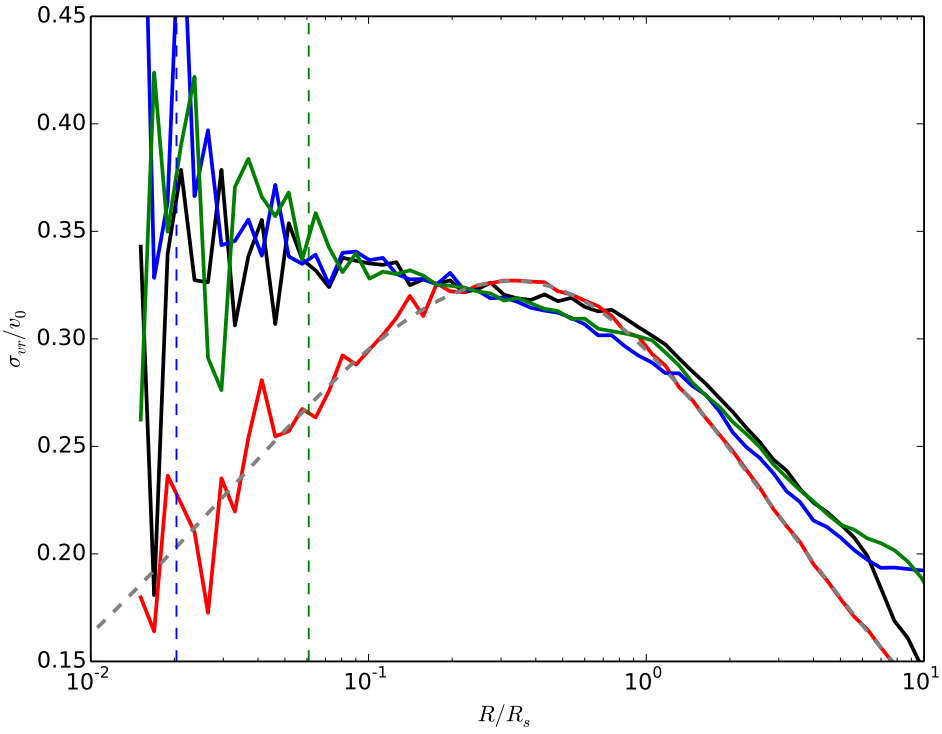

Figure 2.6: Snapshots of Hernquist profiles showing the dispersion σ_0 in units of $v_0 = a\sqrt{4\pi G\rho_0}$ where $\rho_0 = M/(2\pi a^3)$ and $a = 2.26$ where these units attempt to normalize the halos such that they evolve in the same scaled way (Koda & Shapiro, 2011). The cross section is constant at 10 cm^2 g^{-1}. In dashed grey is the analytical prediction for an ideal Hernquist halo. Each halo was described with about 2 million particles.

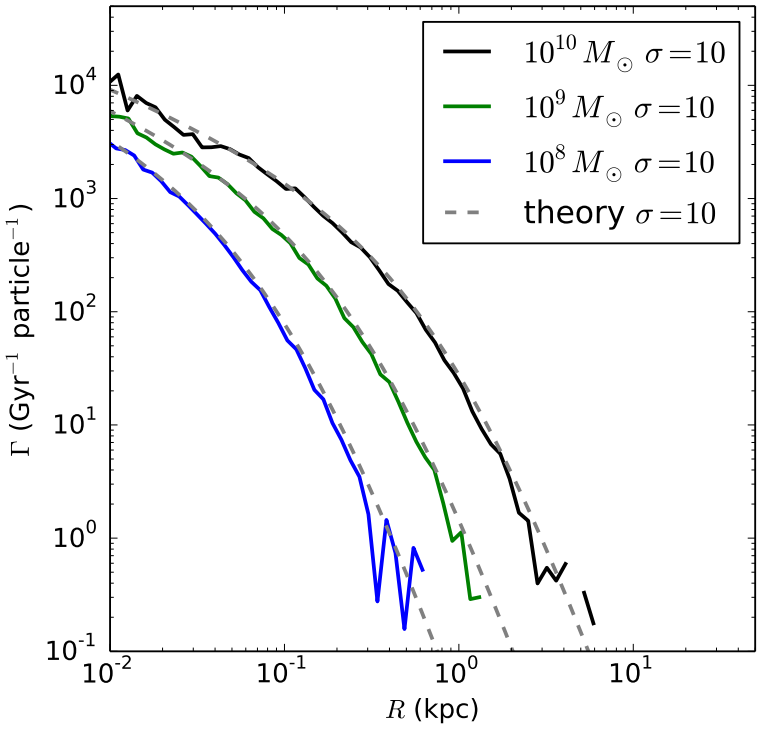

Figure 2.7: Snapshots of a Hernquist profile constant cross SIDM simulation showing the number of interactions that occur per particle per gigayear for the same halos as above. The cross section is 10 cm^2 g^{-1}. In dashed grey is the analytical prediction for each halo respectively. The simulations were run for a period much shorter than the dynamical time of the halo. Each Hernquist profile has a different scaled structure as described in the previous figure. Each halo was described with about 2 million particles.

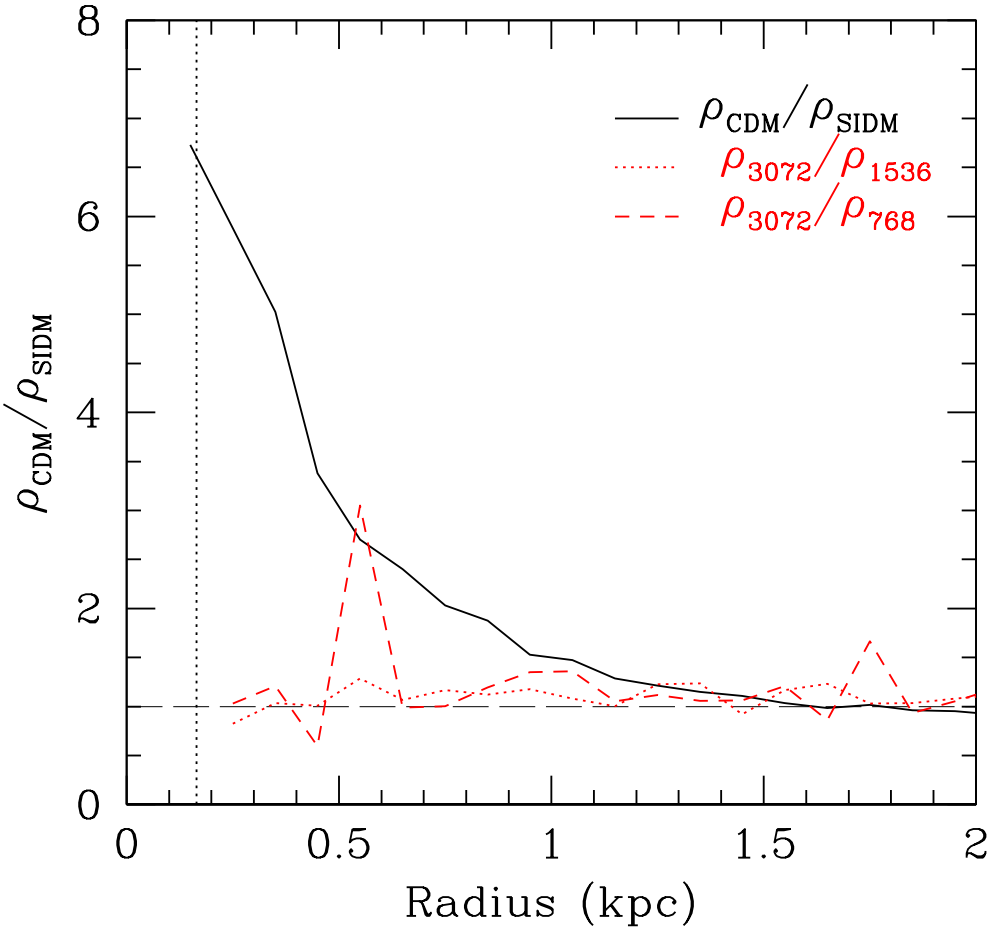

Figure 2.8: The local density ratio as a function of radius between the high resolution SIDM version of halo h516 (ρ_{SIDM}) and its lower resolution counterparts (ρ_{1536}) and (ρ_{768}) Results in the low res versions converge at $\sim$ two softening lengths, as typical of CDM-only simulations.

2.3 Simulations

We focused our hydrodynamical simulations on the largest galaxies formed in the filamentary regions h516 and h2003. These are two well studied fields: h2003 is the same halo simulated in Governato et al. (2015) while h516 is the main halo of Governato et al. (2010) and referenced by the moniker 7 dwarfs studied in Shen et al. (2014) and Madau et al. (2014). The SF parameters in our study were identical for all CDM and SIDM simulations. They also correspond to the fiducial g5 runs in Governato et al. (2015), where we explored the effects of different feedback and SF recipes in the context of comparing the formation of dwarfs in CDM vs Warm scenarios. Here we emphasize that our SF implementation creates repeated starbursts and gas outflows with significant loading factors (gas mass ejected from the center divided by star formation rate). Multi-wavelength evidence for outflows, analysis of the stellar populations in the SDSS dwarfs and realistic CMDs give strong support to our implementation of SF. This approach differs from Vogelsberger et al. (2014) where less bursty feedback does not create substantial DM cores. The SF and feedback prescriptions have been shown to form CDM galaxies with SF effi- ciency, photometric, and kinematic properties close to those of real ones (Christensen et al., 2014a; Munshi et al., 2013).

For h516 and h2003 stars form at a threshold of 100 amu cm^{-3}, stars form stochastically from gas colder than 10^4 kelvin, the IMF is Kroupa 2001, early stellar winds, supernova deposit 10^{51} ergs in their blast radius, and the coupled SN energy is 1. The density threshold of SF at 100 amu/cm^3 limits SF to dense regions and concentrates feedback energy (Christensen et al., 2014b; Agertz & Kravtsov, 2015).

The second set of simulations is h937 and h148. Halo h937 is also known as the 40 thieves. The 40 thieves has been analyzed in (Governato et al., 2015) and additionally a description of these galaxies and their detailed star formation is in preparation by Munshi et al. 2015. In addition to metal line cooling the simulation labeled g1HbwK1 includes non-equilibrium abundance and cooling processes of H_2 (Christensen et al., 2012). The forty thieves and h148 are analyzed extensively here as DM only runs, but runs with SIDM+baryons are in progress. The resolution for many of the simulations here is equivalent to a uniform grid of 4096^3 particles over the entire original volume of 25 Mpc, see the tables for specifics. For

this particular resolution, we expect numerical fragmentation effects due to finite force and mass resolution to become important at a few $\times 10^7$ $M_\odot$. We obtain a significant sample of DM halos in a range of environments by using the zoomed-in approach (Katz, 1992). The 40 thieves simulation has a gravity resolution of 60pc, a SPH resolution of 6pc (when gas present), and DM particles have a mass of 6650 , 1410, and 422 $M_\odot$ for DM, gas, and stars respectively (when present).

We use the Amiga halo finder (Gill et al., 2004; Knollmann & Knebe, 2009) to identify all the halos in this work. We use the analysis software pynbody (Pontzen et al., 2013) to generate many of the intermediary results.

DM only simulations				
Run ID	DM ($cm^2\ g^{-1}$, km/s)	DM part. mass ($M_\odot$)	Force Soft. (pc)	halo mass range ($M_\odot$)
h516vSIDM1	$\sigma_0 = 16$, $v_{max} = 18$	1.6 $\times 10^4$	86	$\times 10^9$-5$\times 10^{10}$
h516CDM	CDM	1.6 $\times 10^4$	86	$\times 10^9$-5$\times 10^{10}$
h2003CDM	CDM	0.67$\times 10^4$	64	4$\times 10^8$-1$\times 10^{10}$
h937CDM	CDM	0.81$\times 10^4$	64	4.2$\times 10^8$ - 2.4$\times 10^{10}$
h937cSIDM	$\sigma_{DM} = 2$	0.81$\times 10^4$	64	4.2$\times 10^8$ - 2.3$\times 10^{10}$
h937vSIDM1	$\sigma_0 = 16$, $v_{max} = 18$	0.81$\times 10^4$	64	4.2$\times 10^8$ - 2.3$\times 10^{10}$
h937vSIDM2	$\sigma_0 = 35$, $v_{max} = 10$	0.81$\times 10^4$	64	4.2$\times 10^8$ - 2.3$\times 10^{10}$
h937cSIDM.hr	$\sigma = 2$	0.24$\times 10^4$	64	1.25$\times 10^8$ - 2.7$\times 10^{10}$
h148CDM	CDM	1.93$\times 10^4$	86	10^9 - 1.3$\times 10^{12}$
h148SIDM	$\sigma = 2$	1.93$\times 10^4$	86	10^9 - 1.3$\times 10^{12}$
hc148SIDM	$\sigma_0 = 16$, $v_{max} = 18$	1.93$\times 10^4$	86	10^9 - 1.3$\times 10^{12}$

Table 2.1: Dark matter only simulations analyzed and compared in this work. The DM parameters correspond to whether the run used a constant cross section, σ_{DM}, or a classical regime velocity dependent cross section with a normalization value σ_0 at the given v_{max} value. The mass range shows halos with at least 50,000 DM particles within their virial radius. The main halos in each volume are studied with several million particles each. The DM-only subsample is one of the first to simulate a sample of field and satellite halos at similar mass and spatial resolution. This approach allowed us to study the effect of the environment on the DM distribution of the halos in the two populations.

ΛCDM Reference Simulations				
Run ID	physics model	DM/Gas part. mass ($M_\odot$)	Force Soft. (pc)	halo mass range ($M_\odot$)
h937g1MbwK1C52	SF	$0.67\times10^4/1.4\times10^3$	115	10^7 - 5×10^{10}
h937g1HbwK1	SF+H2	$0.67\times10^4/1.4\times10^3$	115	10^7 - 5×10^{10}
h516CDM	SF	$1.6\times10^4/3.3\times10^3$	86	10^9 - 5×10^{10}
h2003CDM	SF	$0.67\times10^4/1.4\times10^3$	64	4×10^8 - 1×10^{10}

Table 2.2: Standard cosmology simulations with stars use for comarison in this work. The mass range shows halos with at least 50,000 DM particles within their virial radius.

SIDM Complete Simulations				
Run ID	physics model	DM/Gas part. mass ($M_\odot$)	Force Soft. (pc)	halo mass range ($M_\odot$)
h937vSIDM1	SF,H2	$.81\times10^4/3.9\times10^3$	115	-
h516cSIDM	SF	$1.6\times10^4/3.3\times10^3$	86	10^9 - 5×10^{10}
h2003cSIDM	SF	$0.67\times10^4/1.4\times10^3$	64	4×10^8-1×10^{10}

Table 2.3: Self-Interacting dark matter simulations with stars analyzed in this work. The mass range shows halos with at least 50,000 DM particles within their virial radius. The run ID h937vSIDM1 corresponds to the variable cross section SIDM model $\sigma_0 = 16$, $v_{max} = 18$, which is currently in progress.

Chapter 3

THEORY

We can categorize the most relevant theory that goes into this research into three main branches 1 the astrophysical effects of galaxy formation 2 the fundamental physics of Self-Interacting dark matter models and 3 the dynamics of galaxies.

3.1 Galaxy Formation

How do baryons effect the evolution and structure of galaxies in the presence of Self-Interacting dark matter? Supernovae release about 10^{53} ergs of energy when they explode, but most of this energy is locked away in the suicide notes of the universe – neutrinos. Supernova have $E_{SN} = 10^{51}$ ergs of energy that is readily coupled to particles in the standard model. Of this 10^{51} ergs of available energy we take in our simulations that 100% of this energy is coupled to the surrounding gas. The choice of this parameter depends upon simulation resolution, star formation recipes, the stellar initial mass function, and gas cooling recipes. It is rather certain that this coupling value is not strictly correct: the dynamics of supernovae feedback is sub-resolution. Sub-resolution models are validated a posterior by observations and so the parts of the physical model that are missing or wrong are accounted for by over or under estimating other parameters.

Massive stars in the final stages of evolution form instabilities that lead to collapse when they run out of nuclear fuel. Their interiors collapse, and likely due to the generation of tremendous amounts of neutrinos their outer envelopes are driven out in detonation. The outer parts of the star expand at relativistic speeds. The energy from a supernova is initially in a shock wave which rapidly thermalizes. The amount of energy deposited into the interstellar medium depends strongly upon the ambient temperature, ionization state, and density. Theoretically, we can separate the the coupling into kinetic fraction ($f_{kin} = E_{kin}/E_{SN}$), thermal fraction ($f_{therm} = E_{therm}/E_{SN}$), and gas momentum fraction

($f_P = P/P_{SN}$). There are different models for what fraction of energy that should couple, but they range between a few to more than one hundred percent. In Walch & Naab (2014) they run three-dimensional high resolution hydrodynamical simulations of supernova and find for dense regions of $n \approx 100$ (particles/cm^3) the Sedov and snowplow phase of the explosions end quickly ($\sim$0.01 Myr) and compactly ($\sim$100 pc) due to radiative cooling which limits $f_{therm} \approx 0.01$, $f_{kin} \approx 0.05$, and $f_P \approx 9$. Without cooling these values may go up by orders of magnitude or in a in a preionized interstellar medium they may go up by 50%. The heated interstellar medium can do work and clear out voids; however, the rate at which it cools can also change as it does this work.

The amount of energy deposited depends upon the interstellar medium state in a non-linear way: isolated supernovae couple differently (inefficiently) compared to supernovae occurring in clustered superbubbles driven by multiple supernovae (efficiently). Multiple continuous supernovae inject energy within hot dilute regions and create termination shocks; these so called superbubbles are over-pressured and drive themselves outward (floating radially away from dense central regions in the simulation) well after the shock has become radiative. Lower resolution simulations from the previous decades were not able to resolve star formation into small molecular cloud density ($\sim$50 m_H cm^{-3}) knots where clusters of stars would form. Intense radiation pressure from these regions results in explosive decompression that launches the galactic outflows.

This entire problem is degenerate with the initial mass function: only higher mass ($\leq 1M_\odot$) stars undergo supernovae. The initial mass function determines the number of stars that are created at a given mass. Under-creating massive stars but coupling their energy more tightly will have (up to a point) similar results if massive stars were over-created, but coupled less weakly (Agertz & Kravtsov, 2015). The initial mass function also determines how young stars feedback. Young stars inject blackbody sourced ultraviolet radiation into the interstellar medium that heats the gas to the surface of the young massive stars (which is near 10^4 Kelvin for an OB star). Over the lifetime of a massive star ($\leq 1M_\odot$), they emit more energy than supernovae in Lyα photons, around 10^{52} erg, but these photons do not couple well to the interstellar medium.

A widely used initial mass function is Salpeter where the number of stars goes as $dN =$

$\xi(m)dm$ where dn is the number of stars with mass between m and $m + dm$ $\xi(m) = km^{-\alpha}$. In the Salpeter formulation $\alpha = 2.35$ for masses greater than $M_{\odot}$. In this work we use a Kroupa initial mass function where the values vary from $\alpha = .3$ to 2.3 over masses of .08 $M_{\odot}$ to greater than 1 $M_{\odot}$. The challenge of producing the right number of stars is insensitive to the number of massive stars produced because the massive stars are such a minority by number, however massive stars dominate in UV flux and generate the supernova feedback that alters the potentials of halos. The IMF and supernovae couplings in our simulations are consistent with observations of dwarf galaxies, however this consistency does not mean they are the true model parameters. We find that we can create realistic dwarf galaxies that match predicted stellar mass to halo mass relations (Munshi et al., 2013) with CDM and our current parameters. Yet by changing the slope of initial stellar mass function at the high end or by changing the strength of supernovae coupling to the interstellar medium we could still create realistic dwarf galaxies with SIDM.

Supernovae drive the distribution of matter in a galaxy to a cored profile. This works through multiple brief baryonic outflow events that occur at time scales below the dynamical time scale of the DM. If the gas outflows are faster than the local circular velocity this will cause the DM to migrate outwards through multiple outflows events (Pontzen & Governato, 2012). This mechanism can only work in galaxies that have significant outflows generated by supernovae. Galaxies with stellar masses less than $10^{6.5}$ $M_{\odot}$will have difficulty generating enough energy to create cores. The energy required to create a core with SN feedback is a strong function of the original DM inner distribution such as concentration, final core size, and so the cost scales exponentially as $\sim M_{halo}^{.3-.7}$ for core sizes less than 1 kpc (Maxwell et al., 2015). Estimates of the amount of energy to create a core have been revised by recent studies: the mass does not have to redistributed at the virial radius, it can be pushed just out of the core radius. Summarily, baryonic outflows are a verified effect of CDM that naturally explains the cores of intermediate mass galaxies. However, if baryons are responsible for core generation then there may be some expectation of at least small correlation between core size and luminosity of the galaxy.

Supernova feedback modulate galaxy formation and structure as soon as the first starbursts in a galaxy are generated (Dekel & Silk, 1986), but even before this event the density

of nascent halos is determined by the background density of the universe when the galaxies first began to form and so the mass within the central regions of dark matter halos today is related to the depth of the gravitational potential well at formation (Cole & Lacey, 1996; Bullock et al., 2001a). Dwarf halos collapsed much less than a billion years after the big bang and during the epoch of reionization (Planck Collaboration et al., 2014). When the building blocks of hydrogen were formed in the early universe it was only free protons and electrons. Neutral hydrogen formed during recombination ($\sim$380,000 years after the Big Bang) and later when the integrated ultraviolet flux arising from hot young massive stars and QSOs was sufficient the bulk of the universe became reionized. The UV background of the universe present at and during reionization suppresses star formation in dwarf galaxies (Bullock et al., 2000; Wyithe & Loeb, 2006; Milosavljević & Bromm, 2014) and may even explain the observed common mass scale relations that begin at $V_{circ} = 30$ km s^{-1}. Robust reionization suppresses gas accretion onto low-mass halos such that most halos will be dark unless they accreted substantial amounts of gas before reionization.

3.2 Models of Self-Interacting Dark Matter

What model of Self-Interacting dark matter should we choose? Dark matter self interactions depend upon physics in the dark sector. The dark sector is a theorized domain of physics that includes everything beyond the Standard Model (SM) that doesn't have strong interactions, other than gravity, with SM particles. The concordant ΛCDM cosmological model is 96% dark. Dark energy is 76% of that energy, dark matter is 24% of that energy, and the remaining small fraction of the Universe's energy budget is rounded out by SM particles. There are epistemological reasons to assume the simplest model is favored until it is demonstrated unfeasible, but the complex observations that the dark sector can explain compel us to look at interactions beyond the SM. The discovery space of dark matter remains vast despite years of efforts to create or detect dark matter directly and indirectly. The observational evidence for dark matter may also be the best evidence for physics beyond the standard model.

This work focuses on elastically scattering Self-Interacting dark matter with cross sections limited by observational data. There are a myriad of theoretical physical models that

could produce this behavior. Generally an $\sim$ MeV scale dark sector force carrier particle ϕ could generate self interactions required to isotropize DM halos and if this mediator particle decays to standard model particles it has implications for indirect and direct detection experiments. There are limits to the strength of interactions beyond the standard model (Davé et al., 2001). Velocity dependence is a natural way to avoid constraints from larger (high velocity systems) such as dissociative velocity clusters or $L_\star$ galaxies. Conveniently a range of SIDM models with massive force carriers would have significant velocity-dependent interactions (Feng et al., 2010).

The characteristic SIDM cross section explored is around 1 cm^2 g^{-1} or around 10^{-24} cm^2 GeV^{-1} c^2 this is many orders of magnitude larger than the weak scale cross section (10^{-36} cm^2). The canonical DM particle beyond the minimal gravitational interaction only dark matter particle is the WIMP, but SIDM is not the standard WIMP nor does SIDM depend upon the WIMP model being correct at all. WIMPs are predicted by various theories such as supersymmetry. SIDM is predicted by deviations from CDM structure at small scale. The primary measurables for WIMP models are the mass m_χ (theoretically 10 GeV to a few TeV) and the thermally averaged cross section times the velocity σv. Note that the WIMP's interaction cross section is for interactions through the weak force (coupled to the dark sector). The cross section that we seek is for SIDM is through the dark sector.

The mediators of the dark sector are by some theoretical opinions more likely than not to connect to the standard model or an observable in some way. For example there could be an allowed decay of the ϕ into SM particles before big bang nucleosynthesis. Bound state formation and Sommerfeld enhanced annihilation after chemical freeze-out could reduce the DM relic density. Compton scattering off hidden photons could delay kinetic decoupling and this would suppress small-scale structure. DM annihilation in early halos (z$\sim$30) would be amplified trough Sommerfeld enhancement. Finally, the mediator may lead to a present day path to direct detection or collider production. If the SIDM model (or the WIMP model, or any DM model) gathers observational evidence for a particular interaction model then these observational signatures will be sought as confirmation of the model. Currently, all of the observational signatures just described above are not seen: they are constraints on what DM is not.

3.2.1 The Cross Section

The microphysics of the dark sector interaction are well below the resolution limit of our simulations. Our model does not currently include the possibility of bound states, decays, or dark photons, or even angular dependence. Some of these theoretical possibilities would violate our assumption of elastic energy conserving interactions and are highly constrained, for example CMB observation constraints allow that at most 5% of the DM is interacting in any dark atom and dark photon model (Cyr-Racine et al., 2014). The lack of angular dependence is in our model is not ideal, but it is consistent with other literature. The way we treat our cross section borrows several conventions and definitions from plasma physics. They define the conductivity cross section σ_C and transport σ_T as

$$\sigma_C = \int (sin^2\theta)\frac{d\sigma}{d\Omega}(\theta)d\Omega \qquad \sigma_T = \int (1-\cos\theta)\frac{d\sigma}{d\Omega}(\theta)d\Omega. \tag{3.1}$$

These cross sections depend upon the azimuthally symmetric and momentum independent differential cross section $d\sigma/d\Omega(\theta)$ (where Ω is the two-dimensional solid angle) which describes the change in impact parameter necessary to cause a given change in trajectory defined by the angle θ. The conductivity or viscosity cross section σ_C evenly weights forward and backward scattering and is not our parameter of choice. The transport cross section σ_T, or sometimes referred to as the momentum-transport cross section, is an effective particle cross section that describes the average momentum transferred from a particle when it has a collision. The $1-\cos\theta$ weights the transfer cross section by the angle θ to which the DM particle is scattered such that in the case $\theta \to 0$ or $\theta \to \pi$ the horizontal momentum component is zero and all non-horizontal momentum transfer will cancel out on average.

The differential cross section $d\sigma/d\Omega$ depends upon the DM particles approach angle and relative velocity. The standard cross section is the integral over all angles $\sigma = \int d\Omega$ $(d\sigma/d\Omega)$, but this cross section does not take into account scattering which has a strong angular dependence which is the case for light mediators that are likely for SIDM. For light mediators there is a strong forward scattering enhancement; however, this enhancement is nullified because the net DM particle trajectories are unchanged. Perpendicular scattering is more efficient at thermalizing the DM halo and altering the shape of observable astrophysical

structure formation. For these reasons we proceed to work with the transfer cross section which is consistent with the literature. All cross sections we use are in terms of σ_T.

Another consequence of the hidden microphysics of the DM interaction is that the cross section that we work with is $\sigma_{dm} = \sigma_T/m_\chi$ which has the reasonable units of centimeters squared per gram. If an identifiable dark matter particle existed it would not be necessary to state the cross section in terms of the DM particle mass in all situations, but in our numerical simulations where a single SPH DM particle represents an ensemble of many DM particles it would still be convenient.

3.2.2 Velocity Dependent Cross Sections

There are three different cross section scenarios that we explore: the constant regime, the classical regime, and the resonant regime. These regimes are extrapolations of the consequence of SIDM being mediated by a force carrier particle that is a light elementary scalar or vector ϕ in the dark sector. The mediator force carrier particle distorts the wave function of DM particles in the interaction which may suppress or enhance the cross section. The full scope of the particle physics of such an interaction is beyond the scope of this thesis, but relevant resultant phenomenology will be discussed here. We have chosen velocity dependent models with the collaboration of Tulin et al. (2013). In order to move beyond the generic to the specific we explore how the dark matter cross section would be velocity dependent under the case of a Yukawa potential, $V(r) = \pm\alpha/re^{-m_\phi r}$, with α as the dark fine structure constant (Loeb & Weiner, 2011). DM scattering falls into the perturbative (Born) regime where $m_\chi\alpha/m_\phi \ll 1$ or the non-perturbative regime (classical or resonant) where $\alpha m_\chi/m_\phi \geq 1$.

The Sommerfeld enhancement is an elementary effect in nonrelativistic quantum mechanics, which accounts for the effect of a potential on the interaction cross section. For the purpose of illustration let us demonstrate velocity dependence with a classical situation (Arkani-Hamed et al., 2009) that is analogous: Sommerfeld enhancement as the quantum version of gravitational focusing. Consider a particle traveling through a field of stars. As it approaches a star of radius r it observes the star to have an impact cross section of $\sigma_0 = \pi r^2$,

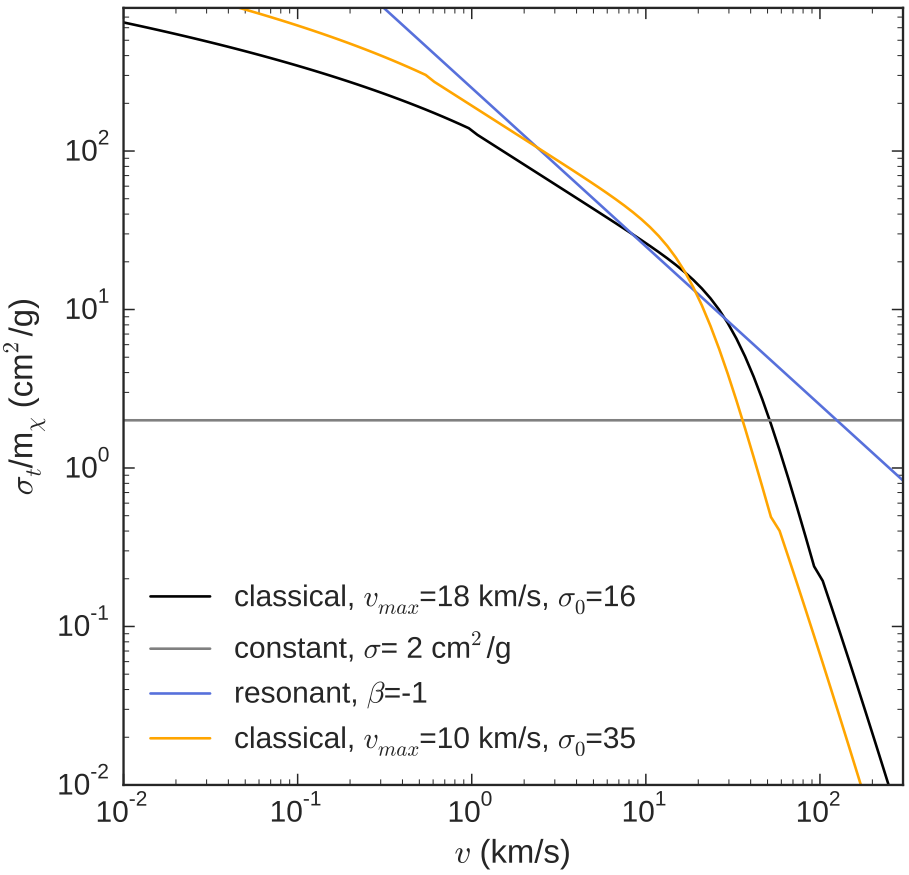

Figure 3.1: A comparison of the constant, classical, and resonant cross section models used in the simulations of this work. The classical cross section is normalized such that it takes the value of approximately σ_0 cm^2 g^{-1} at the given v_{max} value. The normalization for the resonant cross section is chosen such that the cross section is 25 cm^2 g^{-1} at 10 km s^{-1}. The resonant regime is defined as normalization factor times v^β; the units of the normalization factor change with the choice of β. In this work the grey line corresponds to model cSIDM, the black line corresponds to model vSIDM1, and the orange line corresponds to the model vSIDM2.

however the mutual gravity of the particles alters this cross section. In particular the slower the particle's velocity relative to the star the longer the gravitational force has time to act and increase the probability of a collision. Thus when with the added effect of gravity is taken into account $\sigma = \sigma_0(1 + \frac{v_{esc}^2}{v^2})$ where we have used the classical escape velocity: $v_{esc} = 2GM/r$. In the quantum case interaction cross section enhancement depends on the Compton wavelength of the force carrier (Feng et al., 2010).

One particular implementation of velocity dependent SIDM we explored was the non-perturbative classical regime $vm_\chi/m_\phi \gg 1$. The transfer cross section for $\beta = 2\alpha m_\phi/(m_\chi v^2)$ is

$$\sigma_T = \frac{\pi}{m_\phi^2} \begin{cases} 4\beta^2 \ln(1+\beta^{-1}) & \beta < 10^{-1} \\ 8\beta^2(1+1.5\beta^{1.65})^{-1} & 10^{-1} \leq \beta \leq 10^3 \\ (\ln(\beta) + 1 - \frac{1}{2}\ln^{-1}\beta)^2 & \beta > 10^3 \end{cases} \tag{3.2}$$

This formula is a reasonable match to particle physics parameters with the dark matter particle in the mass range of 100 GeV to 10 TeV. However the assumption of isotropy fails becoming forwardly peaked for $\beta \leq 1$. Unfortunately this function crosses into this regime at the knee of the function or at the v_{max} value; thus in this region we are under estimating the number of dark matter interactions. Although it would be favorable to have β transition to near unity at a velocity outside the region of interest in the simulations, it is exactly this change in strength of interaction at this velocity range that could lead to observable differences in small ($v_{circ} = 30$ km s^{-1}) to large ($v_{circ} = 60$ km s^{-1}) satellites.

We also explore the resonant regime where $vm_\chi/m_\phi \leq 1$ and with the proper choice of DM particle mass the resonant cross section would scale as $\sigma_T \propto v^{-2}$. This cross section increases at low velocity and decreases for high velocity and is S-wave scattering which is isotropic.

In figure 3.1 we see the functional forms of some cross sections explored in this work. We implement equation 3.2 by scaling by σ_T by $\sigma_T^{max} = 22.7/m_\phi^2$ and $\beta = \pi v_{max}^2/v^2$ which is equivalent to the previous definition. The classical cross section has σ_T and v_{max} as free parameters wich scale the absolute normalization and knee. The resonant regime

is implemented in our code and seen in 3.1 with a free parameter which scales absolute normalization and a free parameter β which is value of the exponent; thus only if $\beta = -2$ the model is the resonant regime.

3.3 Theoretical Dynamics

How do galaxies respond to Self-Interacting dark matter? Galaxies with Self-Interacting dark matter halos will have unique equilibrium solutions for the combined potential of the DM and baryons. Dark matter self interactions conduct heat from the hotter outer halo to the cooler inner core of the halo through DM collisions. This heat conduction via SIDM flattens or cores the density profile of dark matter. Self interactions drive the DM distribution to be more isothermal. We find that simulations with SIDM+baryons are more cored than simulations with SIDM alone. Our simulations show that SIDM or baryons lead to core formation that matches observations. It is difficult to predict the behavior of dark matter and baryons dynamically without simulations, for example Kaplinghat et al. (2014) finds that for their simulations of an $L_\star$ galaxy without baryonic feedback that SIDM+baryons creates smaller and denser cores.

In the small dwarf galaxies we are concerned with here the DM velocity dispersion (or DM temperature) increases with increasing radius for small radii ($\leq R_s$). Elastic scattering between dark matter particles tends to increase the temperature of the inner region (see figure 2.2). The radius where at least one scattering event has occurred (see figure 3.2 and the following two figures) characterizes the core size, but there is a limit of this scattering radius that depends upon the scale radius where heat can still be transported: a larger cross section should create more scatterings and a denser core region, but this can only be true up to the radius where heat is available to be conducted inwards.

We could theoretically conceive of a dark quenching scenario where the DM potential becomes so shallow that it wont attract baryons, or the baryons will be easily stripped by stellar outflows or tidal disruption. Dark quenching could be an explanation for the missing satellites problem: if at very low velocities SIDM sees an exponential enhancement in interaction rate then the smallest halos could dissipate themselves to the point that galaxies do not collapse.

In order to characterize how galaxies respond to SIDM we would like to model a galaxy's generic matter distribution and then look at how the model is perturbed by the stars or DM. The density profile of realistic systems cannot be described by a single power law. A double power law where there exists an inner slope and an outer slope can describe our galaxies. There are many general forms for the density of matter in a galaxy as a function of radius. Let us take a particularly general form at the cost of several free parameters.

$$\rho = \frac{\rho_0}{(r/r_s)^\gamma (1.0 + (r/r_s)^\alpha)^{(\beta-\gamma)/\alpha}} \tag{3.3}$$

where, γ sets the inner slope of the profile, β sets the outer slope, and α controls the transition between the inner and outer regimes. This form of the density profile allows us to consider many particular classes from the literature, for example in the case that $\gamma = 1$, $\alpha = 1$, and $\beta = 3$ then we get back the familiar form of the NFW profile

$$\rho = \frac{\rho_0}{(r/r_s)(1.0 + (r/r_s))^2} \tag{3.4}$$

And we can recover a pseudo-isothermal profile with the parameters $\alpha = 1/2$, $\beta = 2$, and γ=0. We define a dark matter halo as the region in which the density is larger than $\Delta = 200\rho_{crit}$ where ρ_{crit} is the critical density ($\rho_{crit} = 3H^2(z)/8\pi G$) of the Universe; the value of 200 is an approximation of the result of a assuming a primordial density perturbation in the form of a top hat function collapsing in a ΛCDM cosmology. Densities below Δ are indistinguishable from the background of the Universe and we choose Δ as 200 to facilitate comparison to the literature. For example, the central density scaling ρ_0 for a standard NFW density profile is $\delta_0 = \frac{\Delta}{3} \frac{c^3}{\ln(1+c) - c/(1+c)}$ in terms of its concentration $c = r_\Delta / r_s$ where r_Δ is the radius where the galaxy density falls to $\Delta\rho_{crit}$. Concentration values for realistically simulated halos have been found to be a weak function of mass or c $\propto M^{-1/9}(1+z)^{-1}$ (Neto et al., 2007). At higher redshift the size of halo of a given mass is smaller than the size of the same halo mass at a lower redshift or today; halos are more compact and dense at high redshift.

Observers are severely limited in the number of ways they can reconstruct the density distribution of galaxies. Is there any particular signature that SIDM would imprint that

would be observable in the phase space of matter for these dwarf galaxies? Dwarf spheroidal galaxies have dispersion of the order $\sim$ 10 km/s that is constant out to where the surface brightness falls to the background. Some well studied local satellites including Carina, Draco, Fornax, Leo I, Leo II, Sculptor, and Sextans show an order of magnitude variation in luminosity, yet occupy halos of similar mass. The observer's method for reconstructing the mass distribution of a galaxy begins with photometric and spectral observations of stars in the direction of the galaxy. The spectra of each star is fit for line-of-sight velocity (v_{los}), effective temperature, surface gravity, metallicity abundance, and other instrumental, nuisance, and error parameters. The line-of-sight velocity, surface gravity, and metallicity are all strong discriminators for separating the target galaxy's stars from interloping stars which would otherwise systematically distort the resultant mass distribution found for the selected galaxy.

Even if the full orbital parameters of each star in the galaxy was known the mass distribution would not be uniquely defined. This is the self-consistency problem of dynamics. Given only a density ρ we can find the potential Φ with the Poisson equation $\nabla^2\Phi = 4\pi G\rho$. Given only the potential Φ we can find the orbits of the particles using Newton's laws. Given only the orbits how do we go back to the density consistently? Standard Jeans analysis constrains only the mass enclosed within the luminous scale radius. Standard Jeans analysis does not constrain the internal dark matter distribution in a model-independent way. A recent approach is to realize mass enclosed measured at two distinct locations in a galaxy from chemo-dynamically distinct stellar subcomponents allows the slope of the density distribution to be found (Walker & Peñarrubia, 2011). The mass enclosed at the half light radius $r_{1/2}$ and stellar velocity dispersion (σ_{los}) are equal to $M_{1/2} = M(r_{1/2}) = 3G^{-1}\langle\sigma^2_{los}\rangle r_{1/2} \simeq 4G^{-1}\langle\sigma^2_{los}\rangle R_e$ where R_e is the projected 2D half light radius (Wolf et al., 2010). In the following work r is the 3D deprojected radius and R is the 2D projected radius of the galaxy. Then assuming spherical symmetry, dispersion-supported, collisionless system at equilibrium we have then Jeans equation 1.7 which can be rearranged to find the total gravitating mass profile

$$M(r) = \frac{r\sigma_r^2}{G}(\gamma_\star + \gamma_\sigma - 2\beta) \tag{3.5}$$

where $\gamma_\star = -d\ln n_\star/d\ln r$ and $\gamma_{sigma} = -d\ln\sigma_r^2/d\ln r$. Unfortunately trying to reconstruct the mass from this equation is not possible because only $\gamma_\star$ is observable. This mass profile has a contribution from all components of the galaxy including the stars themselves $m_\star(r) = \rho_\star/n_\star$ where $\rho_\star$ is the 3D stellar mass density and $n_\star$ is stellar number.

The Jeans equation relates the tracer particle's dispersion and number density to the total gravitational potential Φ. In the Jeans equation we used $\sigma_r(r)$ which is the radial velocity dispersion of the stars which can be inferred from $\sigma_{los}(R)$ if β and the surface brightness profile $\Sigma(R)$ is known. First we need the 3D density of stars given the observed projected stellar stellar density $\Sigma(R)$. For a spherical system with a 3D luminosity distribution $\nu = n_*(r)$ then an observer (in the far limit) observes a projected 2D surface brightness distribution that is

$$\Sigma(R) = 2\int_r^\infty \nu(r)dz = \int_R^\infty \nu(r)\frac{rdr}{\sqrt{r^2-R^2}}. \tag{3.6}$$

The inverse of this function is the 3D luminosity function itself

$$\nu(r) = n_*(r) = \frac{-1}{\pi}\int_r^\infty \frac{d\Sigma}{dR}\frac{dR}{\sqrt{R^2-r^2}}. \tag{3.7}$$

To find σ_r given $\sigma_{los}(R)$ and $n_\star$ we have:

$$\sigma_{los}(R) = \frac{2}{\Sigma(R)}\int_R^\infty n_*\sigma_r^2 r\left(1-\frac{R^2}{r^2}\beta(r)\right)\frac{dr}{\sqrt{r^2-R^2}} \tag{3.8}$$

To find the mass of the galaxy we would need an analytic form for $\Sigma(R)$ (like the Plummer profile for example), a parametric model for $M(r)$, and then find halo parameters that best fit the dispersion profiles observed from equations 3.8 and 3.7 (Walker et al., 2009). The anisotropy parameter β (defined in equation 1.8) quantifies the difference between the radial and tangential velocity dispersion. In most analysis it is assumed, just as it is assumed that galaxies are spherical, that isotropy guarantees β to be $\sim$1. Even if the assumption of isotropy is not valid, for example the velocity dispersion is dominated by stars on tangential orbits ($\bar{v_\theta^2} \gg \bar{v_r^2}$), the mass distribution from equation 3.5 will give us a lower limit on the mass of a galaxy when considering that the true value of β must be less than unity.

3.3.1 Implications of SIDM for direct detection

Direct detection experiments of DM particles with SM particles in the laboratory could potentially reveal the velocity distribution of DM, a velocity distribution which would be altered by SIDM. The direct detection interaction rate R depends upon the particle physics of the interaction $\mathcal{R}$, the local density of the dark matter, and the integrated local velocity distribution of DM T (Jungman et al., 1996)

$$R(E,t) = \mathcal{R}\rho_0 T(v_{min}(E),t) \tag{3.9}$$

and where the integrated local velocity distribution of DM is

$$T(v_{min}(E),t) = \int_{v_{min}(E)}^{\infty} \frac{f_v(t)}{v} dv \tag{3.10}$$

where there is a minimum velocity of dark matter that is detectable:

$$v_{min}(E) = \left(\frac{E(m_\chi + m_n}{2m_\chi^2 m_n} \right)^{1/2} \tag{3.11}$$

The distribution of the DM $f_v(t)$ is a function of time to account for the Earth's orbital motion about the Sun, the v_{min} that is detectable depends upon the given experiment and the mass of the nucleon of the target m_n. Determining the integrated local velocity distribution $T(v_{min}(E),t)$ is an important input into DM particle searches that astrophysicist must assist with. DM interactions thermalize the DM velocity distribution towards a Maxwell-Boltzmann distribution. The velocity distribution of SIDM differs from that of CDM to a greater extent in the inner cores of a halo. At large radii the decreased overall DM density leads to less interactions and SIDM and CDM velocity distributions converge. A large constant cross section SIDM model will have an isotropic Maxwellian distribution even at very far radii (out to 10kpc for a 10 $cm^2\ g^{-1}$ model); CDM does not have a Maxwellian velocity distribution.

The direct detection signal depends upon the ambient passage of galactic dark matter through the detector. The rate of DM particles passing through the detector depends upon

the local DM velocity phase space with respect to the motion of the solar system and the Earth; it is expected that there will be an annual modulation of the signal due to the Earth's orbit. The extremes of the modulation signal for the current epoch are around June ∼2nd and December ∼2nd — the Earth orbits the Sun that orbits the galactic center and on June ∼2nd the velocity of the Earth is tangential to (and adds constructively to) the velocity of the Sun around the MW and we see a larger apparent flux of background particles and then on December ∼2nd the Earth's orbital velocity adds deconstructively. SIDM can lead to a reduction in the total average interaction rate at the 10% level or an amplification of the annual modulation portion of the signal of 25% (Vogelsberger & Zavala, 2013) for SIDM models that are not ruled out by astrophysical considerations in the generous range of .1 to 35 $cm^2\ g^{-1}$ for the Milky Way.

A familiar result with SIDM is that it is more spherical especially for large constant cross sections (see section 3.3.3). Strong SIDM interactions may make the light, mass, and velocity distribution shapes more spherical through DM scattering that isotropizes the DM orbits and thus the potential shape of the halo. For a typical galaxy there is more anisotropy in the velocity distribution ellipsoids in the inner regions of halos than in the outer regions. The velocity distribution of DM f_v along the principal components of the velocity dispersion tensor will be nearly identical for the inner regions of halos with significant DM interactions. For example, the ratio of f_v along the semi-major axis versus the semi minor axis will be nearly unity for a large constant cross section of greater than 1 $cm^2\ g^{-1}$ at a radius of 1kpc. This is important for the prospects of DM detection in laboratory experiments.

It is difficult to compare constraints on SIDM from real galaxies or simulated galaxies because the velocity dependence sets a moving target. Let us take the velocity dispersion in the center of the galaxy as the velocity that sets the velocity dependent interaction cross section. The dispersion for CDM DM-only low mass dwarfs is low at the center, then rising up to the core radii then falling again, but for simulations that include baryons with strong stellar feedback, SIDM, or both, the dispersion is much flatter– the dispersion in the core is the same as the dispersion at the scale radii. For h516 these values are ∼55 km s^{-1} and for h2003 it is ∼40 km s^{-1}, thus in comparison to the velocity dependent models seen in figure 3.1 we see that h516 has the same effective cross section as that of the constant density

case, but that for h2003 the effective cross section would be a factor of a few higher.

We have characterized the number of interactions in terms of an e-fold radius. In the top panel of figure 3.5 we see the radius where the number of interactions in the inner 500 pc falls to $1/e$ as a function of time, and in the bottom panel we see the average number of interactions per particle that have occurred inside 1 kpc as a function of time.The e-fold radius for h516 with SIDM+baryons and a constant cross section seems very large but remember that this quantity is not the scale radii necessarily at all. An examination of figure 3.2 indicates that as time progress an inner core of $\sim$1 interaction per particle is forming, but if we scale this same figure by time as in figure 3.4 we see that the number of interactions per particle in the core is falling with time, but the number of interactions per particle per Gigayear is constant outside the e-fold radius. The velocity dependent case results in the smallest e-fold radius, but the largest absolute number of interactions: the slope is high and smoothly decreasing.

The rate of scatterings per particle we find here agrees broadly with the literature. Robertson et al. (2015) finds for constant cross section models the scattering rate peaks at late times near $z \approx 5$ (or 1.2) Gyr for 10^{10} $M_{\odot}$halos and for Yukawa potential velocity dependent cross section models the cross section peaks at much earlier times near $z \approx 20$ (or .2 Gyr) for 10^{10} $M_{\odot}$halos. Thus in our cSIDM model, seen in figure 3.2, the cumulative number of scatterings per particle is still rising rapidly at present and more than half the interactions will occur after $z \approx 1$. Thus in our vSIDM1 model, seen in figure 3.3, the cumulative number of scatterings per particle slows down greatly as $z = 0$ approaches and most interactions have already occurred by $z \approx 2$. The rate of interactions in the center of the halo scale differently than rate of interactions within the whole halo: in figure 3.4 we see that outside the scale radii, $\sim$2 kpc, the rate of interactions per particle per gigayear continues to increase towards the present, but in the core it falls towards the present.

In figures 3.6 and 3.7 the surface density of cumulative number of interactions per particle for halo h516 with constant cross section SIDM is shown. When gas is included, as in figure 3.6 the surface density of interactions is much lower and spread out over a much larger area than in the DM only simulation as seen in figure 3.7. This is not surprising because in figure 3.5 we see that dark matter only simulations overestimate the number of interactions per

particle that will occur in the central (1 kpc) region of a halo. These images do not show a map of where DM interactions are occurring today necessarily, rather these images shows the location of where particles that have had interactions are today (and for this particular DM simulation particle mass). In order to transform this image into an instantaneous flux expectation for self annihilating DM we would need, among other things, a DM particle mass. The code developed in this work could easily be adapted to produce such maps. We conclude that in order to accurately predict the J-factor for a given annihilating DM model gas and stellar physics are important.

The spatial distribution of the number of interactions that occur has implications for indirect detection experiments. On a fundamental level DM annihilation, like DM self interaction, is a function of the velocity dispersion and density. DM annihilation doesn't significantly redistribute the real or phase space distribution of DM whereas SIDM does. Any astrophysical effect that redistributes the phase space of DM, or the J-factor, will alter the expected DM annihilation signal. Stellar feedback will make the peak of the signal more diffuse. Models which combine self-interactions plus annihilation are bizarre because they combine WIMP models and dark sector models. In these cases the expected DM annihilation signal would be even more diffuse and the signal would evolve in time: distant dwarfs in early formation stages would have more compact emission regions. This would be a difficult signal to detect indeed.

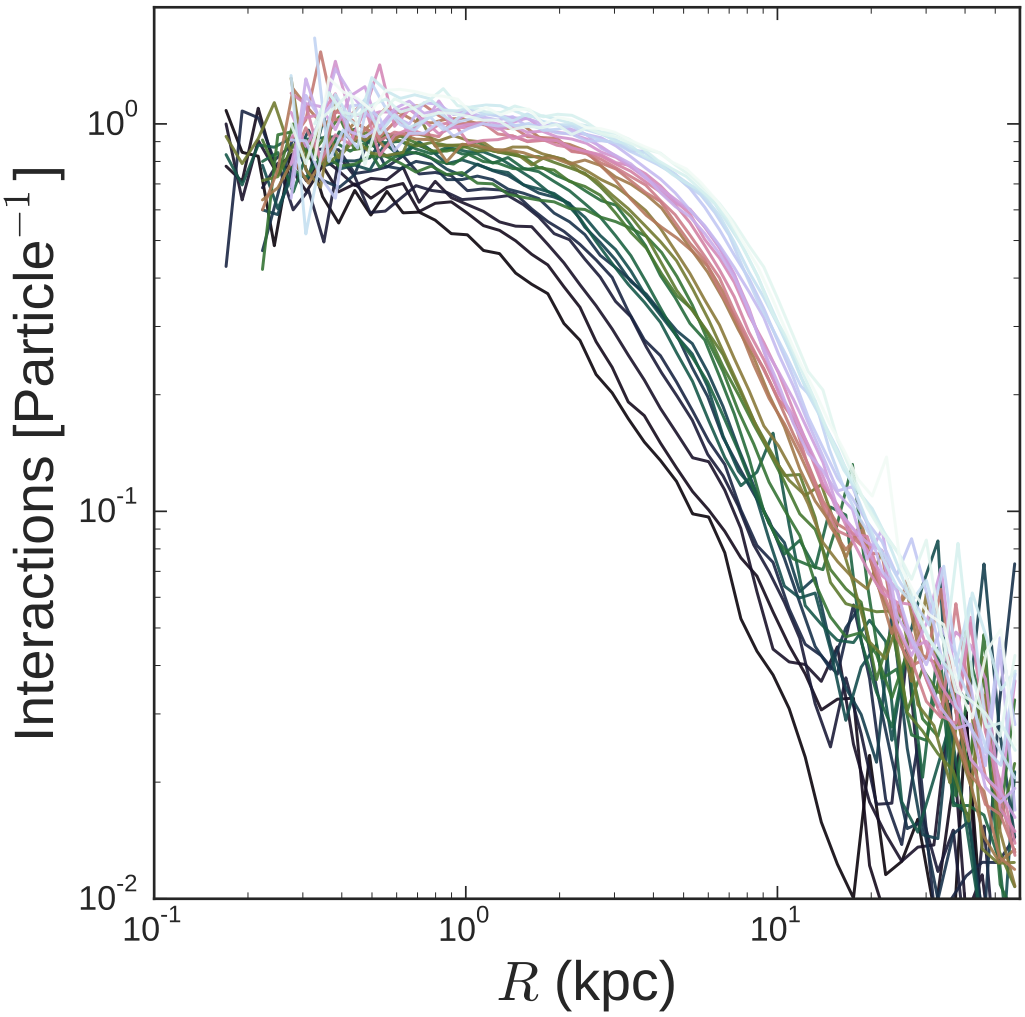

Figure 3.2: The number of interactions that occur per particle as a function of radius for halo 516 run with full baryonic physics and with a dark matter cross section of 2 cm^2 g^{-1}. Each line represents the galaxy at a given redshift from the early universe at ∼3 Gyr to today as the line evolve from dark (blueish) to light (white). A particle at any radius has more interactions as time passes. At late times (white) more particles have had more interactions, but this is may be due to the fact that merely more time has passed.

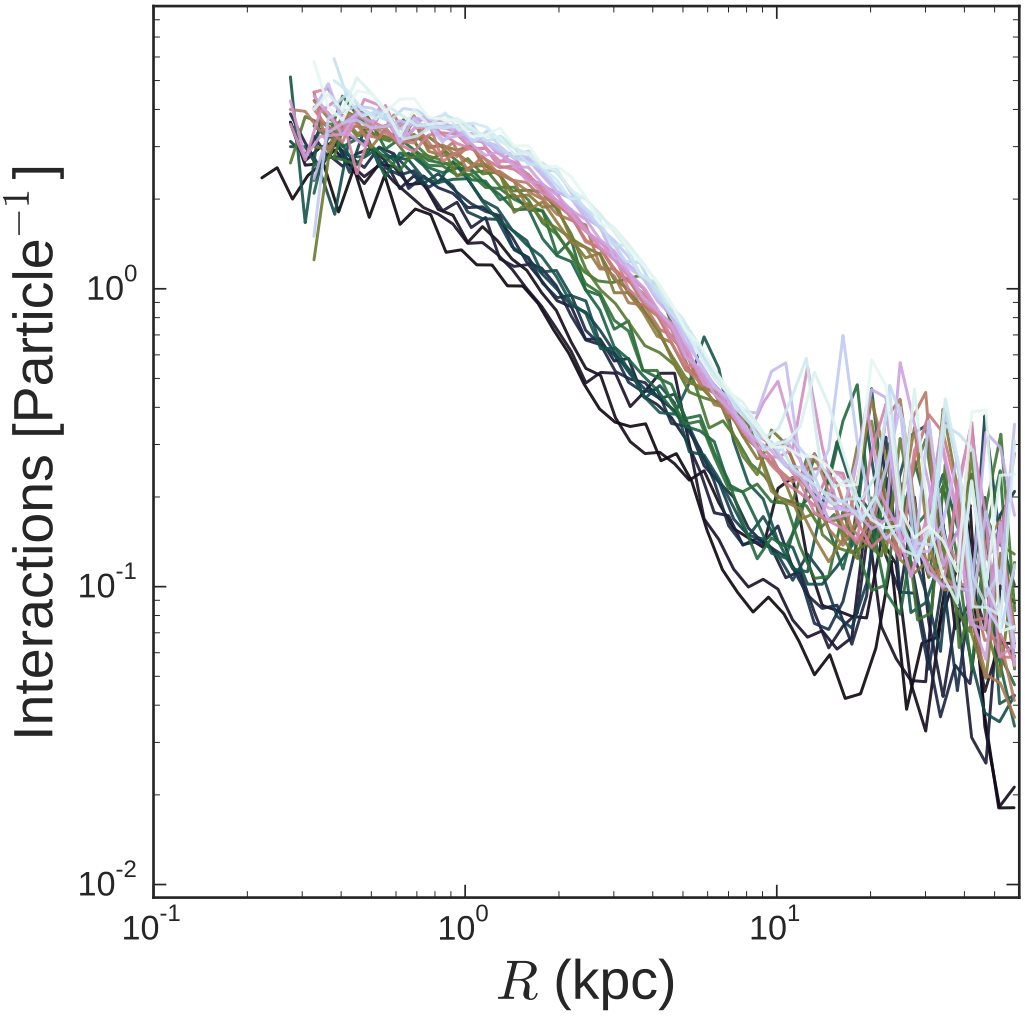

Figure 3.3: The number of interactions that occur per particle as a function of radius for halo 516 run with dark matter only and with a classical cross section normalized to 16 cm^2 g^{-1} at 18 km s^{-1} . Each line represents the galaxy at a given redshift from the early universe at ∼3 Gyr to today as the line evolve from dark (blueish) to light (white). Compared to the constant cross section and gas run the number of interactions per particle is a factor of 3 times greater in the center ∼ kpc and the number of interactions remains higher at larger radii, a flatter outer slope. This run has a similar flatter outer sloped as to that of the h516 dark matter only run with a 2 cm^2 g^{-1} cross section.

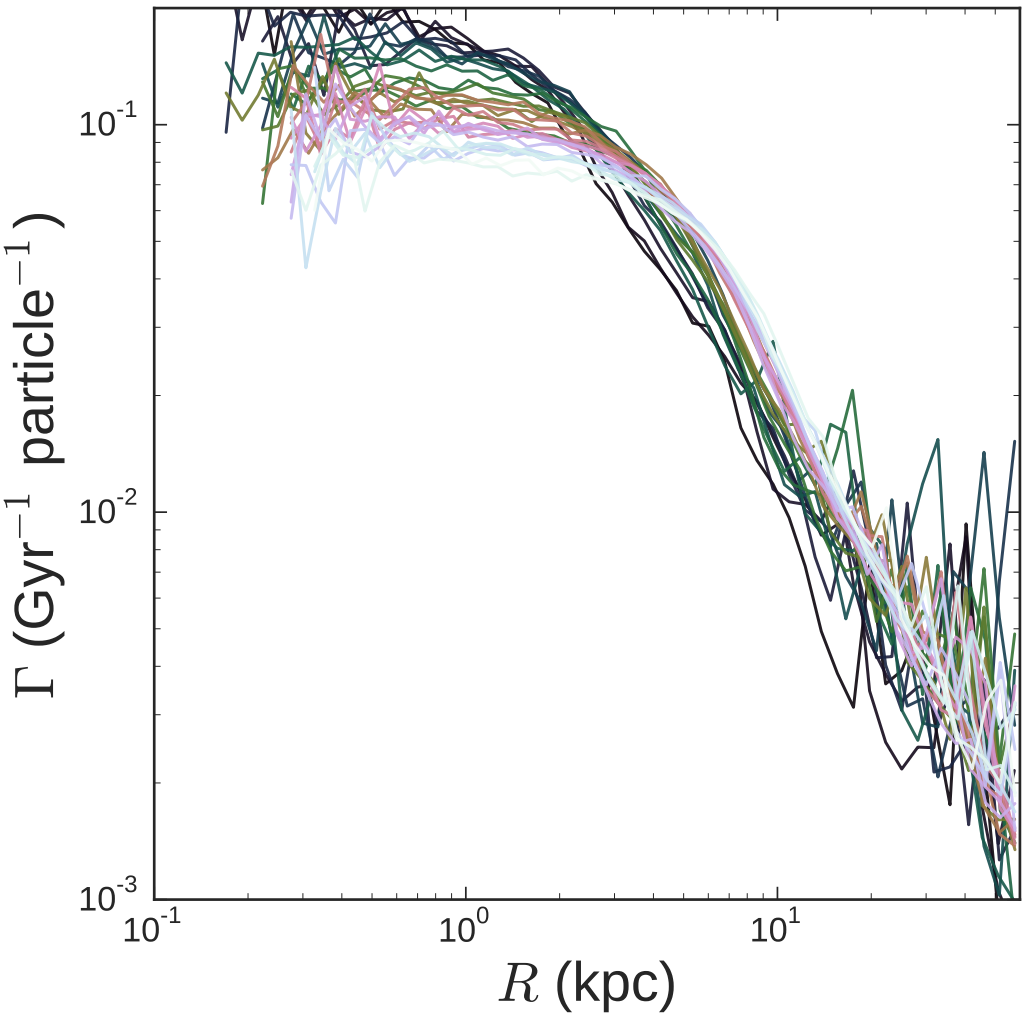

Figure 3.4: The number of interactions that occur per particle per Gigayear as a function of radius for halo 516 run with full baryonic physics and with a dark matter cross section of 2 cm^2 g^{-1}. Each line represents the galaxy at a given redshift from the early universe at $\sim$1 Gyr to today as the line evolve from dark (blueish) to light (white). Notice that when adjusted per Gigayear the number of interactions are an order of magnitude lower than if not adjusted as seen in the other figures. The trend for more interactions with time is reversed in the inner region as compared to the other figures: at late times particles in the core undergo less interactions likely because the galaxy has created an equilibriated core.

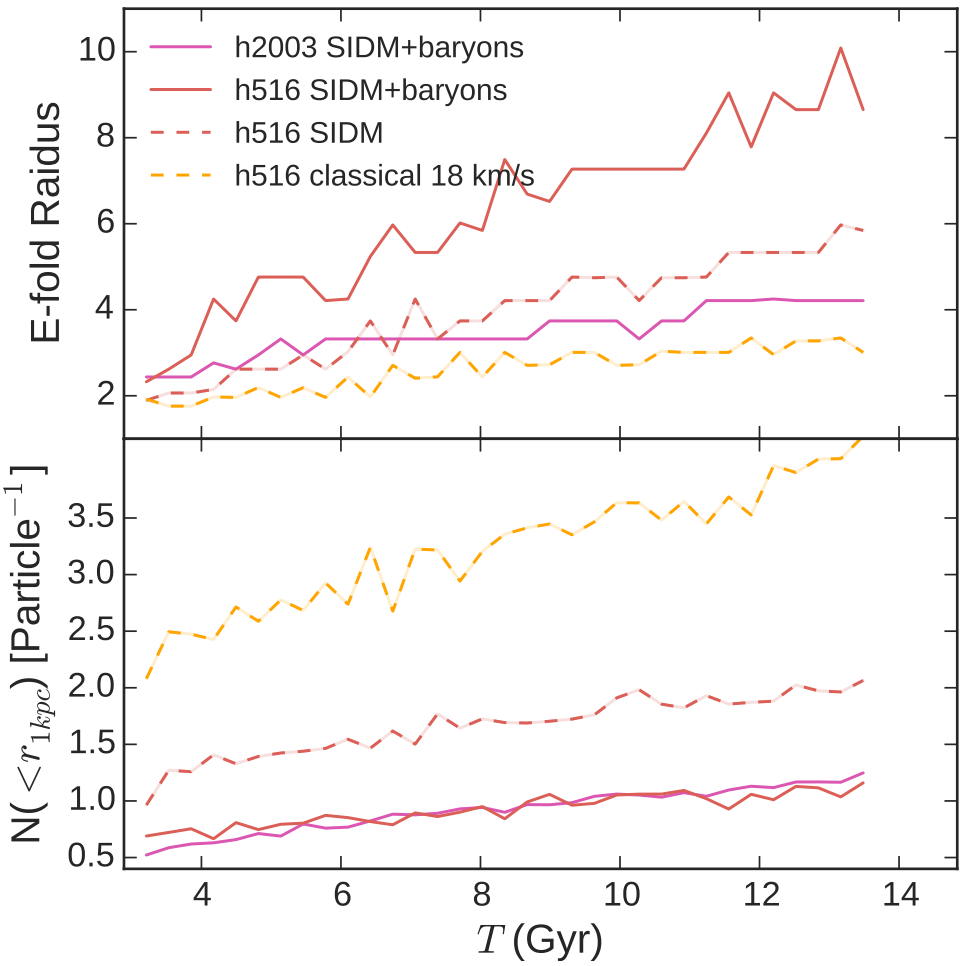

Figure 3.5: Top: the radius where the number of interactions falls to the value of $1/e$ times the average number of interactions occurring for particles inside 500 pc as a function of of time. Below: the number of interactions per particle that have occurred inside 1 kpc as a function of time. The inner halo will be pseudo-isothermal because the number of scattering will be one or greater, the outer halo will be the same as the CDM expectation because the scattering will be much less than one on average.

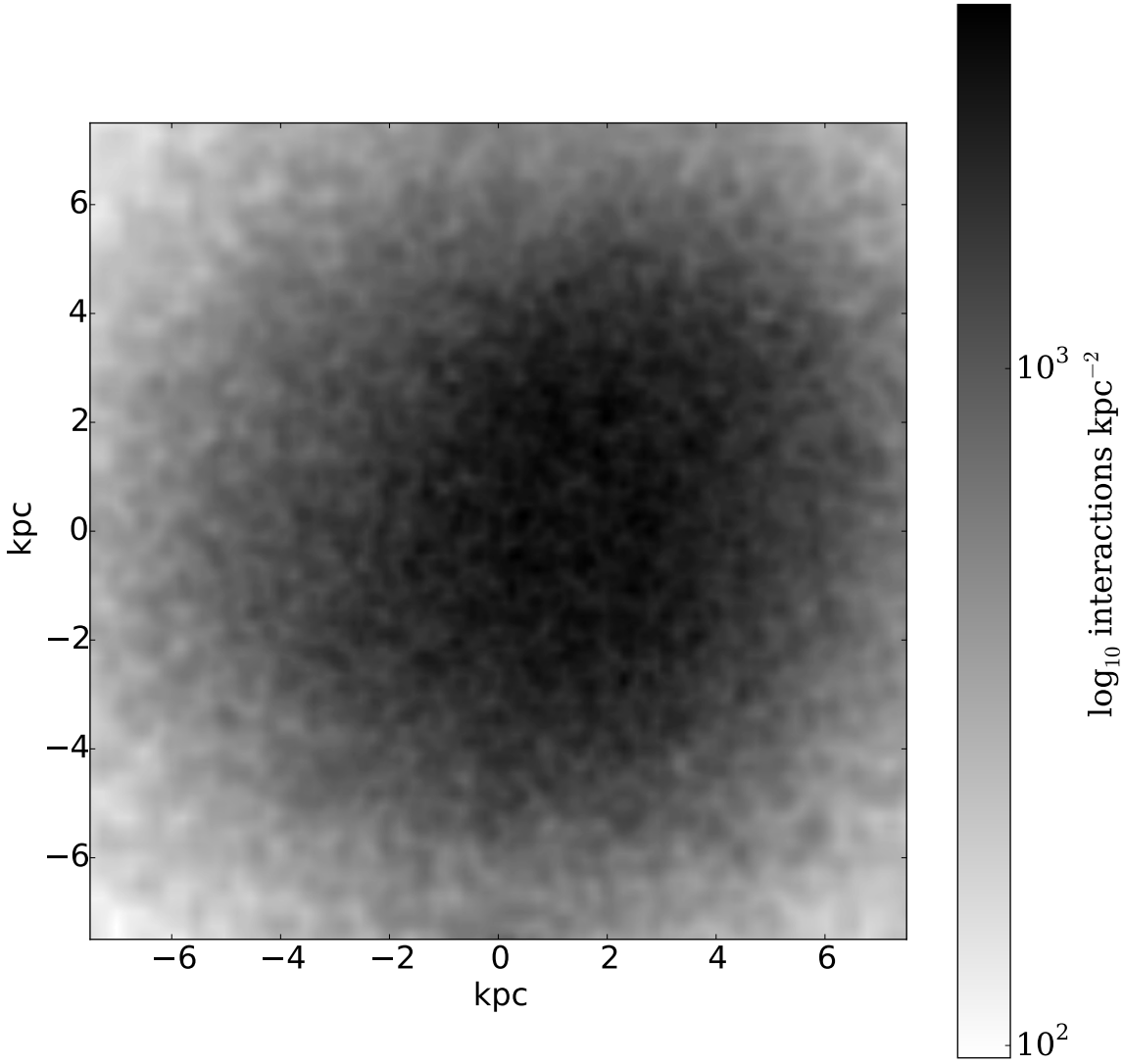

Figure 3.6: The cumulative total number of interactions per surface area of halo h516 with the cSIDM model and baryons at $z = 0$. At a radial distance of $\sim$100 kpc an object with a transverse size of $\sim$2 kpc spans about 1 degree.

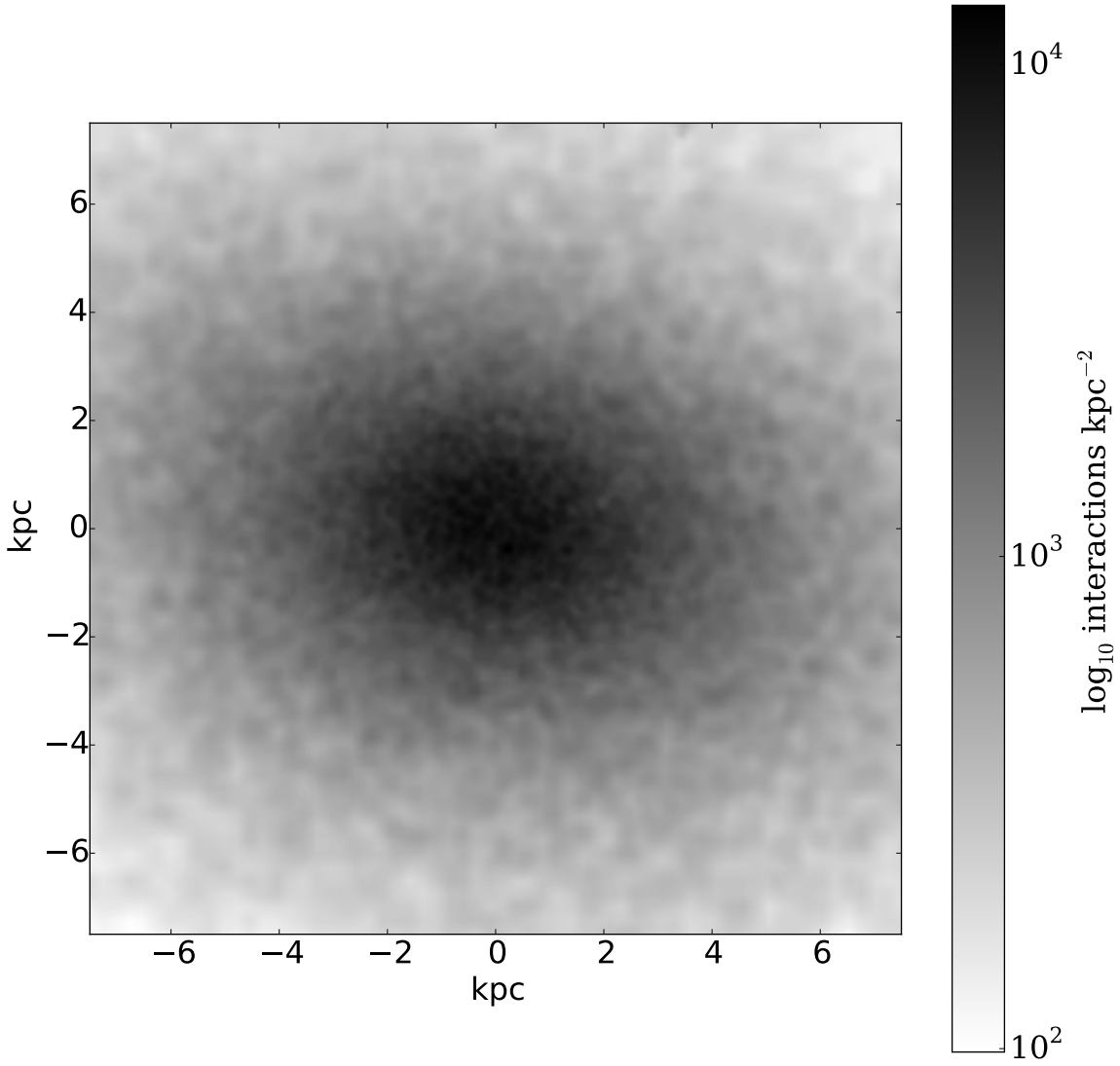

Figure 3.7: The cumulative total number of interactions per surface area of halo h516 with a dark matter only simulation of cSIDM $z = 0$. The current location of particles with significant numbers of interactions is very centrally peaked compared to figure 3.6. Most of the interactions have occurred within ∼2 degrees if this object was at a distance of 100 kpc.

3.3.2 Characteristic Interaction Timescale

Under certain simplifying assumptions theoretical solutions for the density and velocity distributions of DM halos are possible. When the the mean free path of DM particles, $\lambda = 1/\rho\sigma_{DM}$, is much much greater than the Jeans length (or gravitational scale height) $H = \sqrt(v^2/4\pi G\rho)$ an accurate self similar solution exists (derived from a combination of hydrostatic equilibrium, the first law of thermodynamics, and a heat conduction equation) for spherically symmetric halos. In Lynden-Bell & Eggleton (1980) they derive a thermal conduction formula for a collisional, gravitationally-bound system and derived an analytical solution that describes the self-similar collapse of a star cluster (leading to gravitational thermal or gravothermo collapse) that also applies to some regimes of SIDM. Conducting fluid models for SIDM models quantify a local relaxation time of $\tau_r = 1/(a\rho\sigma_{DM}v)$ where a is the constant equivalent to $\sqrt{16/\pi}$ corresponding to the collision rate of particles that following a Maxwellian distribution. Some of the figures in this chapter were represented in dimensionless units that resulted from this self similar analysis that avoid the singularities at the center using $v_0 = a\sqrt{4\pi G\rho_0}$ and $\rho_0 = M/(2\pi a^3)$ (Koda & Shapiro, 2011). These dimensionless scaled models work well for isolated halos.

One method of classifying the regimes of SIDM is the dimensionless Knudsen number, Kn, quantifies the ratio of the SIDM scattering mean free path over the system size. Early N-body results questioned whether gravothermal collapse was possible for a range of Kn systems, and indicated that SIDM may violate observations. In Balberg et al. (2002) they find a self similar solution for $Kn \gg 1$, this solution shows isolated halos would would collapse in a finite time, but a time greater than a Hubble time, and a time longer than that compared to a smaller Kn number. In summary, at small Kn heat transfer is restricted by the small SIDM scattering mean free path, and at very large Kn SIDM scattering is unimportant. When Kn becomes comparable to or smaller than unity the self-similar collapse models fail (terms in the heat conduction equation that were neglected become significant). The smaller Kn becomes the slower time evolution is in units of relaxation time becomes. A smaller mean free path suppress particle transport and results in smaller heat conduction. Both long and short mean-free path terms are important in the transitional

regime and this is where N-body simulation are necessary. As we see from figure 3.5 this is a regime all our halos pass through at some radii and some time. In fact for our constant cross section SIDM model the characteristic mean free path at the center of halos with a density of 10^8 $M_\odot$kpc^{-3} is 25 kpc and for the massive h148 halo which has a characteristic density of 10^7 $M_\odot$kpc^{-3} the mean free path is 300 kpc. In each case this is about the virial radius and therefore the $Kn \approx 1$.

Real halo build up over time from the nonlinear growth of primordial density perturbations within the decreasing density background of the universe. Additional mass is continuously falling in. This has been attempted to be modeled (Balberg et al., 2002). Summarily, real halos depart from theoretical heat flux models because the halo is not self-similar when the infall rate during cosmological structure formation drops below the self-similar rate at late times (Koda & Shapiro, 2011).

We approximate the characteristic maximum timescale (ignoring the factors of unity for theoretical self-similar halos) on which a given halo is stable by taking the number of interactions that occur per particle and setting it equal to unity for a halo with $v = V_{max}$ =max($\sqrt{GM/r}$)

$$\tau_{SI} = \frac{1}{\rho v_{max} \sigma_{dm}} \tag{3.12}$$

A comparison of τ_{SI} within the center of the halo to the age of a halo is an approximate way to determine if enough time has elapsed for SIDM effects to become apparent. Small satellite halos could be differentiated from those of their field counterparts by the interaction with the DM halo of a more massive host as the orbital velocity is much higher than the internal velocity of the satellite: under these conditions it may not be the characteristic relaxation time of the halo, but the orbital velocity weighted infall time of the halo that dominates the SIDM interaction.

3.3.3 Halo Shape

Halo shapes are difficult to measure, observe, and interpret due to such factors as orbits in larger halos potentials (Macciò et al., 2007; Maccio' et al., 2007). It may be necessary to look at halo shape as a function of time to rule out periods of large distortion, utilize different kinds of halo shape algorithms of the inertia tensor, and consider the confounding effect of baryons particularly in the center of galaxies. For example, in earlier dark matter only studies (Cole & Lacey, 1996) it was found that halos are generally triaxial, more spherical towards the center, and show no significant trend with mass. In the recent literate only the first conclusion has remained consistent. Robust conclusions about halo shape include 1) more massive halos are more round 2) halos are increasingly rounder at larger radii 3) halos of a given mass are more triaxial at earlier times 4) dissipation processes such as radiative cooling, star formation, and feedback processes make halos substantially rounder at small radii compared to adiabatic systems (Springel et al., 2004). The outer halo shape is unaffected by the presence of a disk, yet the inner halo is aligned such that the minor axis aligns with the disk axis (Bailin et al., 2005) during DM only mergers the final shape depends only on the orbital angular momentum, but with the inclusion of stellar disks substantial changes to shape may occur (Kazantzidis et al., 2004a).

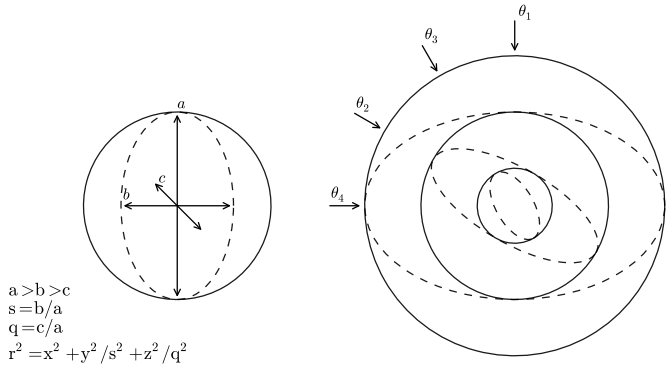

Figure 3.8: The geometry of halo shape analysis.

The shape of a halo is found by determining the inertial tensor of the mass and that defines the axis of maximal variance and defines this as the major axis a. In practice this simple inertia tensor approach may not be sufficient and approaches such as the iterative reduced inertia tensor (Warren et al., 1992) which de-weights the bias introduced by large

sub-halos located on the outskirts of the halo may be necessary (Yoshida et al., 2000). The reduced inertia tensor places more weight at small radii; it is more sensitive to the cumulative mass distribution (Schneider et al., 2012). The definition of halo shape and the inertia tensor should be considered when comparing the absolute values of halo shape analysis from the literature. I define halo axis lengths $a(r) < b(r) < c(r)$ that are functions of the spherical radius so that different halos shapes are allowed at all radii.

There are many different approaches and algorithms for quantifying halo shape. We warn that different algorithms and implementations may not be comparable, but that internally we can quantitatively find self consistent relative differences. The algorithm for halo shape implemented first determines the inertial tensor M_{ij} depending on the position of the particles x that are within a given r and then determines the axis of maximal variance and defines this as the major axis. We use a weighted ellipsoidal moment of inertial tensor:

$$M_{ij} = \sum_{n=1}^{N(<r)} m_n \frac{x_{n,i} x_{j,i}}{r_n^2}, \tag{3.13}$$

where the sum is over all N particles in the elliptical radius r for the indices $i, j = 1, 2, 3$. In practice this function is iterated over for several r defined

$$r = x^2 + y^2/q^2 + z^2/s^2 \tag{3.14}$$

where the axis ratios are given by

$$q = a/b = \left(\frac{M_{yy}}{M_{xx}}\right)^{\frac{1}{2}} \tag{3.15}$$

and

$$s = a/c = \left(\frac{M_{zz}}{M_{xx}}\right)^{\frac{1}{2}} \tag{3.16}$$

where $M_{zz} \leq M_{yy} \leq M_{xx}$ are the axis of maximum variance or eigenvalues a, b, c of M. The axis ratios $p = c/b$, $q = b/a$, and $s = c/a$ are defined such that $s \leq q \leq 1$. In

the first iteration the values of q and s are set to unity and upon each successive iteration the eigenvalues of the reduced inertia tensor are found until the error falls below a given threshold. A simple measure of triaxiality is the minor to major axis ratio s. A simple measure of what way a halo is triaxial is given by (Franx et al., 1991) by

$$t = \frac{a^2 - b^2}{a^2 - c^2} \tag{3.17}$$

A prolate (deflated football for example) halo is $t = 1$, and an oblate (Skittles for example) halo is $t = 0$. The quantity t is not well defined for halos that are close to spherical. The expected result is that CDM produces lower values of s and q (on the order of .6 or .8) at all radii while SIDM may produce higher values of s and q (near unity) at the center of a galaxy and lower values at larger radii (Yoshida et al., 2000).

It is completely obvious that real galaxies are not perfectly spherical. They are not even necessarily smoothly triaxial, but this is our first order approximation. A triaxial halo has box orbits, short-axis tubes, inner long-axis tubes, and out long-axis tubes orbits (whereas an ideal oblate potential has short-axis tube family orbits that dominate and an ideal prolate potential has inner and outer long-axis tube orbits that dominate). Outside the core, there are many radial dependencies. At the largest radii, the long shape of the halo in a triaxial system, the box orbits become boxlets and stochastic orbits. The box orbits supporting these triaxial halos pass arbitrarily close the center of the potential. Baryons can scatter these orbits to reduce triaxiality, but the coupling of baryons and the halo shape is weak because only dense central concentrations of baryons can destroy enough box orbits to cause changes in the halo shape (Debattista et al., 2008; Pontzen et al., 2015).

Halo shape analysis can be carried out at different isodensity surfaces approximated as triaxial ellipsoids. For real halos isodensity ellipsoids are approximately aligned (see figure 3.8) where $\theta_{1...4}$ are changing) with scatter and axial ratios are near constant Jing & Suto (2002) with scatter. Indeed equation 3.13 that we implement iteratively chooses the axis of maximal variance depending on the mass distribution and so allows the alignment of isodensity ellipsoids to vary with radius.

The expected result is that CDM produces lower values of halo axis ratios compared to

SIDM at all radii and that CDM halos are increasingly rounder at large radii. On the other hand SIDM may produce higher values (near unity) at the center of a galaxy and lower values at larger radii Yoshida et al. (2000); Bett et al. (2007) this is because it only is dense enough for at the center where collisions are important dynamical effect. It is also expected that halo shape at inner cores of galaxies will be erratic where the baryons and stellar disc dominate, but it is also in the inner halo where dark matter interactions occur frequent enough to alter the potential of the halo. Shape is a unique constraint on any modified dark matter model, but it's prominence on scales where baryons dominate is a problem. Our analysis in the next chapter finds that for the SIDM models tested here SIDM halos are marginally rounder at all radii, and much rounder at small radii.

Chapter 4

ANALYSIS AND RESULTS

Our simulations with star formation, feedback processes, and SIDM produce galaxies which are consistent with observations. By studying a range of halo masses in the field and in dense environments we explore how SIDM is constrained by current observations. We find that SIDM could have a large cross section (2 cm^2 g^{-1}) in the regime of dwarfs and still be consistent with observations, but to have an observable effect on the smallest dwarfs ($V_{max} < 30$ km s^{-1}) the cross section would have to be even larger, or velocity dependent.

We emphasize that many of the constraints discussed in this work are for constant cross sections; we will attempt to clearly differentiate between constant and velocity dependent models. We begin working with a constant cross section which is simple, but evidence from astrophysics and particle physics strongly favors a velocity dependent cross section. To bring our work here into compatibility with the strict constraints from larger scales we conclude a velocity dependent cross section is necessary. The reader may assume then that the cross section is velocity dependent, but that the dependence is nearly constant in the 10 to 80 km s^{-1} range. A useful note to interpreting figures is that generally SIDM uses warm colors while CDM will use cool colors. The models examined are referenced explicitly by their parameters or by their IDs which

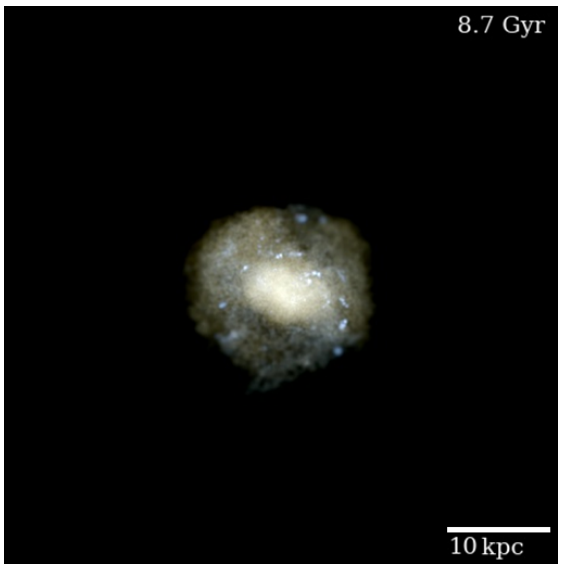

Figure 4.1: An image of h516 in the cSIDM model seen through the Johnson filters I (∼806 nm), V (∼551 nm), U (∼365 nm).

are: cSIDM for the constant cross section 2 cm^2 g^{-1} model, vSIDM1 for the classical cross section model with parameters $\sigma_0 = 16$, $v_{max} = 18$ km s^{-1}, and vSIDM2 for the classical cross section with model parameters $\sigma_0 = 35$, $v_{max} = 10$ km s^{-1}; these models are plotted for reference in figure 3.1.

4.1 Two Well Resolved Halos

We begin by looking at two large galaxies ($M_{halo} > 10^{10}\ M_\odot$) from the filamentary regions h516 and h2003. The star formation parameters in our study are identical for all CDM and SIDM simulations for a fair comparison. This means that star formation creates repeated starbursts and gas outflows with significant loading factors (gas mass ejected from the center divided by star formation rate). Also the SIDM model used for comparison of h2003 and h516 is identical; it is the cSIDM model where 2 cm^2 g^{-1}. Our main results is that the density profiles of h516 and h2003 with constant cross section SIDM are flatter than the fiducial CDM model, however, they are only marginally flatter than CDM models with feedback. The dispersion distributions in these galaxies show how self interactions drive the galaxy to having an isothermal core. The isothermal core is the crucial difference between CDM and SIDM that underlies all of the major differences between these models. Still, this does not make interpretation of the results simple especially in the presence of stellar feedback, for example: for the cSIDM model here the density of h2003 is essentially the same where we examine SIDM+baryons or SIDM alone, but for h516 the baryons have a stronger effect on the core than the SIDM.

The density profiles of the DM component of galaxies h516 and h2003 are seen in figure 4.2. In DM-only simulations halos with masses $> 10^{10}\ M_\odot$ have cuspy profiles. Once baryon physics and outflows are introduced, flatter DM profiles are created in both SIDM and CDM cosmologies. The blue dashed (CDM-only) vs blue (CDM+SF) lines and the red (SIDM+SF) show results for h516. The cyan dashed (CDM-only) vs cyan solid (CDM+SF) lines and the magenta (SIDM+SF) lines show results for h2003, the smaller halo. In both CDM and SIDM models the central cuspy profiles have been significantly flattened inside 1 kpc. For h516, the most massive halo studied with the inclusion of SF, is the one where the central DM density decreases the most. This is consistent with tent with previous findings

(Di Cintio et al., 2014b), showing that the efficiency of core formation peaks in halos with $V_{max} \simeq 50$ km s^{-1}.

The velocity dispersion profiles of halos h516 and h2003 demonstrate the internal transfer of energy to the center of DM halos in SIDM models as seen in figure 4.1. SIDM behaves more like a collisional fluid than traditional CDM. It prevents high density cusps. CDM DM only halos show a decreasing dispersion closer to the halo center while the SIDM halos show a rather flat profile. This difference, a result of the energy transfer to the center of the halo due to collisional processes, had been considered a strong signature of SIDM. However this difference is erased by the introduction of bursty feedback, that creates significant DM cores in the CDM halos. Dynamical heating also causes the velocity dispersion profiles of all halos to flatten out (Pontzen & Governato, 2014). The radius where the maximum velocity dispersion occurs as a function of halo mass (see discussion of an ensemble of h148 and h937 halos in next section) is of order 1 kpc for most halos in the mass ranges we resolve. For a given halo the radius where the maximum velocity dispersion occurs is extremely noisy in the SIDM scenarios because the dispersion is so flat the deviations are dominated by noise. In velocity dependent SIDM scenarios the dispersion becomes even flatter.

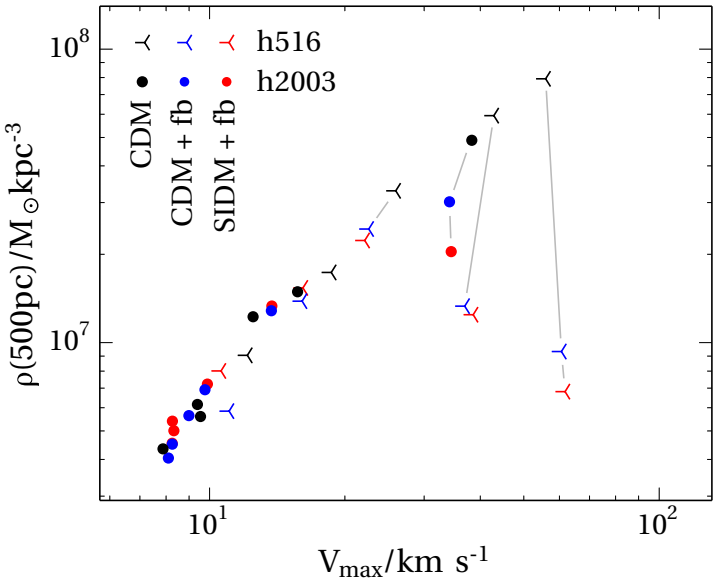

Figure 4.4: The density at 500 pc for CDM (black), CDM+baryons (blue), and constant cross section SIDM+baryons (red) for halos h516 and h2003 (connected by grey lines showing counterparts in different cosmologies. Above V_{max}~30 km/s baryons and SIDM significantly reduce the density, but below this value all halos are cuspy.

Rotation curves generated from our simulations, defined by $V_{circ} = \sqrt{GM/r}$, can be compared to observations. In figure 4.5 we see the circular velocity curves for h516 and h2003 for different cosmologies. These plots are for the constant cross section 2 cm^2 g^{-1} SIDM model. The diminishing effect of cSIDM with radius is clearly seen – at small radii SIDM has an effect of reducing the circular velocity, but at large radii this is not so and SIDM actually has a slightly larger circular velocity at larger radii. The radius where the maximum circular velocity, V_{max} occurs does not show significant trend between CDM and SIDM models. As a function of total halo mass it is occurs at about $\sim$1 kpc for all halos at 10^8 $M_\odot$ and monotonically rises to above $\sim$8 kpc for halos above 10^{10} $M_\odot$. In figure 4.6 and 4.7 we see data for local dwarfs (McConnachie, 2012) in comparison the circular velocity curves for DM only and DM+baryons respectively. The too big to fail problem (that the most massive halos in a given CDM model are too cuspy, V_{circ} too large, at a given radius to fit the data) is not an obvious problem when we examine halo h516 and h2003 here in isolation. The introduction of feedback processes or SIDM lowers V_{circ} out to at least 2 kpc, where mass decomposition based on HI kinematics are crucial. See sections 4.4 and 4.5 for a further discussion of the data in the context of the too big to fail problem.

Here we examine the central densities of halo h516 and h2003 over time. Figure 4.4 shows the DM central density as a function of halo peak velocity with baryonic feedback effects included versus our constant cross section SIDM model. Here the effect of baryons drowns out the effect of SIDM. The central density of CDM and SIDM halos is almost identical over the whole 10 to 50 km s^{-1} range. This result demonstrates that many of the conclusions in this work, and previous work, that do not take into account baryons may overestimate the need for large SIDM cross sections. On the other hand, this could be evidence that baryonic feedback need not be so strong: SIDM can carry some of the burden of creating cores in galaxies. Once we begin to consider velocity dependent dark matter, see figure 4.34 or 4.35, we see that even at very low velocity (10 km s^{-1} range) or halo mass (10^8 $M_\odot$) SIDM can create cores. On the other hand SIDM with a constant cross section is ineffective at forming cores in halos with $V_c < 30$ km s^{-1} this conclusion is largely based on the behavior of the halos at 500 pc. We report many of our results at 300 or 500 pc because this is several times the force softening used in our simulations and additionally 500

pc is a radius that is resolvable by observations, but more practically there is essentially no difference in halo properties at $R_{vir}/2$.

The inner slope α of halo should evolve differently at a range of halo masses. But baryons can eclipse the effect of SIDM rapidly. In figure 4.8 the slope of α at 500 pc is shown for h516, h2003 and a sample of field halos from those simulations is shown. For the main two halos the DM slope evolves rapidly and in a similar way in both CDM and SIDM, as dynamical heating is efficient at this scale; halos larger than $< 10^8$ $M_\odot$ ($V_{max} > 50$ km s^{-1}) have had cored profiles since z$\sim$4. In the most massive halo h516 SIDM actually forms a core more slowly than baryon feedback does. For the less massive halo h2003 the core formation is more gradual due to lower SFR and longer time scale for SIDM interactions. In smaller galaxies below $< 10^8$ $M_\odot$ SF efficiency is too low (Di Cintio et al., 2014b) and the SIDM interaction rate is too low to create cores: early star formation is inhibited by the cosmic UV field and the SIDM interaction rate per particle is very low (the time for this constant cross section model is larger than a Hubble time, also see figure 4.33 for the interaction rate at 500 pc for h937 where α here is being measured). The discussion here has been for constant cross section SIDM models. When looking at velocity dependent models, as

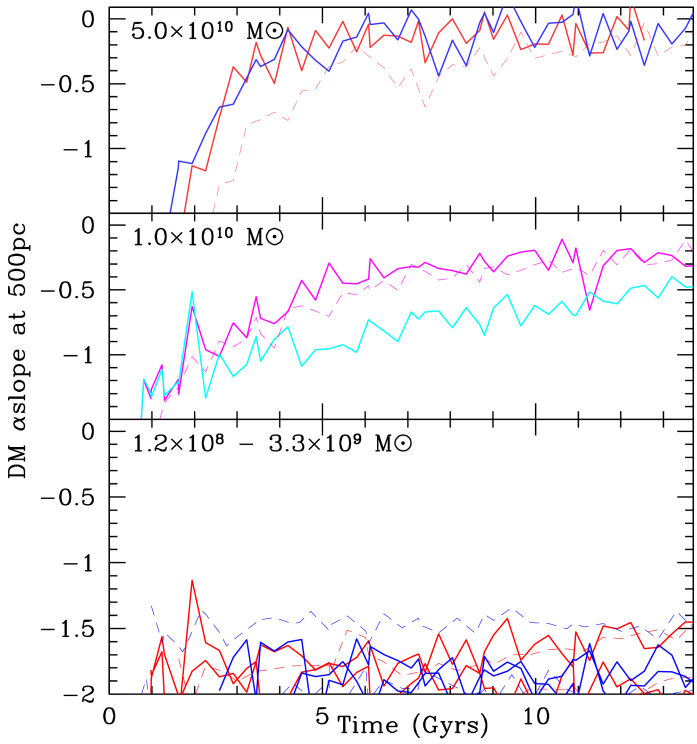

Figure 4.8: The inner slope α of the density profiles for CDM in blue and SIDM in red. The solid lines are baryon and DM runs, the dashed lines are DM only runs. The top is halo h516, the middle is halo h2003, and the bottom shows field halos with total mass $< 10^9$ $M_\odot$.

seen in figure 4.21 for the 40 thieves simulation, the interaction rate per particle is boosted enough to begin to create mild cores, $\alpha > -0.75$, for the majority of small halos $< 2 \times 10^8$ $M_\odot$ even at $z = 2$ (3.3 Gyr).

In figure 4.9 the number of interactions that occur per particle per Gigayear for SIDM simulations at $z = 0$ is analyzed. The solid red/magenta curve shows h516/h2003 with SIDM+baryonic feedback and the dashed red/magenta curve shows h516/h2003 with DM only SIDM. SIDM behaves more like a collisional fluid than traditional CDM. It prevents high density cusps. The radius at where it shows significant deviations is about where one interaction per Hubble time has occurred. In figures 3.2, 3.3, and 3.4 in the previous chapter the radial profile of the average number of scatterings per particle was shown. Those plots show an effective dynamical collisional radius of the halos (more accurately when shown per Gigayear). Here we see a direct comparison between the halos and how baryons effect the scatterings: the scattering rate of DM particles is drastically reduced with the introduction of baryons. Additionally we note the consistent spikes in interaction rate at 10 kpc. In hierarchal structure formation models halos such as h2003 and h516 will have substructure satellites. Diffuse outer parts of substructure halos would be stripped off by tidal effects leaving only the high density core. Typically of order 10% of the total mass of a dark matter halo will be in identifiable substructures out to the total virial radius of the halo (Ghigna et al., 1999). We suspect these spikes may be remnants of substructure interactions.

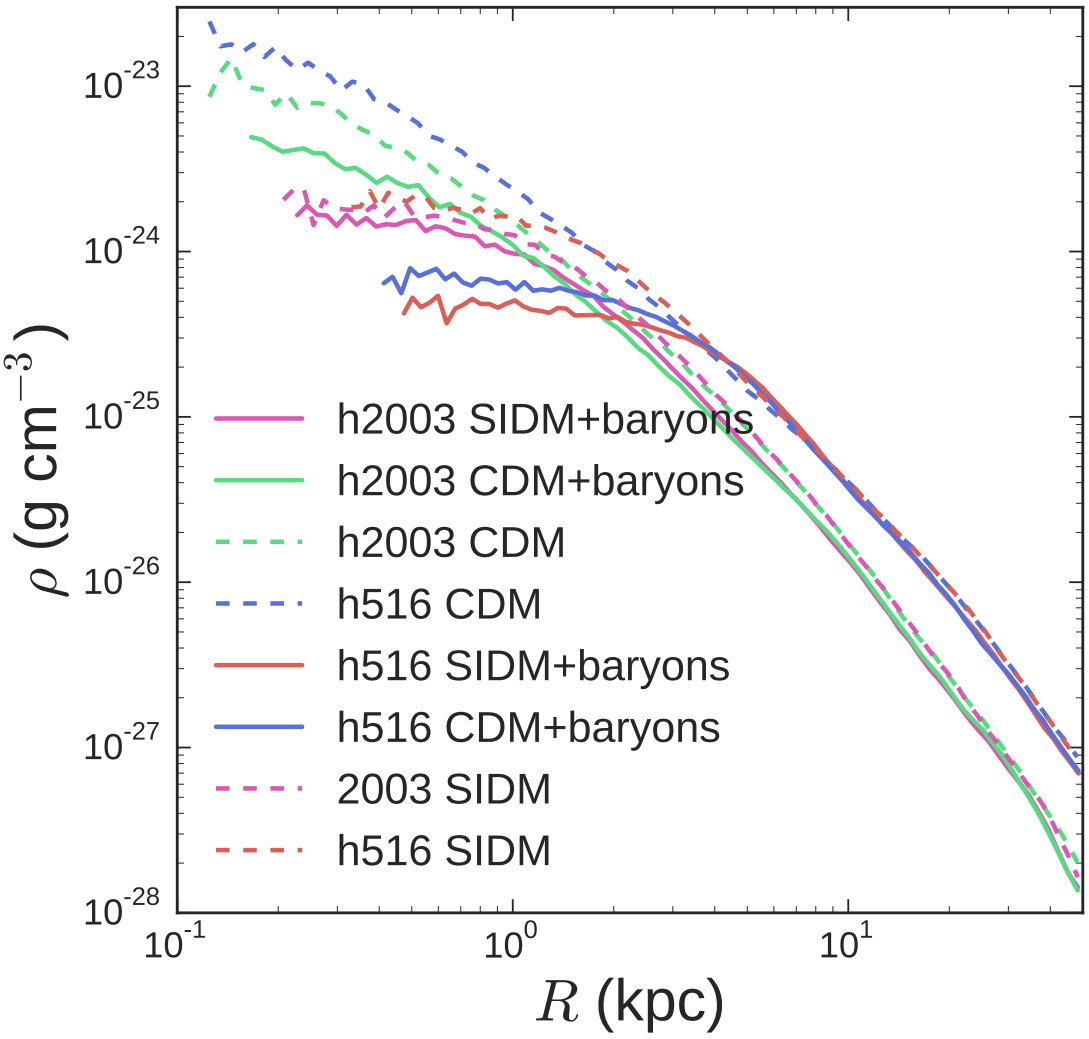

Figure 4.2: The radial density profile of halo h516 and halo h2003 at z=0 showing a very wide range of models.

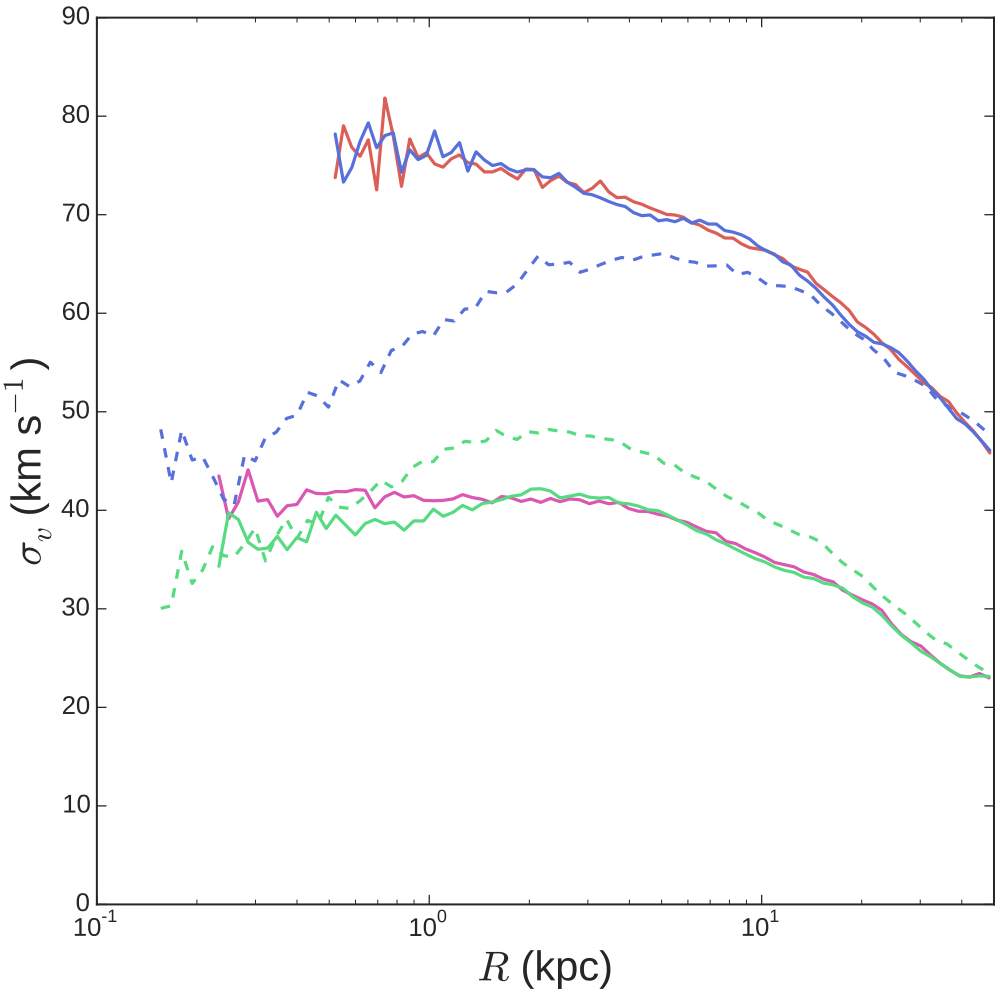

Figure 4.3: The dispersion of halo h516 and halo h2003 measured at z=0. The colors are the same at that seen in figure 4.2. Dark matter only simulations are shown as dashed line. Magenta lines show h2003 SIDM and red lines show h516 SIDM. Green lines show h2003 DM+baryons and blue lines show h516 DM+baryons.

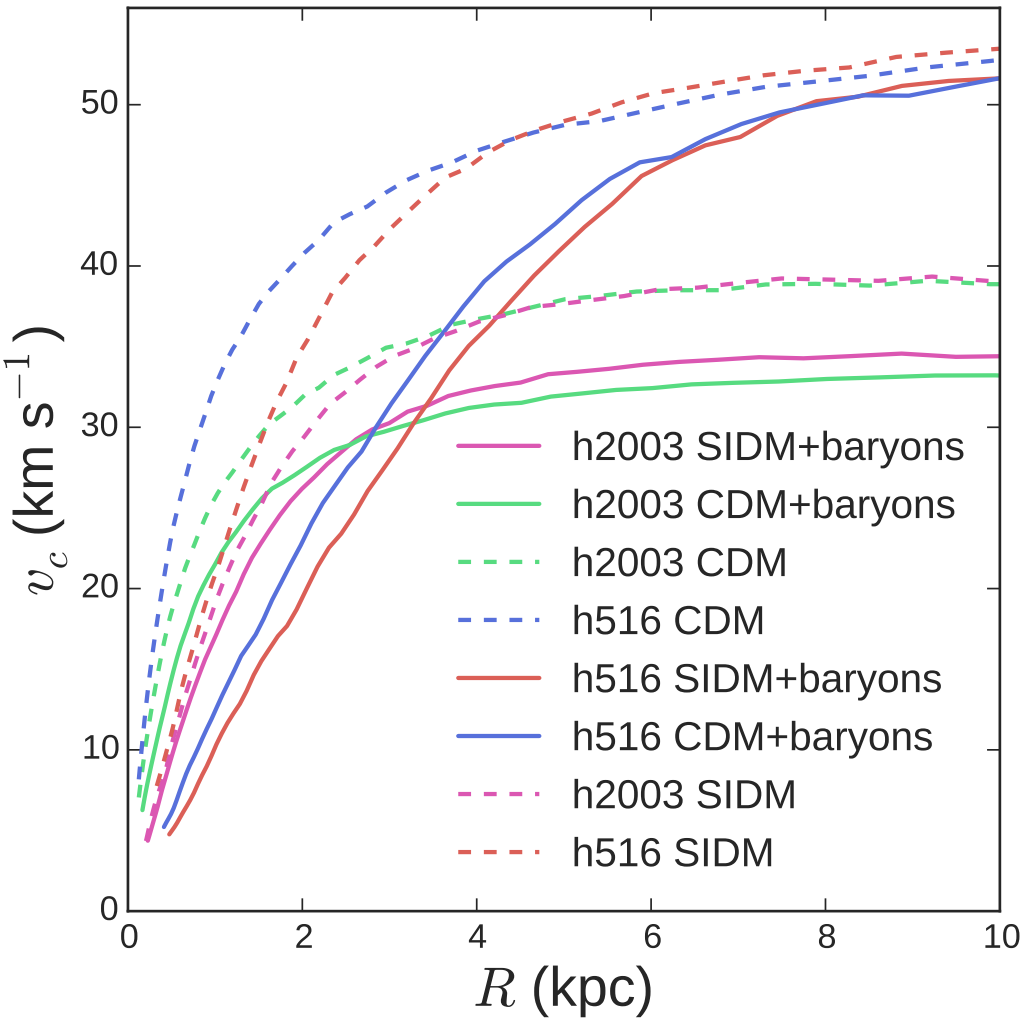

Figure 4.5: The circular velocity of halos h516 and h2003 for a range of simulation parameters. Compared to figures 4.6 and 4.7 we see here the circular velocity at much larger radius: the deviation of CDM versus SIDM diminishes greatly with radius, however note the SIDM actually has a marginally larger circular velocity at large radii.

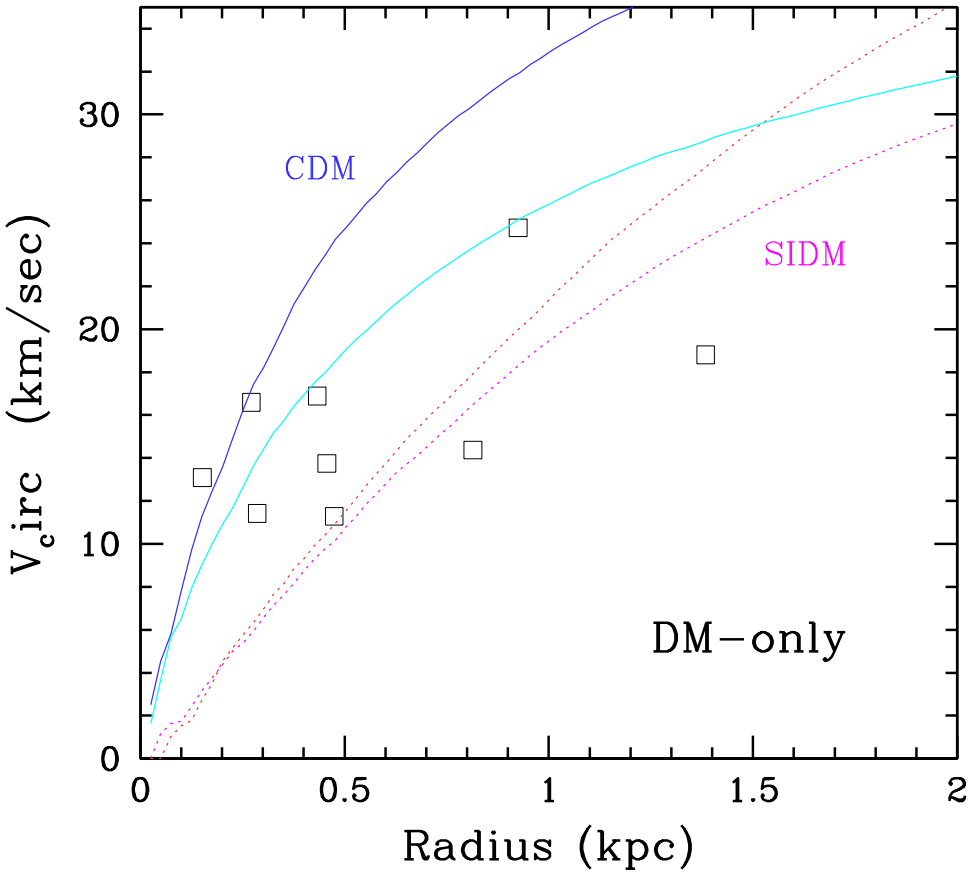

Figure 4.6: The rotation curves for DM only simulations of h516 and h2003 at $z = 0$. The red/magenta curve shows h516/h2003 with a constant cross section SIDM model. The blue/cyan curve shows CDM for h516/h2003. The squares represent local observed dwarfs (Wolf et al., 2010).

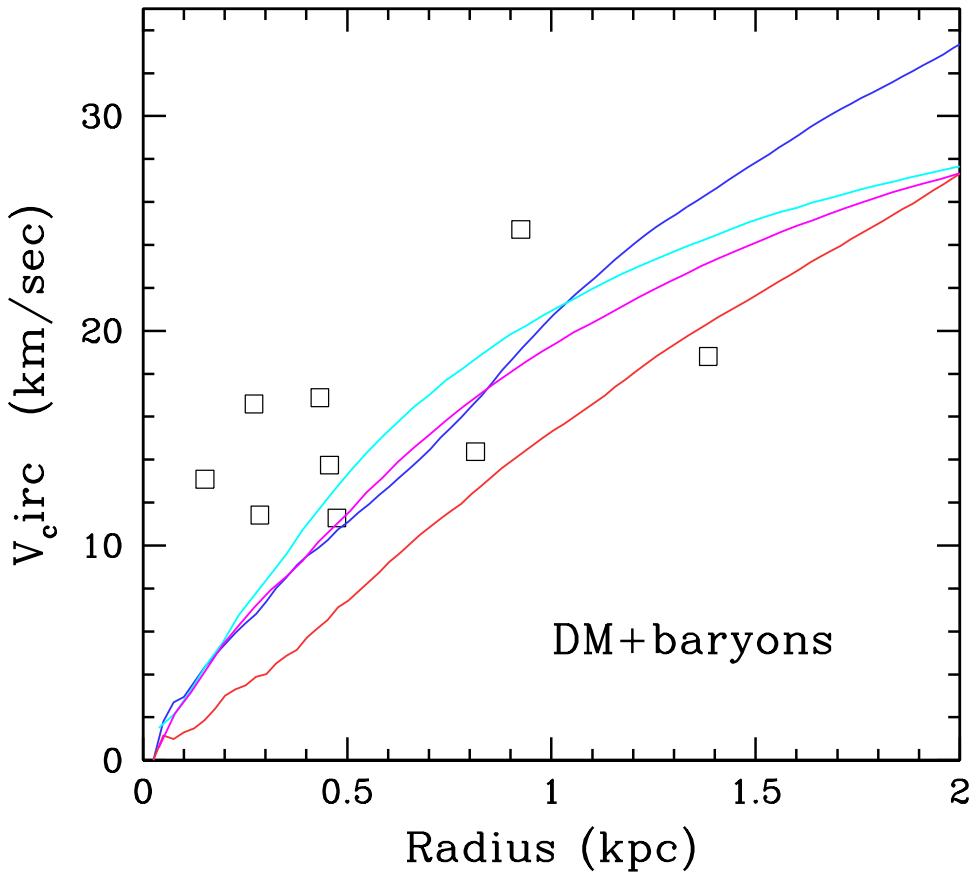

Figure 4.7: Similar to figure 4.6, but for simulations including baryons with feedback at $z = 0$. The red/magenta curve shows h516/h2003 with a constant cross section SIDM model. The blue/cyan curve shows CDM for h516/h2003. The squares represent local observed dwarfs.

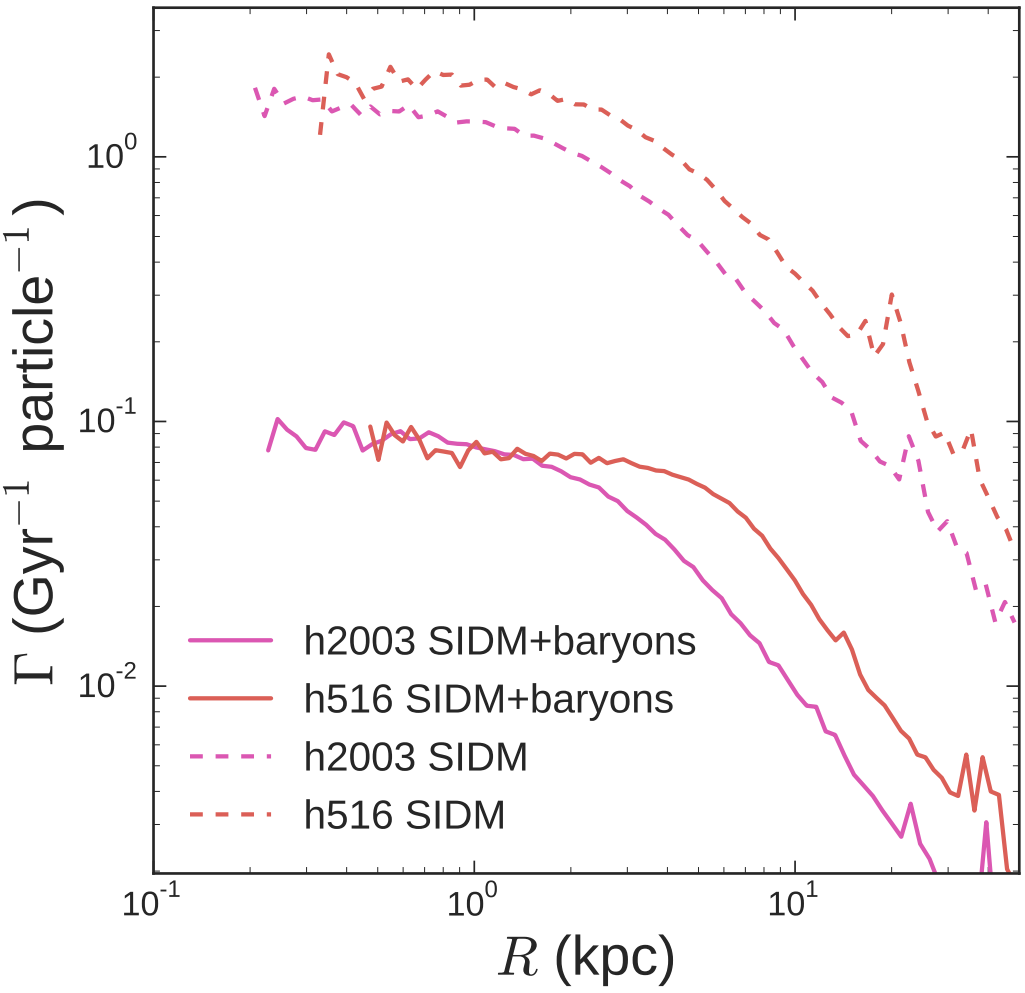

Figure 4.9: The number of interactions that occur per particle per Gigayear for SIDM simulations at $z = 0$. The solid red/magenta curve shows h516/h2003 with SIDM+baryonic feedback and the dashed red/magenta curve shows h516/h2003 with DM only SIDM. Baryonic feedback reduces the central density and so it reduces the interaction rate of SIDM.

4.2 Realistic Star Formation in Realistic Dwarfs

These are the first high resolution simulations that compare SIDM and CDM+baryons together as seen in the Johnson band color image in figure 4.1. In figure 2.1, 2.2, and 2.3 the projected DM, gas, and stellar masses are shown. Galaxies h516 and h2003 both have extended, gas rich disks and negligible bulges. We find DM cores are created though dynamic heating from baryons even with only CDM models. In our simulations the density threshold for SF is 100 amu cm^3 this limits SF to dense regions and concentrates feedback energy thus resulting in coupling of SN energy with the DM potential. The properties of these dwarf galaxies are dependent upon the depth of their potential. These dwarfs form shallow potential well that drives their stellar mass fraction to halo mass fraction down: dwarf galaxies have reduced ($\sim$1 dex lower) gas cooling and star formation efficiency compared to $L_\star$ galaxies which partially attributable to early feedback (Roškar et al., 2014; Trujillo-Gomez et al., 2011). We use a prescription for UV background photoheating after reionization that suppresses star formation and and gas in-fall to our halos at early times.

Star formation histories for nearby dwarfs as well as extreme emission-line galaxies (ie. CANDELS) are consistent with models where the majority of present day stars in dwarf galaxies formed in short-lived bursts at redshifts greater than 1. The ultra faint dwarfs of the Milky Way have a uniformly ancient, 10 Gyr stellar population. Even so, the star formation history of galaxies in the ANGST sample of nearby dwarfs (Weisz et al., 2011) show that most galaxies have had some recent star formation. Nevertheless, most stars formed greater than 10 Gyr ago. In figures 4.11 and 4.12 we see the star formation histories of h2003 and h516. Let us discuss h2003 in detail. The continuous but bursty star formation history of h2003 is consistent with local observations of resolved stellar populations for HST dwarfs (Tolstoy et al., 2009; Governato et al., 2015). Simulated outflows can be driven by not so bursty star formation as well, but there is extensive evidence of bursty SF in smaller galaxies (masses of $\sim 10^8$ $M_\odot$) which may have as much as .85 of their stellar mass fraction formed in bursts (Kauffmann, 2014).

The integrated star formation history, the total stellar mass, is also in agreement with observations. Figure 4.10 shows the stellar mass to halo mass ratio of these simulated halos

compared to local data and the abundance matching technique (Di Cintio et al., 2014b; Garrison-Kimmel et al., 2014; Brooks & Zolotov, 2014).The dashed lines and solid lines show the relation obtained from Local Group data. The stellar mass relation below $\sim 10^{6.5}$ $M_{\odot}$ is an extrapolation due to sample incompleteness. Open circles show the raw data, solid dots show the simulation data correcting for observational and simulation biases (Munshi et al., 2013) in measuring stellar and halo masses. The most massive halo converts about 1% of gas into stars. The rapid drop in SF efficiency at halo masses below 10^{10} $M_{\odot}$ is due to the introduction of early feedback. Overall the simulations produce the right amount of stars showing how baryons cycle (Shen et al., 2014): galactic outflows preferentially remove low angular momentum material (leading to the formation of bulgeless galaxies) due a combination of star formation peaking at high redshift (when the DM potential is shallow) and the existence of a reservoir of high angular momentum gas which provides material for prolonged SF at later times (Brook et al., 2011).

Producing the correct instantaneous and aggregate integrated star formation is necessary in order to estimate the minimum mass at which baryonic processes can originate cores. Analytical and numerical work have shown that feedback lowers the central DM density in galaxies, creating gas outflows and repeated fluctuations in the gravitational potential Velliscig et al. (2014). It is very likely that at the scale of dwarf galaxies with V_{max}=30 to 50 km s^{-1} SN can couple energy to DM efficiently enough to make differences between SIDM and CDM negligible. An open question is whether cores form in galaxies with 1000 times less stellar mass than what we have simulated here, all while remaining within local group observational bounds of half-light radii, metallicities, star formation histories, and stellar mass function.

In our work and in others, SIDM cosmologies consistent form a few percent more stars than CDM models. By $z = 0$ these galaxies have nearly identical masses and SF efficiency to within 20%. Changes of timescale and intensity of the individual SF events could be driven by subtle effects and still differentiate between CDM and SIDM, for example a shallower density profile could drive more gas instabilities that lead to radial inflows and increase the burstiness of SF, or, on the other hand, lower DM densities could slow down the collapse of gas and reduce SF in the SIDM scenario. We quantified the burstiness of

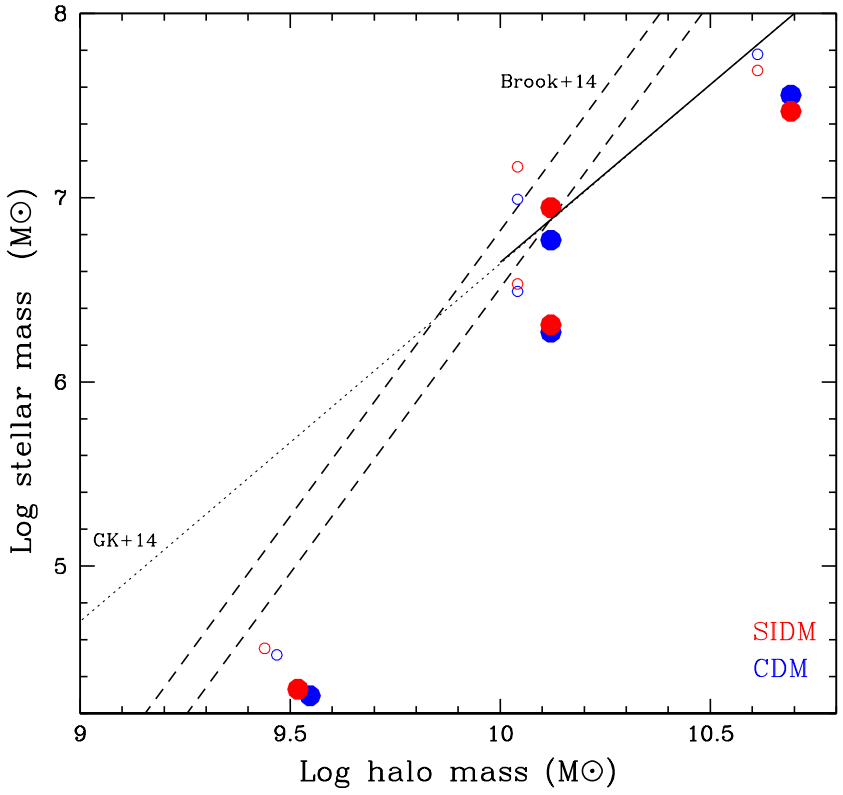

Figure 4.10: The stellar mass to halo mass relation for h516 and h2003. Dashed lines and solid lines show the relation obtained from Local Group data (Di Cintio et al., 2014b; Garrison-Kimmel et al., 2014). The stellar mass relation below $\sim 10^{6.5}$ $M_{\odot}$ is an extrapolation due to sample incompleteness (dotted lines). Open circles show the raw data, solid dots show the simulation data correcting for observational and simulation biases (Munshi et al., 2013) in measuring stellar and halo masses. Overall the simulations produce the right amount of stars. The most massive halo converts about 1% of gas into stars. The rapid drop in SF efficiency at halo masses below 10^{10} $M_{\odot}$ is due to the introduction of early feedback.

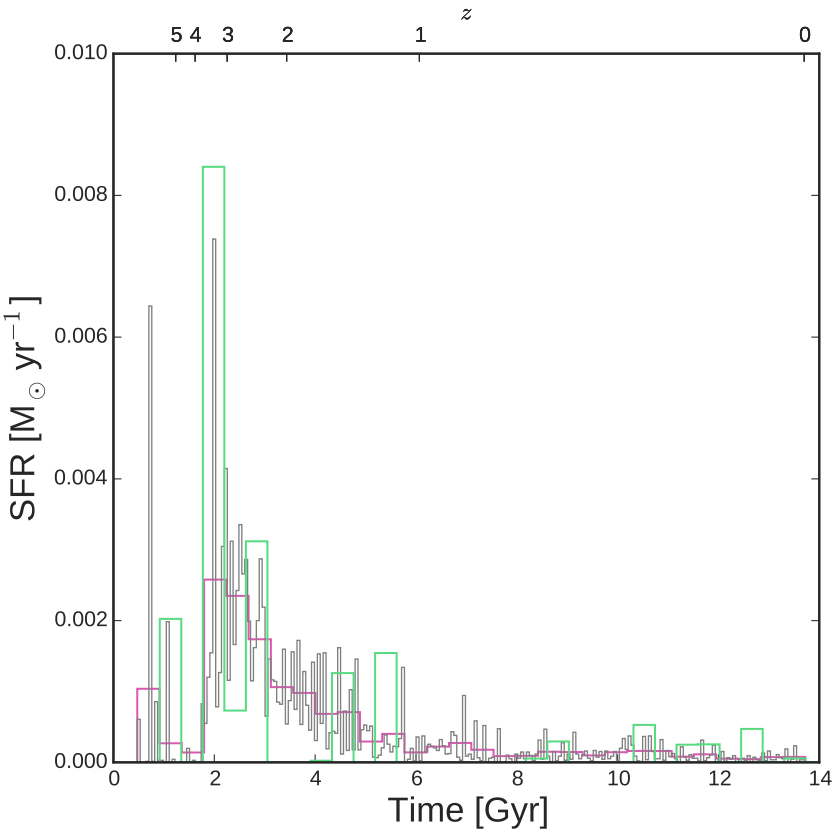

Figure 4.11: The star formation in halo h2003. In green in the CDM case and in magenta is SIDM case. The colored lines are binned on 500 Myr timescales and the grey line is CDM binned at 50 Myrs.

SF in SIDM vs CDM by measuring the dispersion in star formation rates measured by Δ_{TSFR} intervals, where Δ_{TSFR} was varied from 10^6 to 10^9 years. Measuring Δ_{TSFR} over hundreds of randomly sampled intervals for both halo h516 and h2003 in both models we found a SF rate dominated by small time scale fluctuations, with a similar dependence on time scale and halo mass, with the less massive halos having a burstier SF at all time scales (a result seen also in simulations with different feedback models (Hopkins et al., 2014)). Observations (Kauffmann, 2014) strongly support a bursty build up of the stellar content of dwarf galaxies. Within our sample of galaxies, we do not find evidence of large differences in the baryonic content and distribution in galaxies formed in a CDM vs SIDM model.

In figure 4.2 we saw the density profile of h516 and h2003. Noting that the difference

between h516 cSIDM vs CDM+baryons is less than the difference between h2003 cSIDM vs CDM+baryons. We briefly explore this by examining figure 4.13 where the total density of h2003 along with just the stellar density is shown. We see that indeed the SIDM case is much flatter. And not just in DM density, but also in stars. The ratio of stellar mass to DM halo mass as a function or radius is very different between these models. Up to about 1 kpc the ratio is greatly reduced for the SIDM model: the inner core isn't just a lack of DM it is also a lack of stars. Examining the detailed luminosity profile of SIDM galaxies may be a direction for future research.

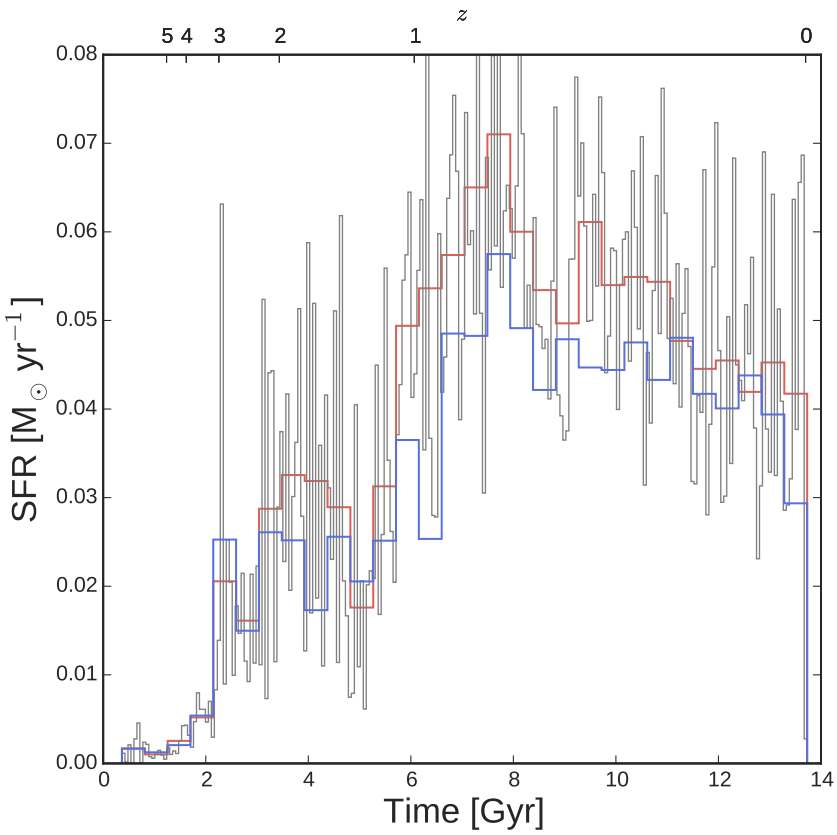

Figure 4.12: The star formation in halo h516. In blue in the CDM case and in red is SIDM case. The colored lines are binned on 500 Myr timescales and the grey line is CDM binned at 50 Myrs.

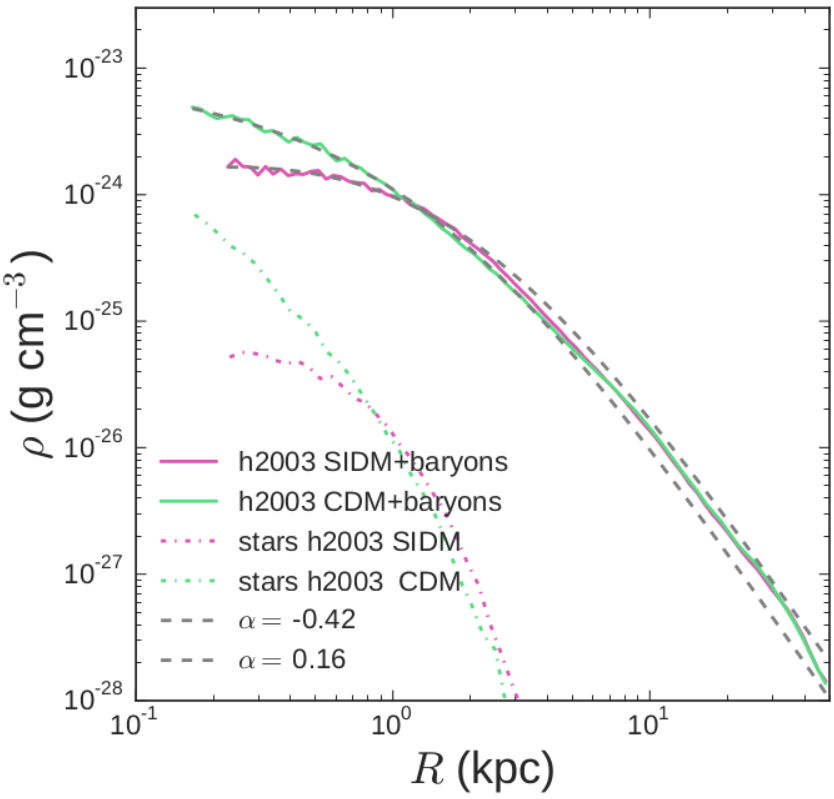

Figure 4.13: The total density, and the density of just stars from h2003.

4.3 Halo Shape

Halo shapes are difficult to measure, observe, and interpret; scatter added by assembly history to the observed shapes large enough that it precludes using a small number of objects to set constraints on SIDM cross sections (Peter et al., 2013; Macciò et al., 2007; Maccio' et al., 2007). It may be necessary to look at halo shape as a function of time to rule out periods of large distortion, utilize different kinds of halo shape algorithms of the inertia tensor, and consider the confounding effect of baryons particularly in the center of galaxies. For example, in earlier dark matter only studies (Cole & Lacey, 1996) it was found that halos are generally triaxial, more spherical towards the center, and show no significant trend with mass. In the recent literate only the first conclusion has remained consistent. Robust conclusions about CDM halo shape include 1) more massive halos are more round 2) halos are increasingly rounder at larger radii 3) halos of a given mass are more triaxial at earlier times 4) dissipation processes such as radiative cooling, star formation, and feedback processes make halos substantially rounder at small radii compared to adiabatic systems (Springel et al., 2004). The outer halo shape is unaffected by the presence of a disk, yet the inner halo is aligned such that the minor axis aligns with the disk axis (Bailin et al., 2005) during DM only mergers the final shape depends only on the orbital angular momentum, but with the inclusion of stellar disks substantial changes to shape may occur (Kazantzidis et al., 2004a).

The shape of a halo is found by determining the inertial tensor of the mass and that defines the axis of maximal variance and defines this as the major axis a. Halo shape analysis can be carried out at different isodensity surfaces approximated as triaxial ellipsoids. For real halos isodensity ellipsoids are approximately aligned (see figure 3.8) with scatter and axial ratios are near constant Jing & Suto (2002). In practice this simple inertia tensor approach may not be sufficient and approaches such as the iterative reduced inertia tensor (Warren et al., 1992) which de-weights the bias introduced by large sub-halos located on the outskirts of the halo may be necessary (Yoshida et al., 2000). We use the reduced inertia tensor defined in equation 3.13 with an ellipsoidal selection window which places more weight at small radii. This equation iteratively chooses the axis of maximal variance

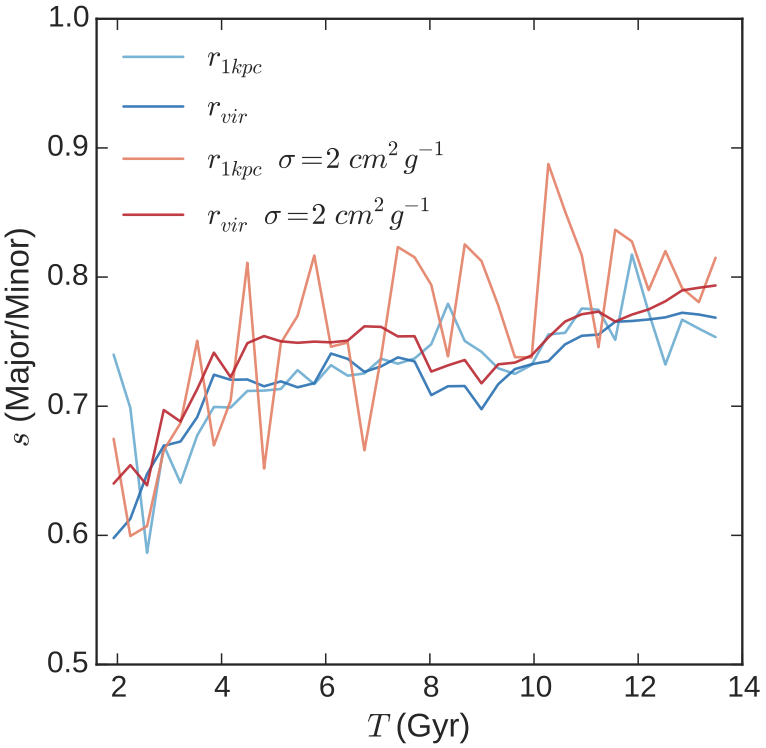

Figure 4.14: The ellipticity of halo h2003 as measured by the ratio of the minor axis c over the major axis a over cosmological time. In red is the constant cross section SIDM model; the fainter line is measured at 1 kpc and the darker line at the virial radius. In blue is CDM; the fainter line is measured at 1 kpc and the darker line at the virial radius.

depending on the mass distribution and so allows the alignment of isodensity ellipsoids to vary with radius; it is more sensitive to the cumulative mass distribution (Schneider et al., 2012). The definition of halo shape and the inertia tensor should be considered when comparing the absolute values of halo shape analysis from the literature. We define halo axis lengths $a(r) < b(r) < c(r)$ that are functions of the spherical radius so that different halos shapes are allowed at all radii. There are many different approaches and algorithms for quantifying halo shape. We warn that different algorithms and implementations may not be comparable, but that internally we can quantitatively find self consistent relative differences.

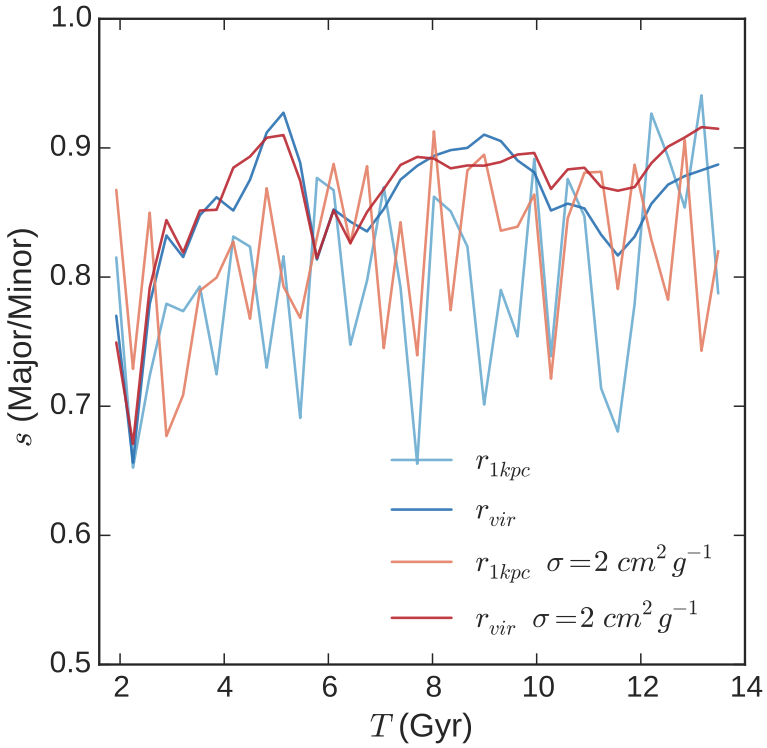

Figure 4.15: The ellipticity, s of halo h516 measured over cosmological time. In red is the constant cross section SIDM model; the fainter line is measured at 1 kpc and the darker line at the virial radius. In blue is CDM; the fainter line is measured at 1kpc and the darker line at the virial radius.

A prolate (deflated football for example) halo is $t = 1$, and an oblate (fly saucers for example) halo is $t = 0$. The quantity t is not well defined for halos that are close to spherical. The expected result is that CDM produces lower values of s and q (on the order of .6 or .8) at all radii while SIDM may produce higher values of s and q (near unity) at the center of a galaxy and lower values at larger radii (Yoshida et al., 2000). SIDM will only be apparent at small radii where collisions are important dynamical effect. It is also expected that halo shape at inner cores of galaxies will be erratic where the baryons and stellar disc dominate, but it is also in the inner halo where dark matter interactions occur frequent enough to alter the potential of the halo. Shape is a unique constraint on any modified dark matter

model, but it's prominence on scales where baryons dominate is a problem. Baryons can scatter these orbits to reduce triaxiality, but the coupling of baryons and the halo shape is weak because only dense central concentrations of baryons can destroy enough box orbits to cause changes in the halo shape (Debattista et al., 2008; Pontzen et al., 2015).

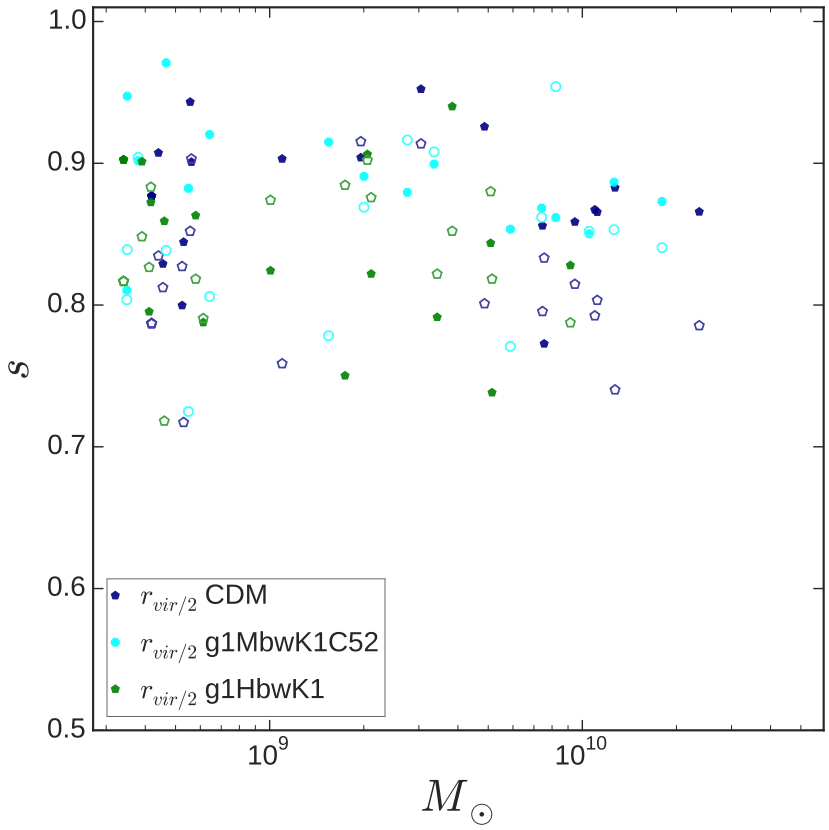

Figure 4.16: The ellipticity (as the ratio $s = a/c$ of the major over minor axis ratio) of halos in the 40 thieves simulation for CDM and CDM+baryons simulations as a function of the total mass of halos. This plot shows halos down to 50,000 dark matter particles. The open points indicate the shape at 1 kpc and the filled points show that shape at half the virial radius.

In figure 4.17 and 4.16 we see halo shape analysis for the 40 thieves at a redshift of zero. The values we find are consistent with the literature, yet on the high end for comparable mass halos using the ellipsoidal selection window (Schneider et al., 2012). The filled points

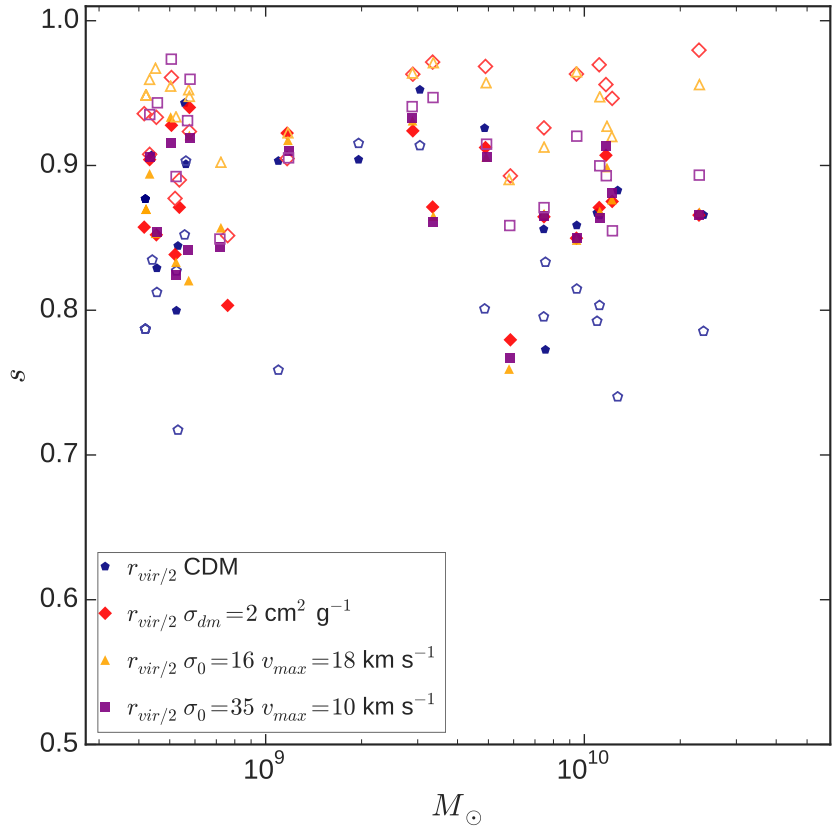

Figure 4.17: The ellipticity (as the ratio $s = a/c$ of the major over minor axis ratio) of dark matter only halos in the 40 thieves simulation for CDM and SIDM simulations for halos with more than 50,000 particles. The open points indicate the shape at 1 kpc and the filled points show that shape at half the virial radius.

are a measurement of the shape at half the virial radius, and the open points show a measurement of the shape at 1 kpc (although 500 pc would be preferred to discern the effects of SIDM, 1 kpc was chosen to maximize signal). Only massive halos that have 50,000 or more dark matter particles are analyzed to ensure fidelity of the results. They show a measure of ellipticity given by $s = c/a$. While s can range from 0 to 1 theoretically in practice it stays close to 1 for realistic halos. Generally we can conclude for the 40 thieves with CDM versus CDM+gas+baryons (figure 4.16) that CDM cosmologies are rounder at

large radii rather than small radii and that baryons can make halos rounder. Generally we can conclude for CDM versus SIDM (figure 4.17) that for the SIDM models tested here that SIDM halos are marginally rounder at all radii, and much rounder at small radii. A CDM versus SIDM discriminating trend in the data is that *a given SIDM halo is rounder at small radii compared to large radii* whereas *a given CDM halo is rounder at large radii compared to small radii*. Note that this is a relative result: for these SIDM models and mass ranges *SIDM halos are marginally rounder than CDM halos at all radii*.

The shapes of the CDM halos show complex trends in figure 4.16. The shape was analyzed by considering the entire matter distribution including DM star, and gas particles inside the given triaxial ellipsoid. The run in the figure labeled g1MbwK1C52 includes metal line cooling, a Kroupa 2001 IMF. The run labeled g1Hbwk1 includes these same physics plus molecular hydrogen. Once molecular hydrogen is included halos have a trend of being more elliptical by a factor of $\Delta s \sim 0.1$ at half their virial radius than a comparable CDM or CDM+baryons simulation at the same radii. In fact the inclusion of molecular hydrogen breaks the generalized result found earlier: for these simulations they are actually more round at 1 kpc.

The shapes of the SIDM halos are very round $s > 0.85$ (see figure 4.17) at 1 kpc. The variable cross section model with the parameters $\sigma_0 = 16$ $V_{max} = 18$ km s^{-1} is the roundest $s > 0.9$ at 1 kpc at all halos masses probed. The constant cross section 2 cm^2 g^{-1} SIDM model halos are very round $s > 0.9$ at 1 kpc for halo masses greater than $\sim 10^9$ $M_\odot$ and the variable cross section model with the parameters $\sigma_0 = 35$ $V_{max} = 10$ km s^{-1} is very round $s > 0.9$ at 1 kpc for halos less than $\sim 10^9$ $M_\odot$; however with the scatter and uncertainty in the data this trend would need futher investigation to be corroborated.

For h516 and h2003 we analyzed the halos with baryons+DM and baryons+SIDM over cosmological time. Halo h516 is rather round as seen in figure 4.15. SIDM is marginally more round at small radii compared to CDM at the same radii. SIDM is marginally more round at large radii compared to CDM at the same radii. For all cases h516 is more round at large radii. Halo h2003, seen in figure 4.14, is on average more elliptical than any other halos examined. It is quite noisy. We could argue that SIDM is more round at all radii and perhaps marginally more round at small radii rather than large radii. This halo shape

analysis reveals the result that SIDM halos halos are rounder at small radii compared to large radii. CDM follows the expected outcome that halos are rounder at large radii. With CDM+baryonic feedback halos shapes are complex.

4.4 The 40 Thieves

In figure 1.1 we saw the large scale structure for simulation h937 or the 40 thieves. Visually, see figure 4.18, the structure of median mass h937 halos is similar when comparing CDM and SIDM cosmologies at large radii, but at small radii we see that SIDM cosmologies form constant density cores. The h937 simulation has been analyzed in different contexts in the literature previously. The dwarf galaxies generated from the 40 thieves show excellent agreement with the present-day stellar to halo mass relationship; they have realistic blue colors and low star formation rates, realistic baryon fractions, colors, and metallicities. Additionally cumulative star formation histories show excellent agreement with local group dwarfs, especially when observational corrections are applied. Currently velocity dependent SIDM simulations with baryons are being run with h937 to make comparison to observations. Here we present analysis of the 40 thieves as DM only runs by comparing CDM and SIDM results.

The three most massive galaxies of h937 are field galaxies in a larger cosmological filament of structure. They have cores with $\alpha = -.5$ or greater. The relative mass enclosed (the mass enclosed at a given radii divided by the mass enclosed in the CDM model) of dark matter halos is shown in figure 4.19 for the three most massive and well resolved halos from simulation h937 with different cosmologies of constant cross section SIDM (red) and variable cross section (purple and orange). To within 3% all cosmologies have the same halo masses of $2.3 \times 10^{10}\ M_{\odot}$, $1.2 \times 10^{10}\ M_{\odot}$, and $1.1 \times 10^{10}\ M_{\odot}$ for the most to least massive halos respectively. The darker lines in the figure correspond to the most massive halos and the lighter lines to the least massive halos: for constant cross section SIDM the most massive halos creates the largest radius core and the largest reduction in mass enclosed compared to CDM.

The circular velocity, V_c, of the three most massive and well resolved halos from simulation h937 with different cosmologies of CDM (blue), constant cross section SIDM (red), and variable cross section (purple and orange) is shown in figure 4.20. The points with error bars are V_c values calculated from Wolf et al. (2010) using the half-light mass, $M_{1/2}$, and radius, $R_{1/2}$, quantities. All circular velocities are calculated using $V_c = \sqrt{GM/R}$. The

observed sample includes nearby dwarf spheroidals within 300 kpc of the Milky Way with $M_\star > 2 \times 10^5\ M_\odot$. To within 1% all cosmologies have the same V_{max} of 49, 36, and 37 km s^{-1} for the most to least massive halos respectively. For constant cross section SIDM models halo core densities scale inversely with V_{max}. In figure 4.20 and 4.19 the most massive $\sigma_{DM} = 2$ cm^2 g^{-1} galaxy (darkest red line) is the lowest circular velocity curve or least mass enclosed relative to CDM curve. But for the variable cross section SIDM models there is no such strong trend. At this galaxy scale of $V_{max} = 40$ km s^{-1} we conclude, similar to other work (Elbert et al., 2014), that cross sections as large as 50 cm^2 g^{-1} remain viable for SIDM cosmologies, however at larger galaxy masses constant cross section models will fail to match observations.

In figure 4.21 the slope of the density inside 500 pc is shown for the 40 thieves sample at present and when the universe is 3.3 Gyr old. For this velocity dependent model at earlier times the slopes for halos are already very flat and over cosmic times the galaxies gain more mass, but do not change their slope significantly. Summarily cores form very early, if they are going to form at all in our SIDM models. The age at which cores and shallow potential wells form in SIDM models has bearing on the missing satellite problem. Early core formation can lead to easier unbinding of baryons through baryonic feedback, merger, or tidal interactions. The star formation rate and cumulative star formation for small galaxies at 3.3 Gyr would be very stochastic: for example the SFR of h2003 peaked right before 3 Gyr and decreased rapidly afterward. We may expect that because core formation occurs in SIDM models early it would make subsequent epochs of star formation highly inefficient, however, this approximate statement should be seen as suspect: in our work and in other work galaxies with halo masses of a few $\times 10^9\ M_\odot$ have slightly increased star formation rates, however this SFR trend will need to be examined for smaller few $\times 10^8\ M_\odot$ and below halos. These slope results should be taken with caution. The profile and slope of a galaxy depends upon the halos accretion history and in particular the time of the last major merger (Colín et al., 2002).

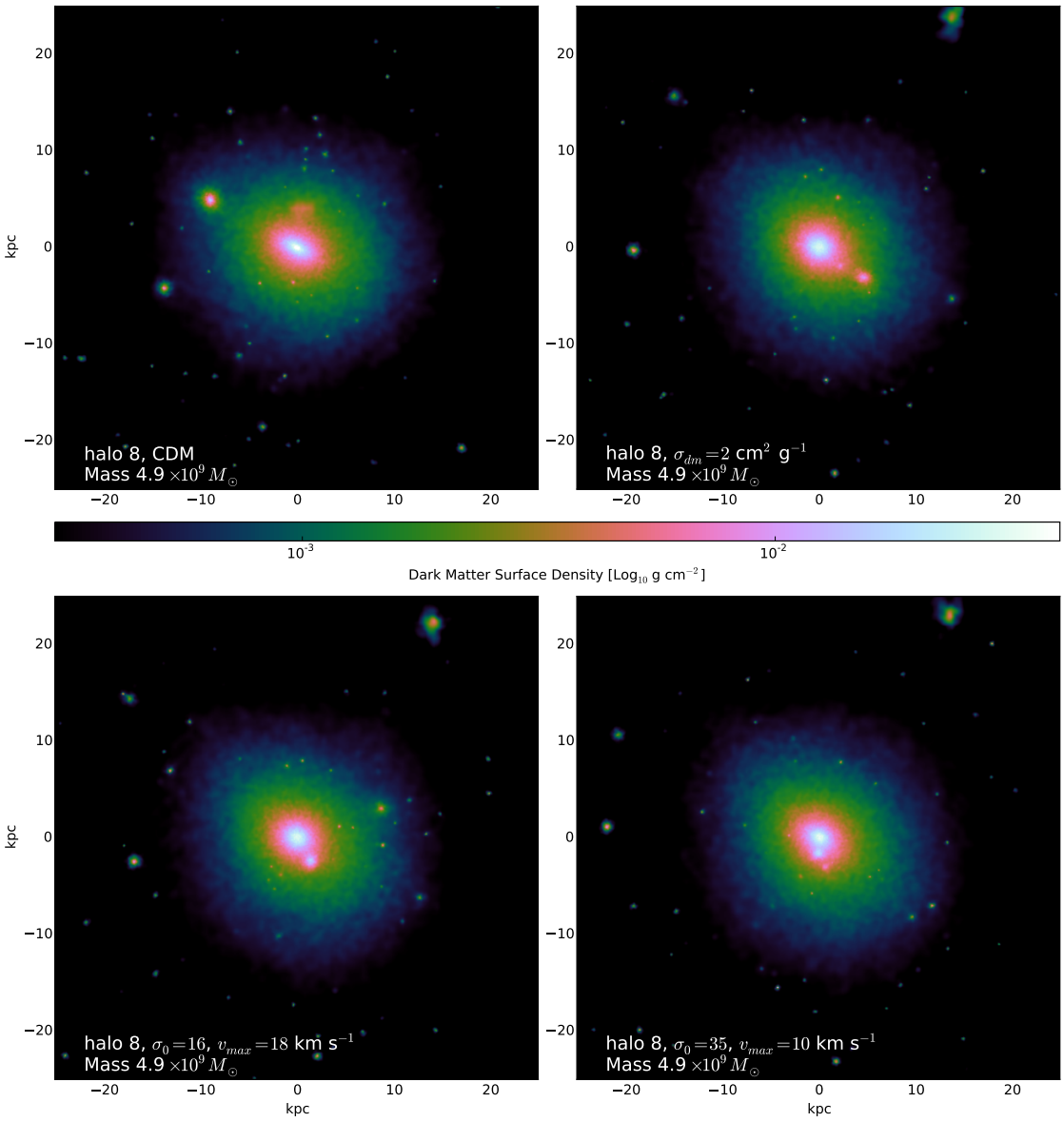

Figure 4.18: A visual comparison of halo 8 from the DM only simulation at $z = 0$ showing the surface density of dark matter for the different cosmologies tested. The slight changes in location of the substructure is generally an effect of the chaotic dynamics of the halo evolution and cannot be directly attributed to the DM model. However, do note that the SIDM models have formed spherical constant density cores in all instances for this 4.9×10^9 $M_\odot$ halo.

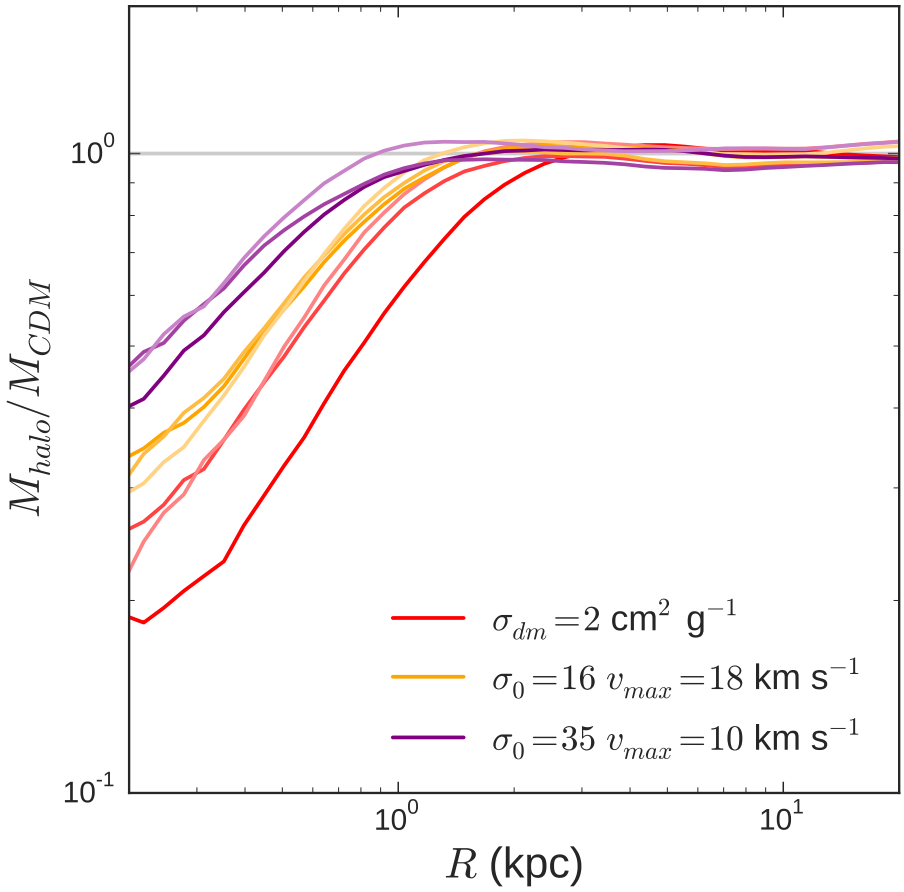

Figure 4.19: The relative mass enclosed of the three most massive and well resolved halos from simulation h937 with different cosmologies of constant cross section SIDM (red), and variable cross section (purple and orange) scaled by the total mass enclosed of the CDM counterpart halo. The darkest lines are the most massive halos. The mass enclosed is nearly identical by ∼2 kpc for the CDM and SIDM cosmologies with the parameters explored here and for this galaxy mass. However, as the total galaxy mass increases the deviation from CDM may continue to large radii, ie. in 4.22, the constant cross section SIDM model shows large deviation from CDM expectations out to 10 kpc.

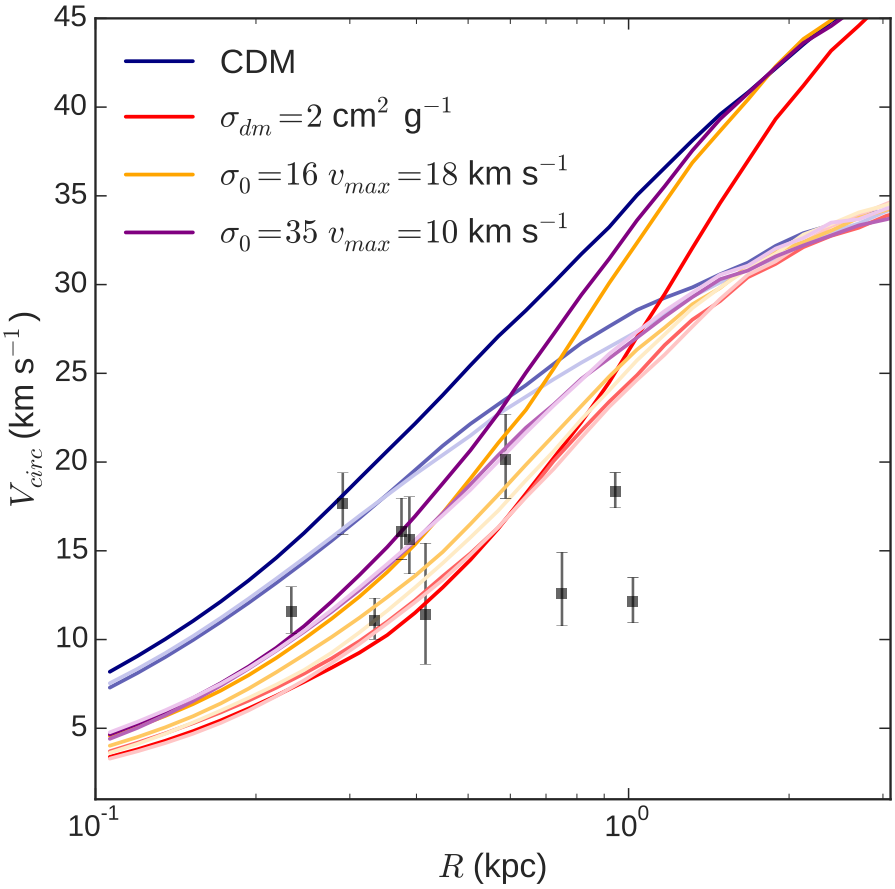

Figure 4.20: The circular velocity of the three most massive and well resolved halos from simulation h937 with different cosmologies of CDM (blue), constant cross section SIDM (red), and variable cross section (purple and orange). The darkest lines are the most massive halos. The points with error bars are V_c values calculated from Wolf et al. (2010) using the half-light mass, $M_{1/2}$, and radius, $R_{1/2}$, quantities. All circular velocities are calculated using $V_c = \sqrt{GM/R}$. The observed sample includes nearby dwarf spheroidals within 300 kpc of the Milky Way selected with $M_\star > 2 \times 10^5$ $M_\odot$ and excluding disturbed satellites. From left to right these are: Leo II, Draco, Carina, Sculptor, Leo I, Ursa Major, Ursa Minor, Canes Venatici I, Fornax, and Sextans.

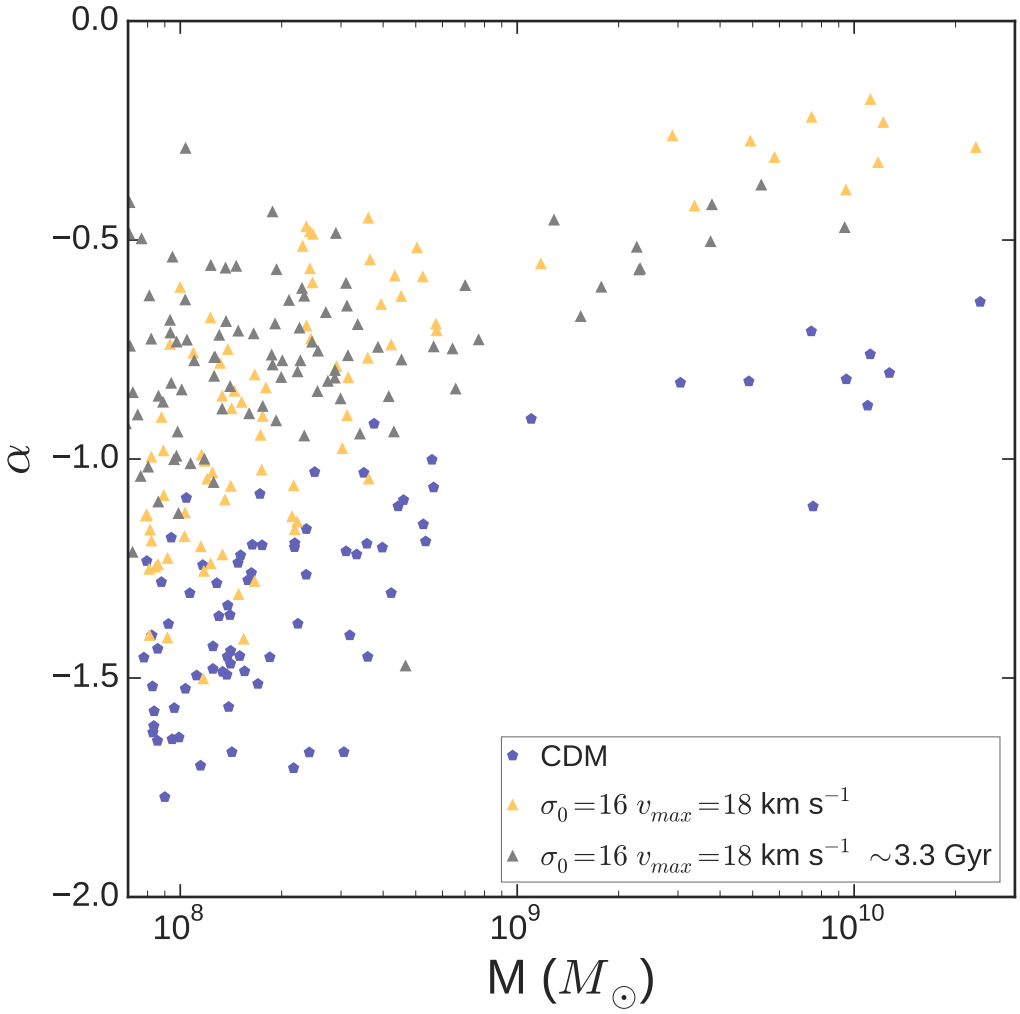

Figure 4.21: The slope of the density profile inside 500 pc, α_{500} for a range of halo masses from the 40 thieves simulations. The bright colored points show α_{500} at $z = 0$ for CDM and a velocity dependent cross section. The faded grey points show the the same velocity dependent model when the universe was 3.3 Gyr old. In SIDM models, if cores are going to form at all, they start to form early as was seen with h516 and h2003 in figure 4.8.

4.5 A Milky Way Analog

Our simulation h148 is a Milky Way like galaxy. Here we compare DM only simulations of h148 run with CDM, a constant cross section SIDM model of 2 cm^2 g^{-1}, and a velocity dependent model with $\sigma_0 = 18$, $V_{max} = 16$ km s^{-1}. In all three cases the total mass of the central massive halo is 1.3 $\times 10^{12}$ $M_\odot$. At this mass the differences between CDM and SIDM are stark: SIDM with a constant cross section of 2 cm^2 g^{-1} is observationally inconsistent with massive, 10^{12} $M_\odot$ galaxies. In figure 4.22 the density profile of h148 is shown. The density in the cSIDM model is reduced by more than an order of magnitude even out to 1 kpc. For smaller halos of $M_{halo} = 10^{10}$ $M_\odot$ the density or mass enclosed is nearly identical by $r \approx 2$ kpc when comparing between CDM and cSIDM cosmologies; however, as the total galaxy mass increases the deviation from CDM may continue to arbitrarily large radii. Here that is 10 kpc. The limiting factor is the age of the universe and the size of the cross section. The models explored in this work result in halos that are nearly identical at radii greater than $0.1R_{vir}$ for all halo masses resolved.

Once SIDM is turned on a pseudo-isothermal profile fit to the density profile works well. The best fit scale radii for the constant cross section model is $r_s = 9.4$ kpc, for the velocity dependent cross section model the scale radii is $r_s = 1.2$ kpc. The inner slope α measured at 500 pc for the constant cross section model is $\alpha = 0$, for the velocity dependent cross section model the slope is $\alpha = -.25$, and for the CDM case the slope is $\alpha = -.74$. At early times $\sim$3.3 Gyr the core this halos have already begun to form and most of the mass missing between the SIDM and CDM models is already gone. The outer slope of these halos show smooth behavior for the CDM and constant velocity SIDM model at $\sim 3.3Gyr$: measured from .1 to .4 times the virial radius ($\sim$366 kpc) the halo the slope is -2.2 for CDM and -2.3 for constant cross section SIDM, but the profile shows a deviation from constant slope for the velocity dependent SIDM model (the best fit is -1.7) possibly indicating that the velocity dependence is choosing some particular radii where equilibrium has not yet been achieved. We have evidence that this is the case. The SIDM timescale, τ_{SI}, during this early epoch measured at 500 pc is 1.7 Gyr for the constant cross section model and 2.9 Gyr for the velocity dependent model. At larger radii the density of the halo drops, but

the circular velocity remains high: the timescale for equilibrium for the velocity dependent model is greater than the age of the halo.

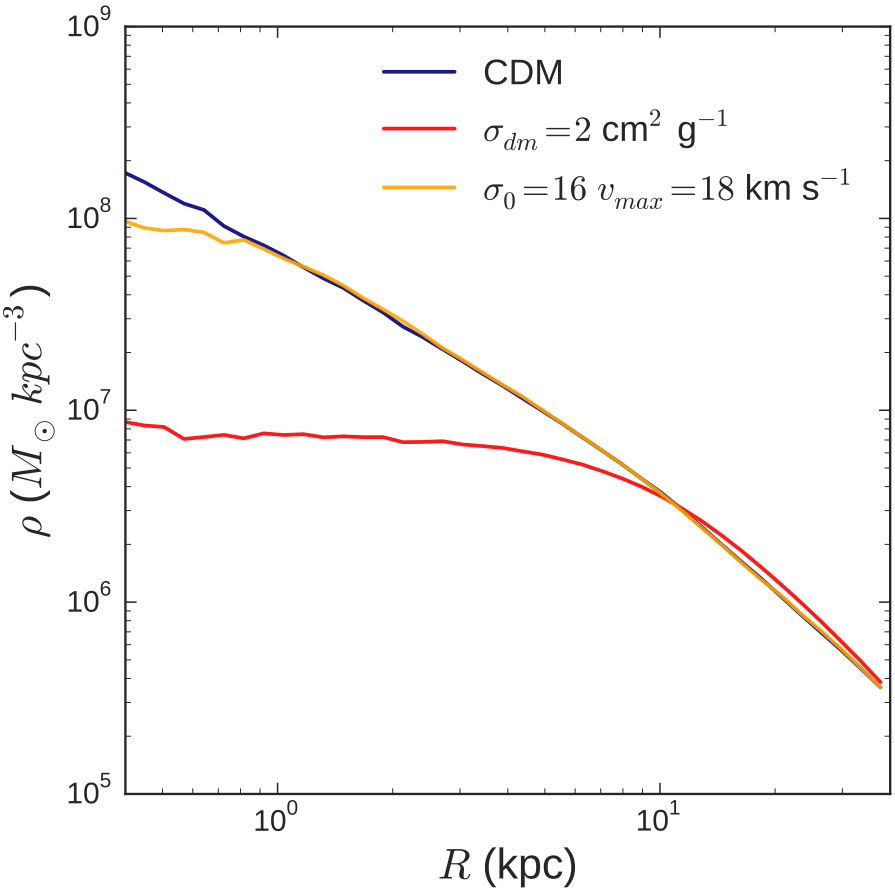

Figure 4.22: The density at $z = 0$ of the massive Milky Way like halo from simulation h148 showing three different cosmologies of CDM (blue), constant cross section SIDM (red), and variable cross section (orange). In all three cases the total halo mass is 1.3 $\times 10^{12}$ $M_\odot$. A pseudo-isothermal profile fit to the density profile indicates that for the constant cross section model the scale radii is $r_s = 9.4$ kpc, for the velocity dependent cross section model the scale radii is $r_s = 1.2$ kpc, and for the CDM case a pseudo-isothermal profile does not apply. The inner slope α measured at 500 pc for the constant cross section model is $\alpha = 0$, for the velocity dependent cross section model the slope is $\alpha = -.25$, and for the CDM case the slope is $\alpha = -.74$.

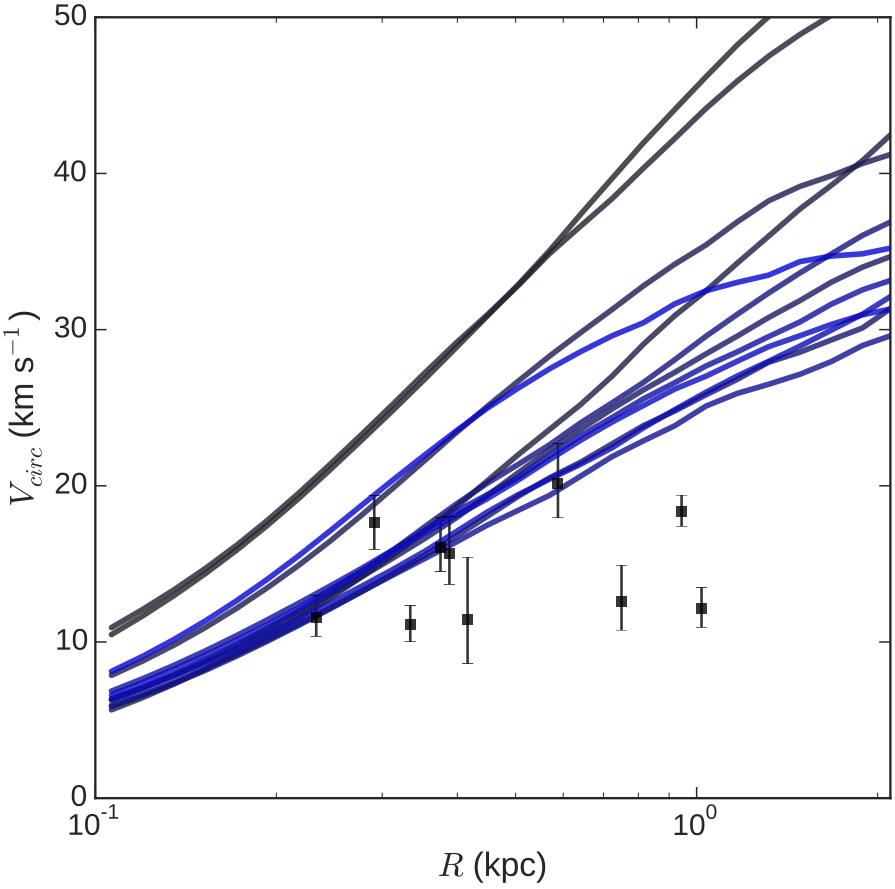

Figure 4.23: The rotation curves of all satellites within the virial radius of h148 which have maximum circular velocities of as least 30 km s^{-1} in a CDM cosmology. The darkest (black lines) are the most massive the most blue lines are the least massive halos. The points with error bars are V_c values calculated from Wolf et al. (2010) using the half-light mass, $M_{1/2}$, and radius, $R_{1/2}$, quantities. All circular velocities are calculated using $V_c = \sqrt{GM/R}$

In figures 4.23, 4.24, and 4.25 we present the rotation curves of all satellites within the virial radius of h148 which have maximum circular velocities of as least 30 km s^{-1}. The points with error bars are V_c values calculated from Wolf et al. (2010) using the half-light mass, $M_{1/2}$, and radius, $R_{1/2}$, quantities. All circular velocities are calculated using $V_c = \sqrt{GM/R}$. The observed sample includes nearby dwarf spheroidals within 300 kpc of

the Milky Way with $M_\star > 2 \times 10^5\ M_\odot$ and excluding disturbed satellites (from left to right these are: Leo II, Draco, Carina, Sculptor, Leo I, Ursa Major, Ursa Minor, Canes Venatici I, Fornax, and Sextans). This sample is not necessarily complete because of the limited survey data available. We are motivated to choose the 30 km s^{-1} selection criteria because

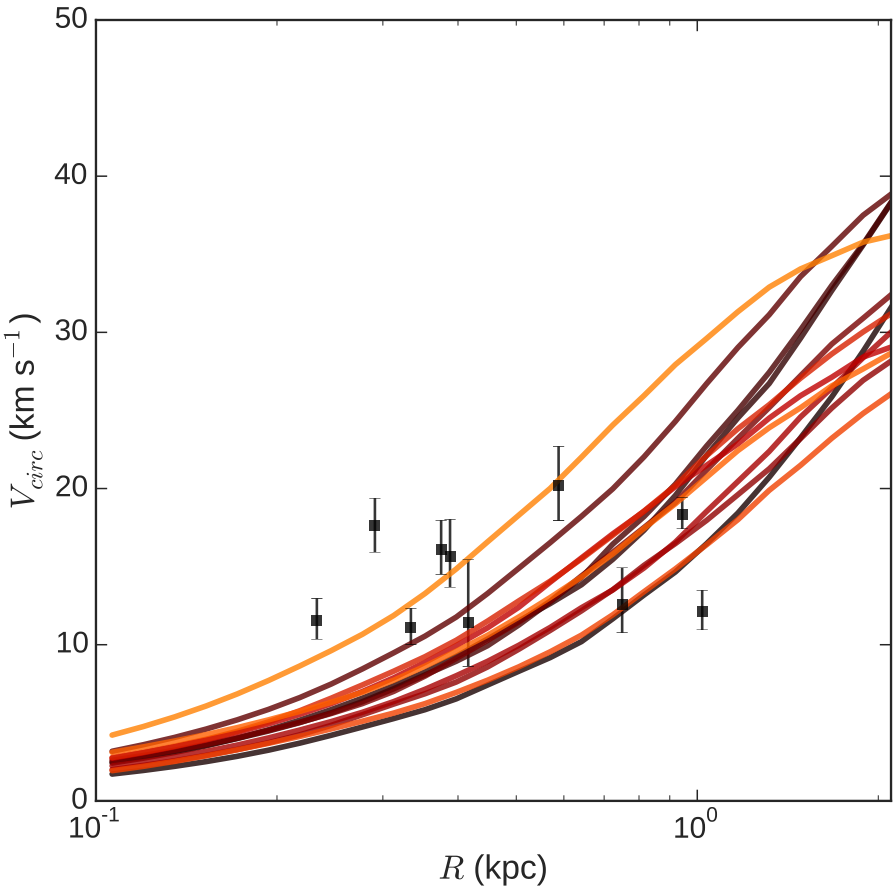

Figure 4.24: The rotation curves of all satellites within the virial radius of h148 which have maximum circular velocities of as least 30 km s^{-1} in a constant cross section SIDM model of 2 cm^2 g^{-1}. The darkest (black lines) are the most massive the most red/orange halos are the least massive. The points with error bars are V_c values calculated from Wolf et al. (2010).

the largest satellite halos in our simulations, with the largest potential wells, should host the largest reservoirs of gas and stars that are retained through reionization. This assumption is derived from work with extrapolating abundance matching relating the stellar and DM mass functions of halos down masses of $M_\star > 10^5$ with observations of MW and M31 satellites

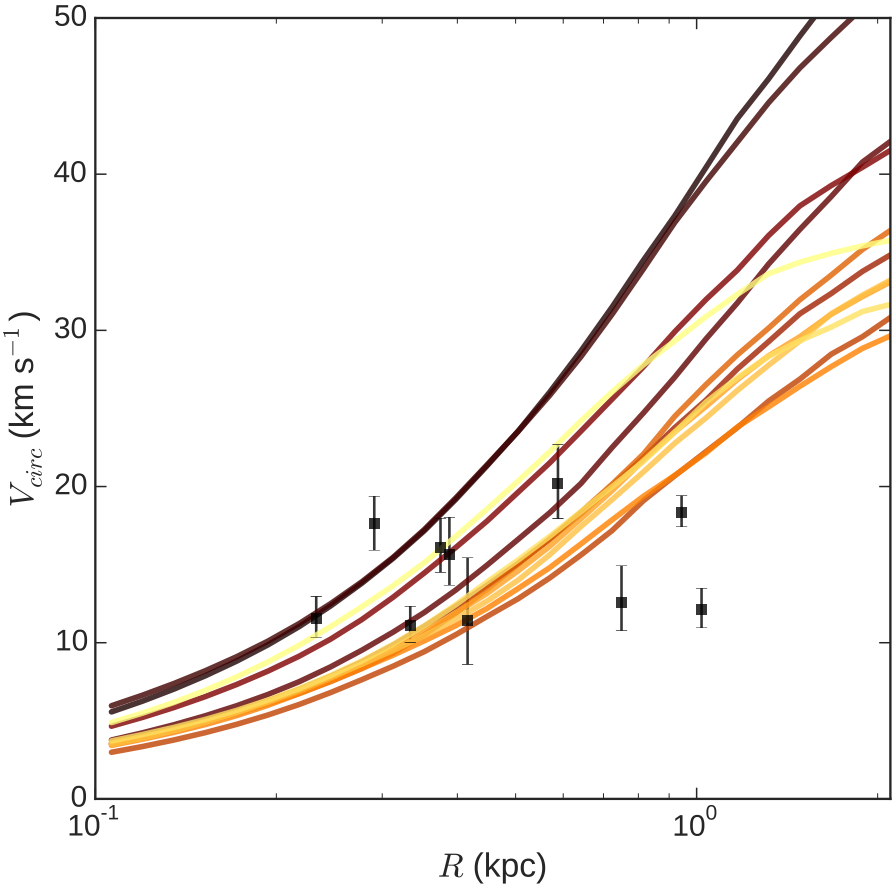

Figure 4.25: The rotation curves of all satellites within the virial radius of h148 which have maximum circular velocities of as least 30 km s^{-1} in a velocity dependent model with $\sigma_0 = 18$, $V_{max} = 16$ km s^{-1}. The darkest (black lines) are the most massive halos and the most yellow/orange lines are the least massive halos. The points with error bars are V_c values calculated from Wolf et al. (2010).

(Brook et al., 2014; Koposov et al., 2009; Kravtsov et al., 2004). The brightest classical dwarf spheroidals of the Milky Way should be hosted in the largest subhalos of the MW, and if h148 is analogous to the Milky Way those most massive subhalos should be comparable to the observed bright satellites of the MW. We can be rather certain of this because the halo mass functions in SIDM and CDM are nearly identical therefore abundance matching relations between SIDM and CDM are unchanged (Rocha et al., 2013).

In every cosmology examined there there were 12 satellites with $V_{max} > 30$ km s^{-1}. These halos have masses of 74.3 to 2.2 $\times 10^9$ $M_\odot$ for CDM, masses of 72.3 to 2.1 $\times 10^9$ $M_\odot$ for constant cross section SIDM, and masses of 73.9 to 2.0 $\times 10^9$ $M_\odot$ for variable cross section SIDM. In all cases the largest halo had a maximum rotational velocity 81 km s^{-1}. The consistency of the V_{max} is expected because at large radii where V_{max} peaks the SIDM interactions are inefficient for all models tested here. The too big too fail problem synthesized from these plots is that in the h148 CDM simulation there are four large mass ($M_{halo} > 2.0 \times 10^9$) and large circular velocity ($V_{max} > 30$ km s^{-1}) satellites that have no observational counterpart; these simulated galaxies are too dense to host the observed brightest satellites.

In all cosmologies simulated here h148 hosts large massive halos of the same total mass, however, the central density of these halos varies considerably and shows different systematic trends in the different cosmologies. In the velocity dependent SIDM model and in CDM the most massive halos also have the largest and fastest rising circular velocity curves (are the most dense), but in the constant cross section SIDM model this trend is inverted: the slowest rising halos are the most massive halos (least dense halos). In the CDM case the discrepancy with respect to observations is the fact that the large dense CDM halos have no observational counterpart. In the velocity dependent SIDM case the discrepancy with respect to observations is that the most massive subhalo we simulated is not dense enough to match observations and less massive halos will only be less dense: a weaker SIDM cross section would help. In the velocity independent case the discrepancy with respect to observations is that the least dense halo simulated is the most massive halo simulated, but there are still observed galaxies that are under-dense with no corresponding halo. For constant cross section SIDM models, at the smallest radii (for this particular cross section

of 2 cm^2 g^{-1} and for this particular mass range and for these radii below $\sim$.3 kpc) the most massive SIDM halos are the least dense (lowest V_{circ}), but at larger radii ($\sim$1 kpc for our model), the massive halos have larger V_{circ} again. For constant cross section SIDM models halo core densities scale inversely with V_{max} (for example the constant core density of the h148 main halo for constant cross section SIDM is $\sim 9 \times 10^6$ $M_\odot$ whereas for the velocity dependent model the core density is $\sim 9 \times 10^7$ $M_\odot$). So less luminous dwarfs could have central densities as dense or denser than galaxies four order of magnitude larger is mass or brightness in some SIDM models.

If the MW is more or less massive that h148 then our summary of simulation discrepancies would change; further, the presence of Andromeda, the LMC, and the SMC, could make the MW a unique system. I do not know if h148 is exactly analogous to the MW such that this comparison is fair, but their are some robust trends regardless. Our SIDM models are actually not dense enough to fill all the observed satellites. And we see the trend that for constant cross section the most massive halos are actually the least dense, a reversal of trend seen in the other models. Boylan-Kolchin et al. (2012) and Boylan-Kolchin et al. (2011) have observed that the Milky Way's nearby dwarf spheroidals with $V_{max} = 40$ km s^{-1} have central masses much less than the central mass of an equivalent $V_{max} = 40$ km s^{-1} galaxy from a CDM simulation. This is a density problem – observed galaxies appear to have much lower central densities than CDM simulations and SIDM cosmologies can solve this problem. SIDM cosmologies that match the stellar mass and inner dark matter density of satellites (Strigari et al., 2008a; Garrison-Kimmel et al., 2014) cannot be ruled out.

4.5.1 Substructure

SIDM can theoretically differ strongly from ΛCDM by suppressing small scale structure, reminiscent of warm dark matter, though generally Self-Interacting models have a much wider range of possible phenomenologies (Buckley et al., 2014). SIDM was in fact originally proposed to evaporate subhalos through interactions with the host halo and therefore solve the missing satellites problem (Spergel & Steinhardt, 2000).

We do not observable a statistical difference between SIDM and CDM models and others have also reported a range of SIDM models that do not suppress small scale structure at the observable limit or even simulation resolvable limit (D'Onghia & Burkert, 2003; Rocha et al., 2013). The number of dwarf galaxies in the field inferred from imaging surveys or the HI surveys disagrees with predictions from CDM (Klypin et al., 1999) and it may likely disagree with SIDM models as well: the number of subhalos is only mildly reduced in many SIDM models. The addition of SIDM with shallower potential wells to baryonic feedback models would theoretically make disruption efficient star formation (and therefore dark MW dwarfs) more likely (Papastergis et al., 2011; Ferrero et al., 2012). It was originally found that SIDM will not change the number of DM halos only their luminous baryon content, but actually large enough cross section (particularly constant cross section) SIDM models will cause subhalo evaporation: the elastic collisions between a small subhalo and a host halo can transfer enough energy to unbind the DM particles of a small halo. This was seen in Vogelsberger et al. (2012) where halos below $\sim 10^8$ $M_\odot$ were reduced by a factor of ~ 2 for a constant 10 cm^2 g^{-1} cross section. Additionally, in Gnedin & Ostriker (2001) they concluded that elliptical galaxies in clusters (which have 25% to 50% of their mass inside their half-light radius and where more elliptical galaxies have a large mass-to-light ratio) would fall beyond the observed scatter of fundamental plane relations if the SIDM cross section was from 0.3 to 10^4 cm^2 g^{-1}. Large constant cross sections are often ruled out at cluster scales indicating that an astrophysically interesting SIDM model is likely velocity dependent.

The missing satellite problem does not necessarily imply missing dark halos. Are there dark halos around the Milky Way with drastically reduced star formation or do the abundant

dark halos predicted by CDM not exist? Missing dark halos are not easily evaporated by SIDM with a variable cross section because the evaporation process requires unbinding DM interactions that are actually suppressed due to the relative velocity of the host and satellite. On the other hand the enhanced cores (shallower potentials wells) created by SIDM (velocity dependent or constant) within the satellites themselves will allow other process to work more efficiently, particularly in the presence of hosts with large discs (Peñarrubia et al., 2010). Processes that are relevant or could work together include: baryonic feedback with efficient coupling of SN with DM, cusp formation at high redshift, and a top heavy IMF (Peñarrubia et al., 2012). SIDM may form cores, but it doesn't necessarily reduce dark substructure.

In our DM only simulations of the forty thieves the number of halos in a given mass range is the same for CDM and all SIDM models down to at least 6×10^7 $M_\odot$ where the halos have at least $2^{13} = 8192$ particles. In our DM only simulation of h148 the number of satellites resolved and counted (for halos with at least $2^{14} = 8192$ particles) varied by only a few percent between models. Down to masses greater than 2×10^8 $M_\odot$ we report that there are 119, 112, and 121 halos around h148 in the CDM, constant SIDM, and variable cross section cosmologies respectively. It is has been found that abundance matching relations between SIDM and CDM remain unchanged because the halo mass functions in SIDM and CDM are identical (Rocha et al., 2013), particularly in the mass range where such abundance matching relations can be applied. In conclusion, we find no statistical difference between the number of dark halos in SIDM and CDM cosmologies, however, we do suspect that significant dark matter interactions would alter the stellar component of small dwarf galaxies.

4.6 Combined Results

Here we examine the detailed properties of an ensemble of halos from the combined h937 and h148 simulations for halos down to $2^{13} = 8192$ particles. The 40 Thieves simulation has halos masses in the range of 10^8 to 3×10^{10} $M_\odot$ with at least 50,000 DM particles in the virial radius. Additionally we have 40 thieves simulations with CDM+baryons (labeled g1MBwk1C52) and CDM+baryons and H_2 (labeled g1HbwK1) which have at least 10^3 star particles for halos with V_{max} greater than 20 km s^{-1} or masses greater than 10^9 $M_\odot$. Complimentary, h148 is a simulation of a Milky Way like halo with satellites of halo masses of 10^9 to 2×10^{12} $M_\odot$ around a MW sized central halo. A pseudo-isothermal fit of the form $\rho(r) = \rho_0(1.0 + (r/r_s^2))^{-1}$ and separately a power law slope fit of the form $\rho(r) = \rho_0 r^\alpha$ was fit to each halo using a non-linear least-squares (Levenberg-Marquardt) minimization method. This psueo-isothermal fit only has two free parameters ρ_0 and r_s that fits SIDM and CDM+baryons halos well, but it fails to fit well CDM only halos.

The 40 Thieves simulation and h148 are our testbeds of environmental effects. The average density of these DM halos as a function of V_{max} is shown in figure 4.26 (Bastidas Fry et al., 2015) where field galaxies are circled and satellites are crosses. Over plotted are lines of fixed τ_{SI} for 1 Gyr and 5 Gyr. SIDM and CDM show similar central DM densities if the typical scale for DM interactions is longer than 5 Gyr. At larger peak velocities and halo masses) with shorter interaction timescales, the SIDM densities decrease compared to their CDM counterparts and fall in a valley between the 1 and 5 Gyr lines, matching results from previous work. SIDM interactions isotropize the velocity distribution of DM and thus force the DM density to drop until, going to smaller and smaller halo masses, the interaction timescale rises to a significant fraction of the Hubble time and SIDM is not effective anymore. This result confirms our simple analytical expectations and clearly shows that even with a significant SIDM cross section, DM cores approach our resolved scale ($\sim$100-200 pc or twice the spline kernel softening) in field halos with virial mass $< 10^9$ $M_\odot$. This confirms the results from Li et al. (2008) and extends them to much smaller halo masses and higher resolution. We verify that the increased τ_{SI} at small halo masses comes from not only a lower velocity dispersion but also lower cusp density, possibly due the later

epoch of collapse of the central regions of the halo.

If we look at the average densities as a function of V_{max}, another difference emerges between the SIDM field (circled red crosses) and satellites (red crosses), with satellite halos showing central densities lower by about factor of two compared to field halos of similar V_{max}. This important environmental difference could be due to the satellites forming their central regions earlier, or to the significant boost to ρ and V_{max} due to orbiting in a large dense host halo with a speed larger than the internal velocity dispersion. In figure 4.31 the environmental difference between centrals and satellites is seen when comparing the mass of a given halo to the slope measured at $0.1R_{vir}$ to $0.2R_{vir}$; the dashed line fit to satellites is elevated above the solid line fit to field galaxies especially for the constant cross section model. This indicates the possibility that satellites will have flatter cores compared to field counterparts.

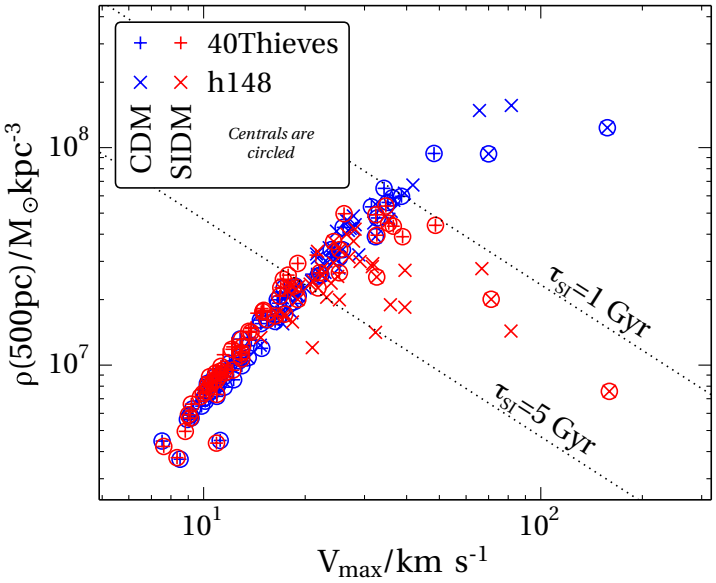

Figure 4.26: The density at 500 pc of DM only simulations (Bastidas Fry et al., 2015). Constant cross section SIDM is in red, CDM is in blue. Isolated field galaxies are shown as circle-crosses, and the satellites are shown as crosses. At the small masses ($V_{max} < 30$ km/s) there is no significant difference between SIDM and CDM. The values of τ_{SI} show the effective time scale for on average one interaction per particle: at low velocity the time scale is large and the cross section is not sufficient (or the time scale is too long) to form cores.

We summarize these results by stating that there seems to an environmental difference: the density at ρ_{500} for halos of the same V_{max} are a factor a few lower for satellite galaxies

compared to the isolated field counterparts. Do satellites in the presence of a large host experience an effective boost in ρ and V_{max} due to a fast orbit of a massive halo? In figure 4.31, where the inner slope α is measured from $0.1R_{vir}$ to $0.2R_{vir}$ it does appear that for the constant cross section model halos are indeed flatter, but when the slope is measured at 500 pc no such environmental discrimination is apparent.

The pseudo-isothermal fit parameters, r_s and ρ_0 at $z = 0$ for halos from simulations h937 and h148 are shown in figure 4.27. The central density of constant cross section SIDM halos scales as $\rho_0 \propto 1/V_{max}$ which is consistent with other constant cross section SIDM work. In the lower panel of figure 4.27 we see that the scale radii is in direct proportion with the V_{max} of the halo for constant cross section SIDM. The central density ρ_0 and r_s are nearly independent of V_{max} for the velocity dependent SIDM or CDM+baryon simulations. The galaxies from h937 with gas and stars have systematically higher ρ_0 and lower r_s, yet there at least a dozen galaxies from the sample that fall within the the scatter of the SIDM models for V_{max} equal to 20 to 70 km s^{-1} and thus objects of this halo mass are not strong discriminators of SIDM and CDM cosmologies. While cores may be created in SIDM or CDM+baryon cosmologies the scatter with which cores are created is a possible discriminator of CDM and SIDM cosmologies. With a large sample of SIDM+baryons and CDM+baryons simulations we could compare the scatter in ρ_0 or $V_{max}/V_{rot}(1kpc)$ (where V_{rot}(1 kpc) is the rotation velocity of the halo at 1 kpc) to V_{max}. Simulations with CDM+baryons with significant supernova feedback have larger variance consistent with observations (Brook, 2015). Whereas simulations with SIDM+baryons with weak feedback may lack the observed variance implying that only models that combine SIDM+baryons with with strong feedback will be viable; however, this claim will have to be tested.

In 4.28 we see the slope of galaxies in a range of different cosmologies as a function of total galaxy mass with solid lines fit to the data. The equation fit to the data is $\alpha = a - \mathrm{Log}_{10}\left((\frac{M}{s})^b + (\frac{M}{s})^{-c}\right)$ and in table 4.6 the fit parameters are shown. The lines show the fit over the range that data was present, but the same fit function was used for all lines. The inner slope at 500 pc is a correlated strongly with halo mass and cosmology. Even by$z = 0$ almost no halo with mass less than a few 10^8 $M_\odot$ in our constant cross section SIDM model has formed a core with $\alpha > -0.5$, but neither has any CDM+baryon galaxy

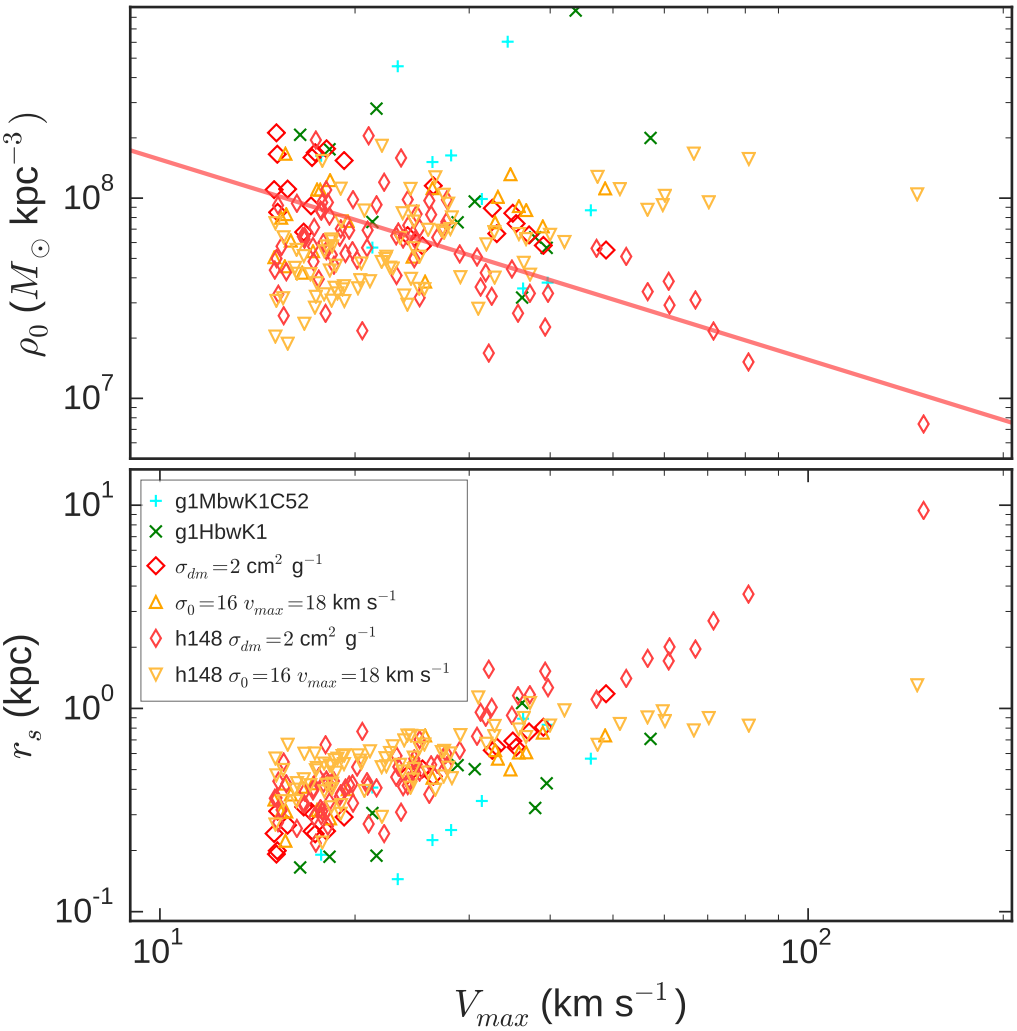

Figure 4.27: The pseudo-isothermal fit parameters, r_s and ρ_0 at $z = 0$ for halos from simulations h937 and h148. In red is the constant cross section model with $\sigma_{DM} = 2$ cm^2 g^{-1} and in orange is the velocity dependent $\sigma_0 = 16$ $v_{max} = 18$ km s^{-1} model. The blue and green crosses are baryon+CDM runs. The plot and the fit were truncated at $V_{max} = 15$ km s^{-1} where the values of r_s begin to fall below 200 pc. The red line is a fit to the constant cross section model's data going as $\rho_0 \propto 1/V_{max}$ which is consistent with other constant cross section SIDM results (Elbert et al., 2014).

that meets the same low mass criteria. For the variable cross section models SIDM halos are NFW ($\alpha = -1$) like only at the very lowest masses. From 10^8 $M_\odot$ to $\sim 5 \times 10^9$ $M_\odot$ the slope is largest for the SIDM velocity dependent models and correspondingly the density is lowest for these models. The $\sigma_0 = 35$, $v_{max} = 10$ km s^{-1}model has the flattest slopes at the lowest masses, but because the knee in the classical cross section model used is only 10 km s^{-1} its interaction strength is truncated. Near $\sim 5 \times 10^9$ $M_\odot$ and above the slope is largest for constant cross section SIDM model and similarly the density is most reduced for constant cross section models.

Run	a	b	c	s
g1MbwK1C52	-1.538	-0.439	1.3710405	4.673×10^7 $M_\odot$
g1HbwK1	-0.223	0.4717	0.7289	7.047×10^9 $M_\odot$
CDM	-0.408	0.121	0.4091	3.528×10^{10} $M_\odot$
cSIDM	-0.155	0.00696	1.00755	1.996×10^9 $M_\odot$
vSIDM1	-0.0513	0.09352	0.694	2.898×10^9 $M_\odot$
vSIDM2	-0.968	-0.3211	3.02646	8.870×10^7 $M_\odot$

Table 4.1: Fit data for the inner slope, $\alpha = a - \mathrm{Log}_{10}\left((\frac{M}{s})^b + (\frac{M}{s})^{-c}\right)$. Only the CDM, cSIDM, and vSIDM1 models have data combined for h937 and h148 which results in more robust fits.

The inner slope measured at 500 pc, α_{500}, is a strong function of halo mass that has a maximum of about $\sim -.1$ near $M_{halo} = 10^{10}$ for our SIDM models. But is the slope at 500 parsecs a robust measurement of the effect of SIDM? If halos are always self similar with an identical constant slope ($\rho \propto r^\beta$) at large radii and if for r less than $r(r_s)$ the density goes as $\rho \propto r^\alpha$ where r_s is the scaled radii then internal to that radii a larger α (more cored) will always result in a smaller mass enclosed. The location of r_s will be monotonically proportional to the amount of missing mass in this cored profile as compared to an ideal cusped profile. However, if the outer slope isn't a constant $\rho \propto r^\beta$ slope then it is possible that a cored profile can contain more or less mass than a cusped profile regardless of where

r_s is. For example in 4.2 we see, especially for h2003, that near the knee in the density curves for the SIDM vs CDM+baryon models that the SIDM models has pushed a small excess amount of mass to near r_s. In this work we see that the slope measured at 500 pc and the fits generated in figure 4.28 are strongly correlated with the density at 300 pc, seen in figure 4.34, or the mass enclosed at 300 pc, as seen in figure 4.35. The slope of α at 500 parsecs is a reasonable measure of the effect of SIDM because our profiles are well behaved, but it is important to consider that if we measure α as a fraction of the virial radius slightly different behavior emerges. Figure 4.29 shows the τ_{SI} value from equation 3.12 evaluated at 500 pc for a range of halos from h148 and h937 in the constant and variable cross section dark matter models; additionally this figure colors codes the the slope, α, of the profile measured at 500 pc in the left two boxes, and measured at at $.1R_{vir}$ to $.2R_{vir}$ in the right two boxes. Lower values of τ_{500} represent shorter SIDM dynamical timescales and stronger SIDM effects. The slope measured at fixed radii, ie. 500 pc, has a different behavior than the slope measured at a fractional value of the virial radius. The figure indicates that for constant cross section models SIDM cores out the central (500 kpc) region of halos until at $\sim 10^9$ $M_\odot$ there is nothing left to core because τ_{500} has approached zero and at this same mass scale α_{500} has transitioned to greater than -0.6. In velocity dependent vSIDM1 model the strength of the SIDM interaction as measured by τ_{500} peaks near $\mathrm{Log}M_\odot = 9.25$ (a mass chosen by the classical cross section model parameter $V_{max} = 18$ km s^{-1}), then begins to decline. It is this peak then decline that makes velocity dependent SIDM enticing as a solution to small scale problems in cosmology, yet also hard to constrain.

In figure 4.31 and 4.31 we compare the α_{500} and $\alpha_{.15R_{vir}}$ values and see an environmental difference for the halos. In these figures the open points are satellite halos fit with a dashed line, and the closed points are field halos fit with a solid line; the fit is a log linear slope (the data in this figure is the same as that of 4.28, but the fit here is a log lienar slope done independently for each field or satellite halo population). First, and reassuringly, we note that whether considering fields or satellites the CDM fits in both figures do not change. But when the inner slope α is measured from $0.1R_{vir}$ to $0.2R_{vir}$ it does appear that for the constant cross section model satellite halos are indeed flatter. There is an inverted trend for vSIDM1: when α is measured from $0.1R_{vir}$ to $0.2R_{vir}$ velocity dependent models

show decreasing slope with halo mass. This is likely due to the scaling of DM halos. The concentration of halos ($c = r_\Delta/r_s$) is a weak function of mass that scales as $c \propto M^{-1/9}$ (Neto et al., 2007). At larger halo masses we are probing beyond any inner core at r_s of the halo that the vSIDM1 model can create, except in the SIDM model where cores continues to grow. In summary the slope as measured scaled to R_{vir} declines (becoming steeper) for our velocity dependent model in the mass range $\sim 10^8$ $M_\odot$ to $\sim 10^{12}$ $M_\odot$. The slope scaled to R_{vir} is increasing for our velocity independent 2 cm^2 g^{-1}model in the mass range $\sim 10^8$ $M_\odot$ to $\sim 10^{12}$ $M_\odot$.

In figure 4.32 we explore how stars may populate cored SIDM halos. Brook et al. (2014) finds a stellar-mass-to halo mass relation fit of $M_\star = (M_{halo}/79.6 \times 10^6)^{3.1}$ for the observed local group of dwarf galaxies in the stellar mass range $10^7 M_\odot < M_* < 10^8 M_\odot$ where the observations are completeness limited; there is likely a more complex than a single power law relation for the stellar-mass to halo mass relation below $M_* < 10^8 M_\odot$. We have used this stellar mass to halo mass relation to infer stellar masses for the DM runs for our halos and have extrapolated our values an order of magnitude lower. Our full baryonic physics simulations produce the right amount of stars and the most massive halos covert 1% of gas into stars. In comparison we find that our SIDM runs with baryons produce the same amount of stars to within a few percent. For stellar masses of $10^7 M_\odot < M_* < 10^8 M_\odot$ SIDM and simulations with CDM+barynos have similar alphas, but below this mass (in a regime where we are extrapolating) SIDM simulations, despite their low stellar masses, still produce cores. Stellar feedback produces the most pronounced cores ($\alpha = -0.1$) at $M = 10^{8.5}$ $M_\odot$ (or $M_*/M_{halo} = 5 \times 10^{-3}$), and below and above this stellar mass the profile is steeper again (Di Cintio et al., 2014b). Unfortunately this corresponds to a halo mass of $\sim 4 \times 10^{10} M_\odot$, which is near the natural turnover in alpha for the SIDM models being explored here.

Whether comparing V_{max} to M_{300}, ρ_{300}, or ρ_{500} a trend is apparent for SIDM. The velocity dependent points for the vSIDM2 model ($\sigma_0 = 35$ $v_{max} = 10$ km s^{-1}) contain the least mass (and have the flattest slopes) at $V_{max} = 10$ km s^{-1}. The velocity independent points for the cSIDM model contain the least relative mass (and have the flattest slopes) at $V_{max} > 30$ km s^{-1}.

In fig 4.33 we see the number of interactions per particle that have occurred for particles at 500 pc (Γ_{500}). The behavior of the central regions of galaxies at 500 parsecs shows stark differences between SIDM and CDM. At 500 pc most particles have had at least one interaction by $z = 0$ for all models except in the case of the cSIDM model for halos below $< 3 \times 10^8\ M_\odot$. The number of interactions per particle is consistently higher for the velocity dependent models, despite the fact that constant cross section models show drastically different behaviors at large mass. This may be because Γ_{500} is a weak proxy for how the total halo mass and velocity has been redistributed given that DM particles may completely scatter out of the core after a single interaction and therefore will no longer be counted as in this measure that examines average particle interaction counts near 500 pc only. Further this value is a total over the entire lifetime of the halo. Velocity dependent SIDM has more interactions in the early universe with the rate peaking at $z > 10$ while velocity independent SIDM has an interaction rate that may remain constant even up to $z = 0$. The points do not seem to show any dichotomous behavior between satellites and field halos.

Figures 4.34 and 4.35 compare the density or mass within 300pc of the center of the halo with the mass or V_{max} value of the halo. These figures are complimentary to each other and to figure to 4.26.

In figure 4.34 we see how the density at 300 pc as a function of total halo mass is reduced for SIDM models; the trend is that for the least massive halos vSIDM2 creates the lowest density cores, whereas at high mass only cSIDM differs greatly from CDM. In figure 4.35 the mass enclosed at 300 parsec as a function of V_{max} is shown; the trend here is that at the lowest velocities, $V_{max} = 10$ km s^{-1}, vSIDM1 halos contain the least mass and at the highest velocities probed, $V_{max} > 30$ km s^{-1}, cSIDM shows a drastic reduction in mass contained of a least a factor of two. In the top panel of these figures we have shown how CDM compares to CDM+baryons simulations, though we caution that stellar physics is not resolved in the halos below $10^9\ M_\odot$. For lower mass halos the density inside a given radius is smaller for our velocity dependent models, but the velocity dependence means that the most massive halos (with $V_{max} \geq 50$ km s^{-1} for reasonable choices of σ_0) will be insensitive to velocity dependent SIDM. But for constant cross section SIDM it is the largest halos that

are dramatically reduced in central density compared to their CDM counterparts. At 300 pc our constant cross section cSIDM model halos contain at twice as much mass as their CDM companions for halos with $V_{max} > 30$ km s^{-1}, yet the CDM+baryon simulations show the same trend.

The radius where the maximum circular velocity, V_{max} occurs does not show a significant trend between CDM and SIDM models. It is occurs at about $\sim$1 kpc for all halos at 10^8 $M_\odot$ and monotonically rises to above $\sim$8 kpc for halos above 10^{10} $M_\odot$. The radius where the maximum velocity dispersion occurs (of order 1 kpc for most halos) for a given halo is extremely noisy in the SIDM scenarios because the dispersion is so flat the deviations are dominated by noise.

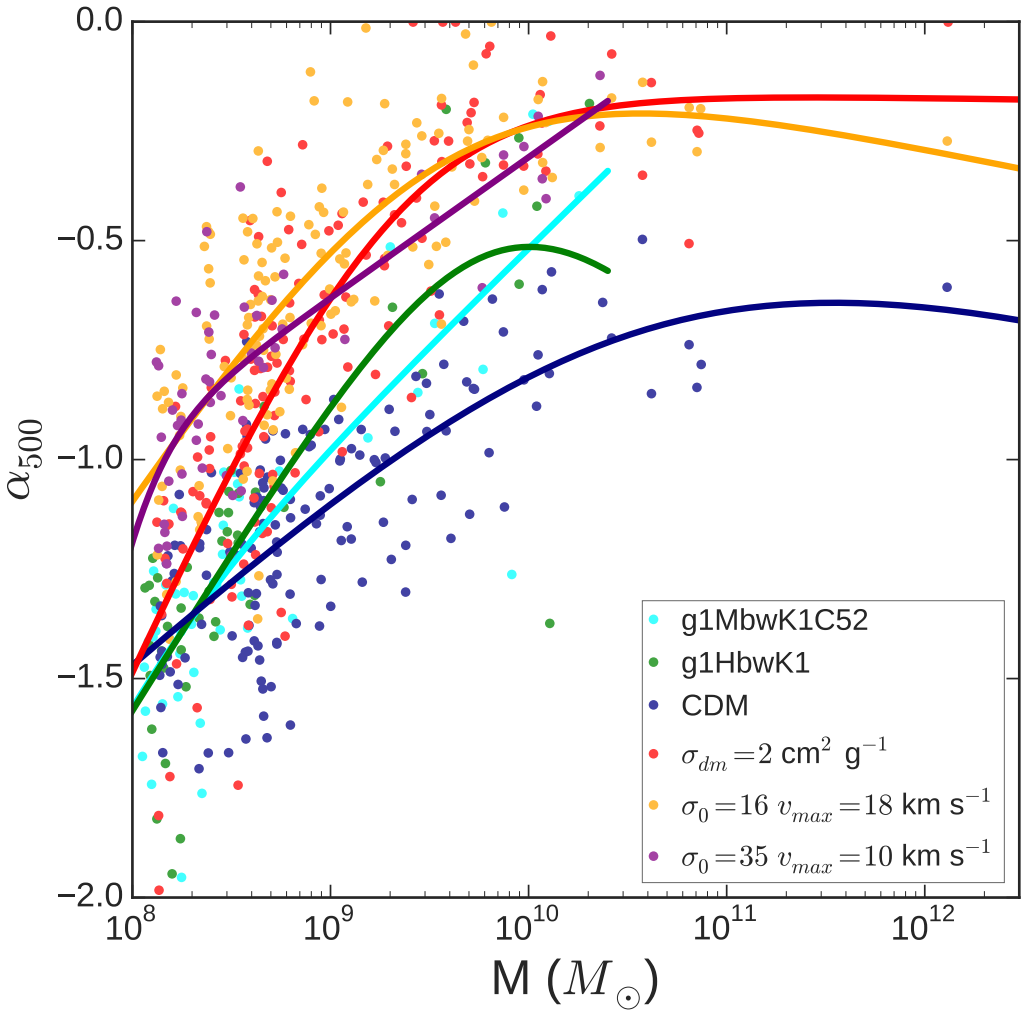

Figure 4.28: The inner slope of halos measured at 500 pc for h937 and h148 for halos with at least 2^{14} DM particles fit with the function $\alpha = a - \mathrm{Log}_{10}\left((\frac{M}{s})^b + (\frac{M}{s})^{-c}\right)$.

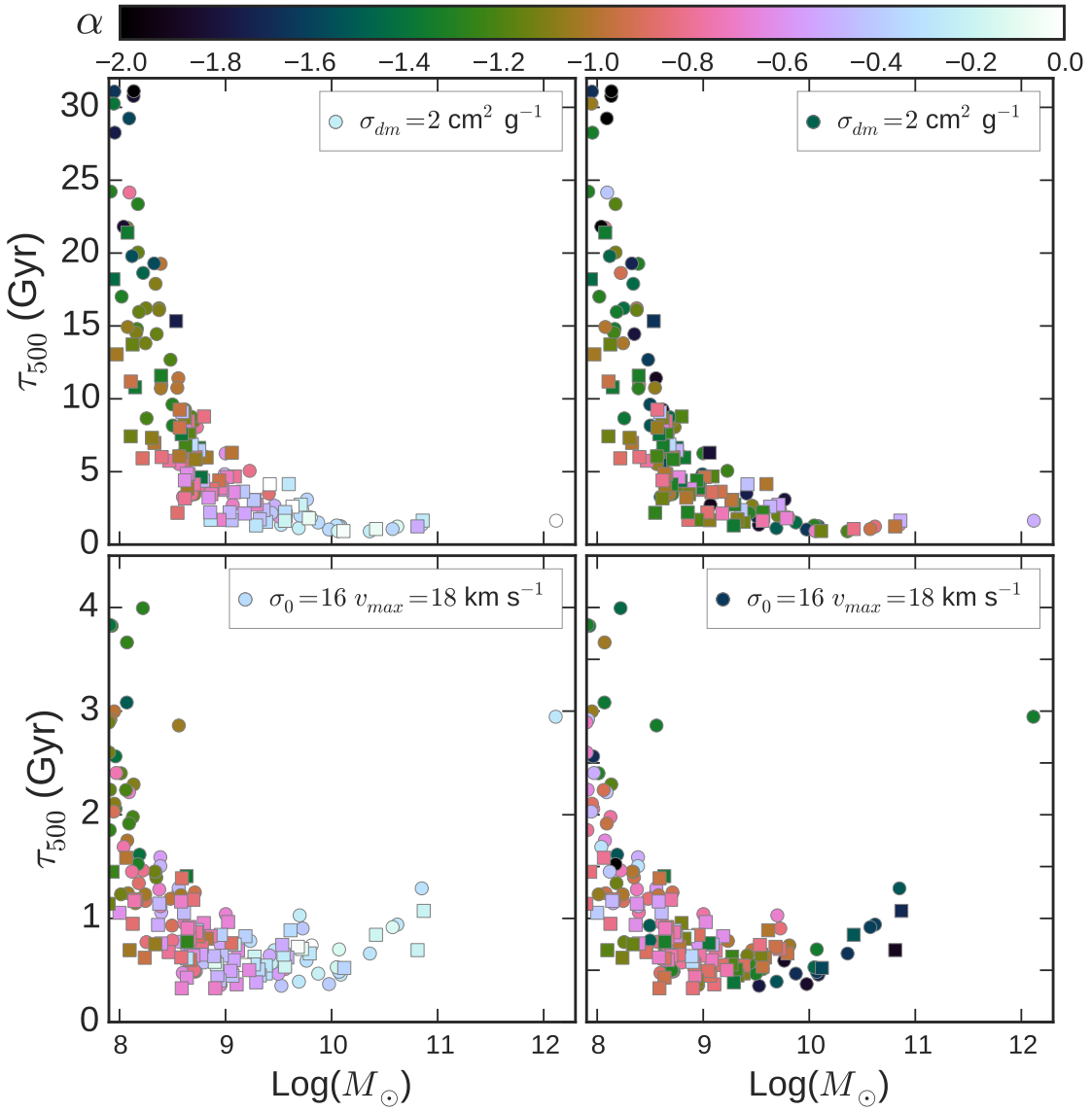

Figure 4.29: The τ_{SI} value from equation 3.12 evaluated at 500 pc for halos from h148 and h937 in the cSIDM and vSIDM1 models. Lower values of τ_{500} represent shorter SIDM dynamical timescales and stronger SIDM effects. Each point is colored corresponding to the slope, α, of the profile measured at 500 pc in the left two boxes, and measured at at $.1R_{vir}$ to $.2R_{vir}$ in the right two boxes. The horizontal axes are shared, but note the vertical axis changes from the top to bottom: in the cSIDM model τ_{500} is larger than the age of the universe for galaxies below 5×10^8 $M_\odot$. The square points represent subhalos and the circle points are field halos.

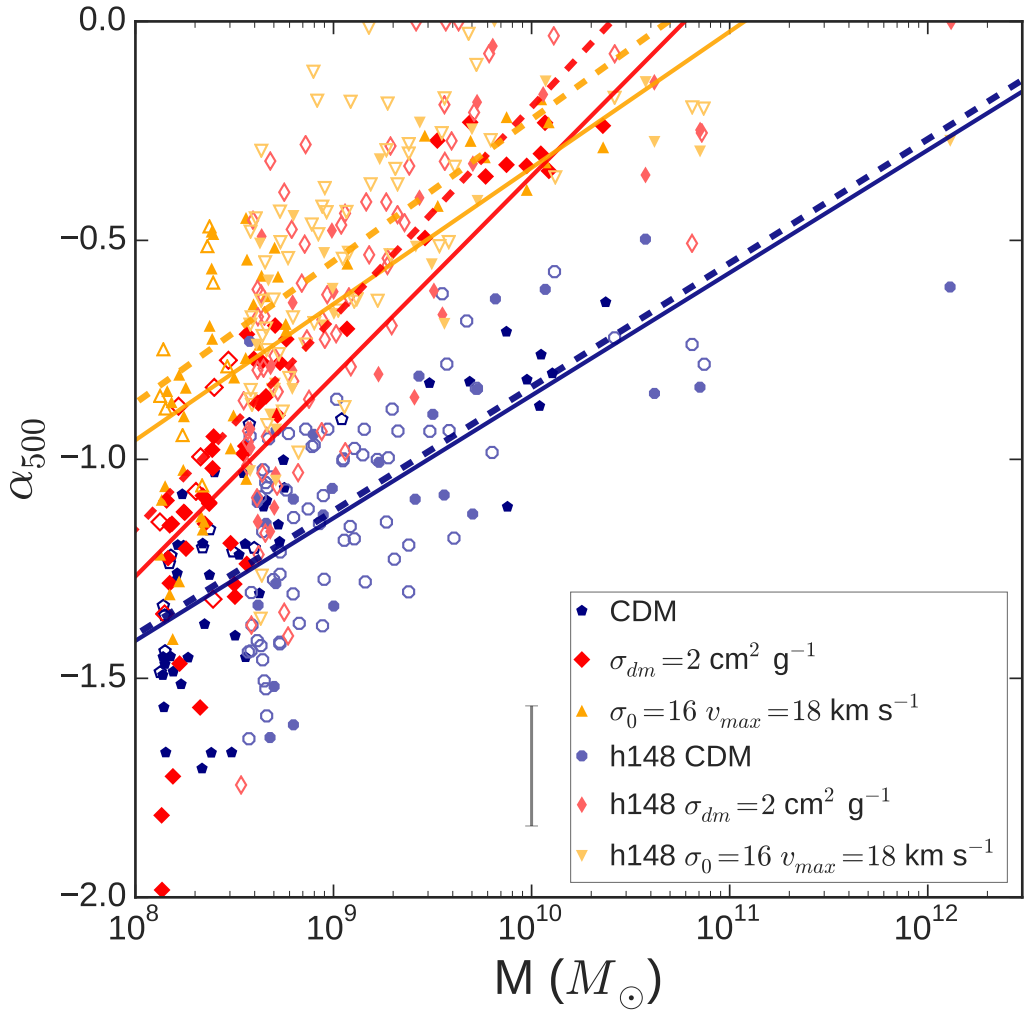

Figure 4.30: The inner slope α of halos measured at 500 pc for h937 and h148. The open points are satellite halos fit with a dashed line, and the closed points are field halos fit with a solid line. The fit is a log linear slope. Generally, including the h148 data makes the fits flatter because of the large field 10^{12} $M_\odot$host galaxy; the dip in the dashed line after 5×10^{10} $M_\odot$is not reliable. This plot shows all halos with at least 2^{14} DM particles. The grey vertical line to the left of the legend shows the average error of α from all points on the plot.

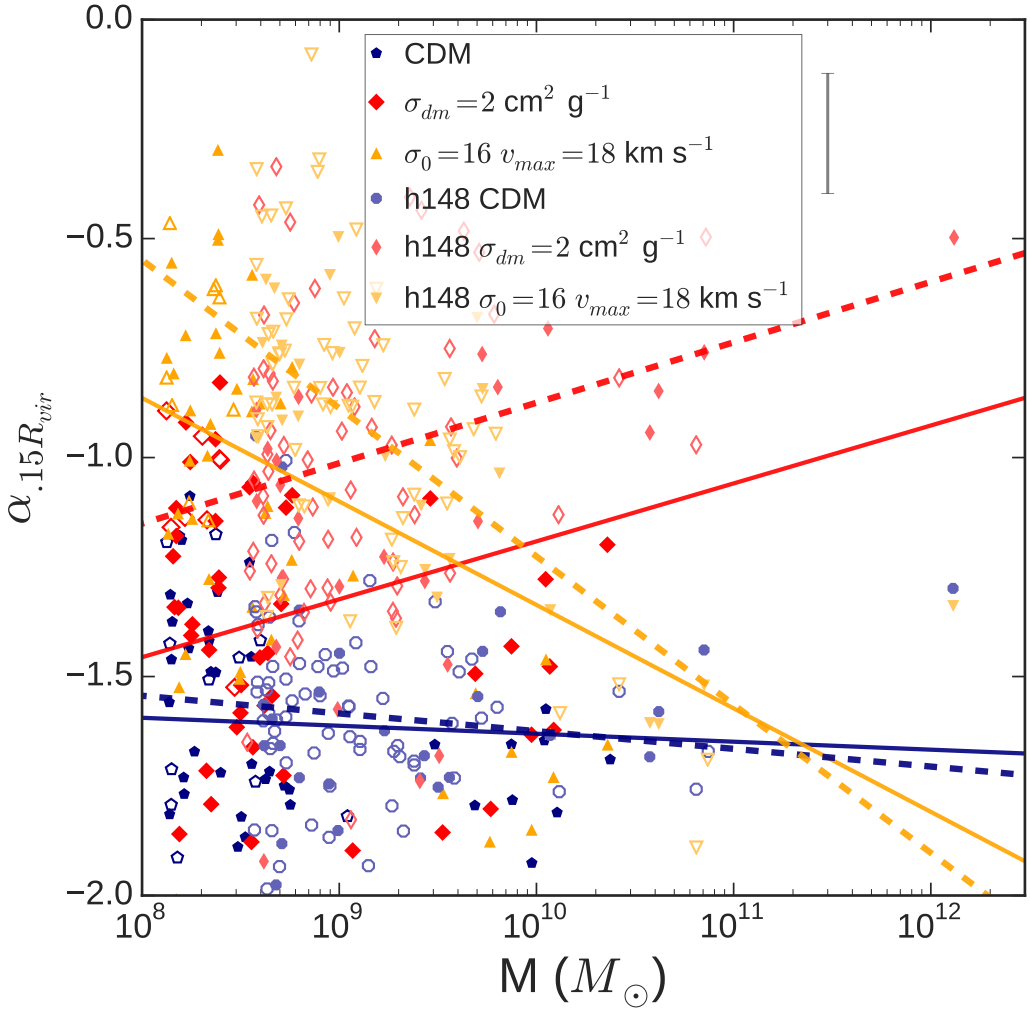

Figure 4.31: The inner slope of halos measured at $0.1R_{vir}$ to $0.2R_{vir}$ for h937 and h148. The open or not-circled points are satellite halos, and the closed or circled points are field halos. The dashed lines are a fit to the combined h937+h148 data of field and satellite halos whereas the sold line is a fit to the h937 data only. The grey vertical line to the left of the legend shows the average error of α from all points on the plot.

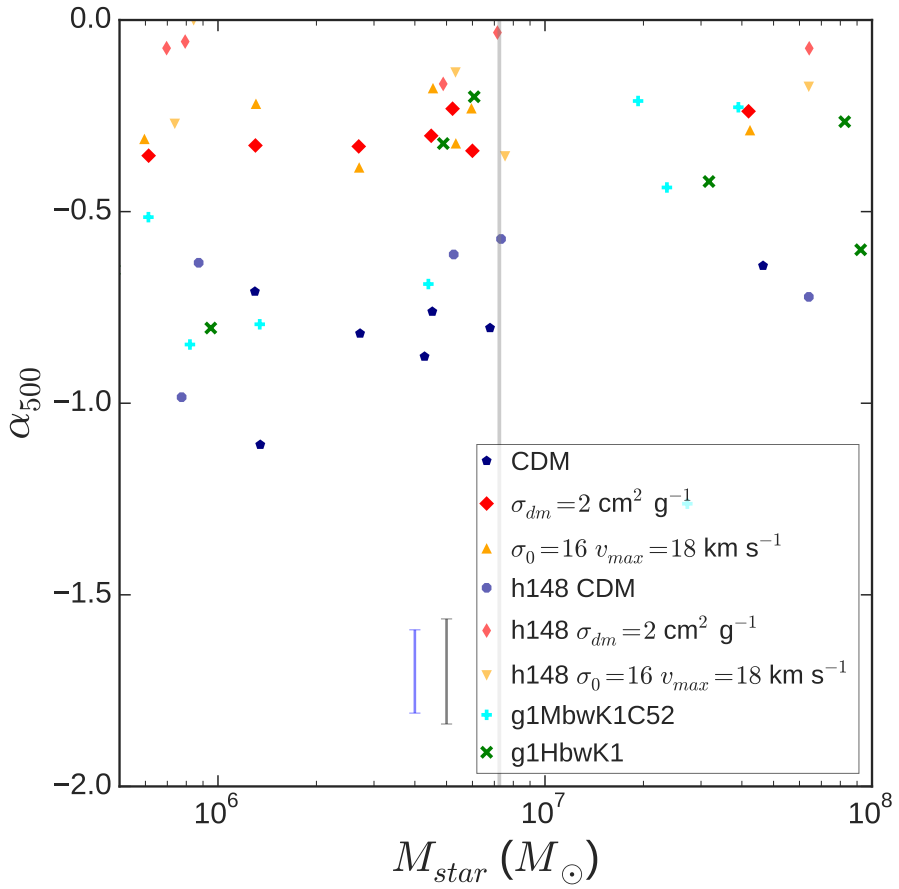

Figure 4.32: The slope at 500 pc as a function of stellar mass for halos run with CDM+baryons from h937 and also DM only simulations from h148 and h937. The stellar masses for the DM runs are inferred from the stellar-mass-to halo mass relation fit from Brook et al. (2014). The stellar masses below the grey line correspond to halo masses of 1.3×10^{10} $M_\odot$and are an extrapolation of the fit due to incompleteness. These points are shown without correcting for observational and simulation biases, though see figure 4.10. The grey line to the left of the legend shows the average error on α for the DM only runs and the blue line shows the average error on CDM+baryon runs.

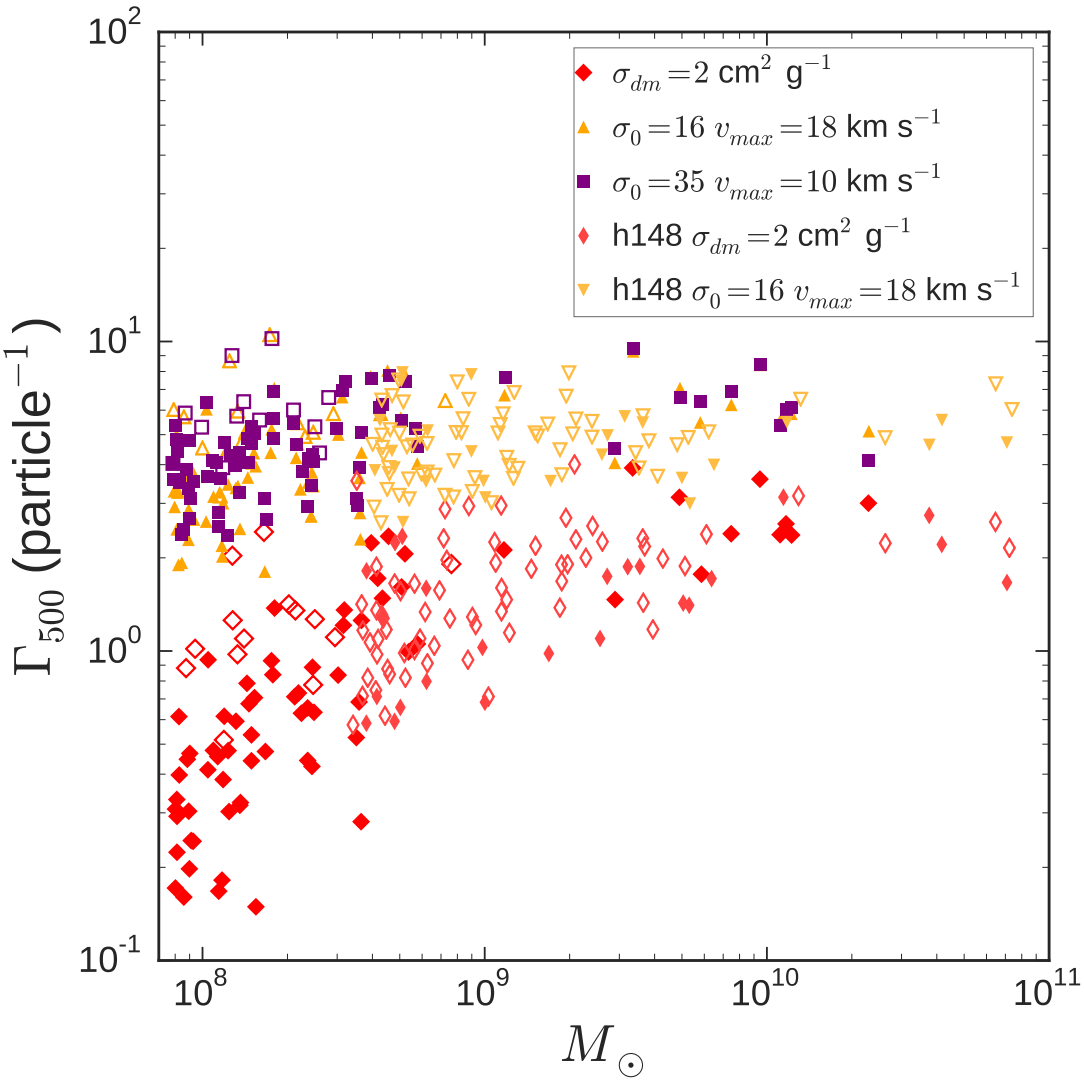

Figure 4.33: The number of interactions per particle that occur at 500 pc for a range of halo masses from the 40 thieves and h148 simulations at z=0. The filled points are field halos and the open points are satellies.

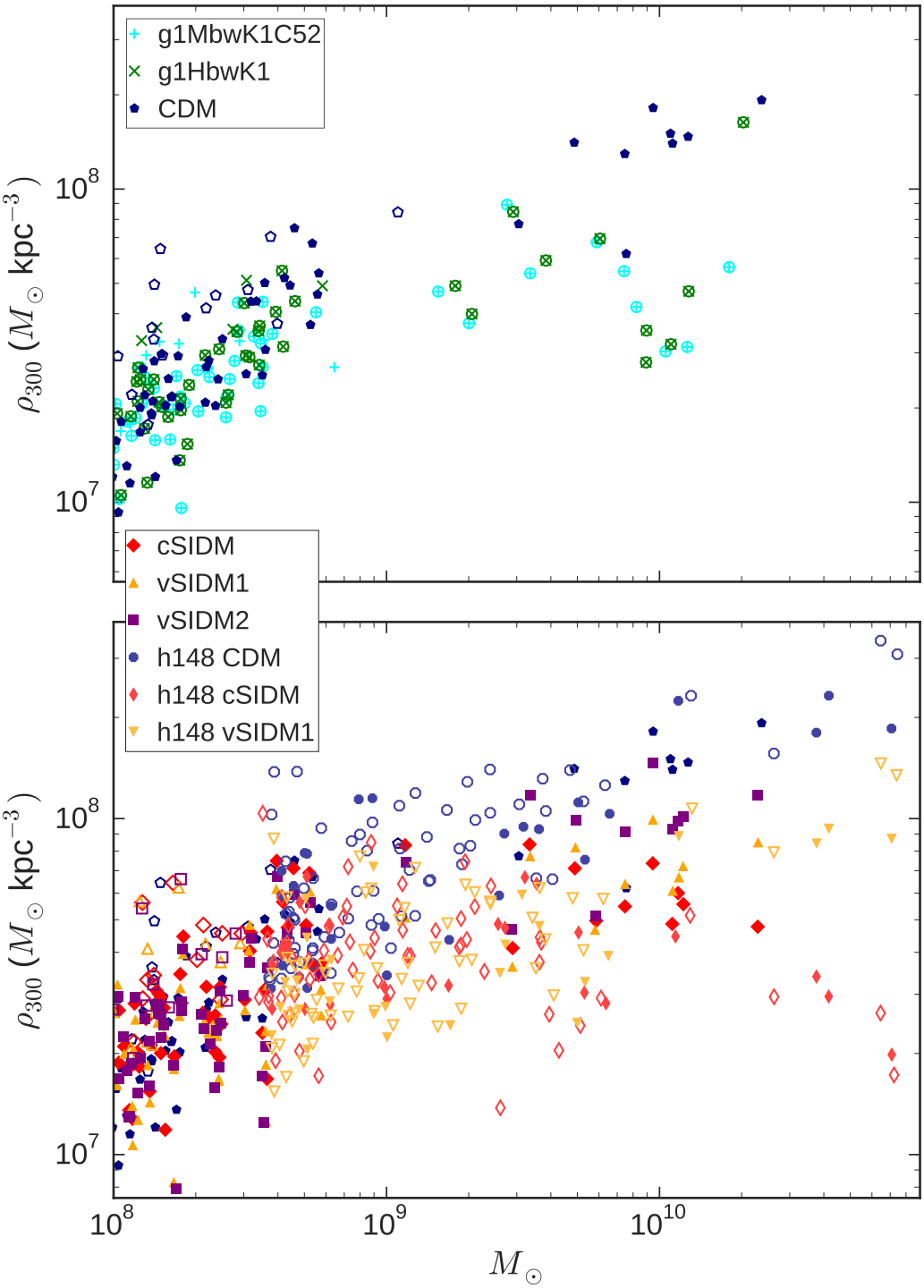

Figure 4.34: The density at 300 pc for a range of halo masses from the 40 thieves and h148 simulations at $z = 0$ down to halos with 2^{13} particles. The top panel shows a DM only CDM run compared to CDM+baryon runs; at masses above 10^9 $M_\odot$galaxies have have at least 10^3 star particles, but below this mass star formation and therefore feedback is not resolved. The bottom panel shows DM only runs. The open or un-circled points are satellites and the filled or circled points are field halos.

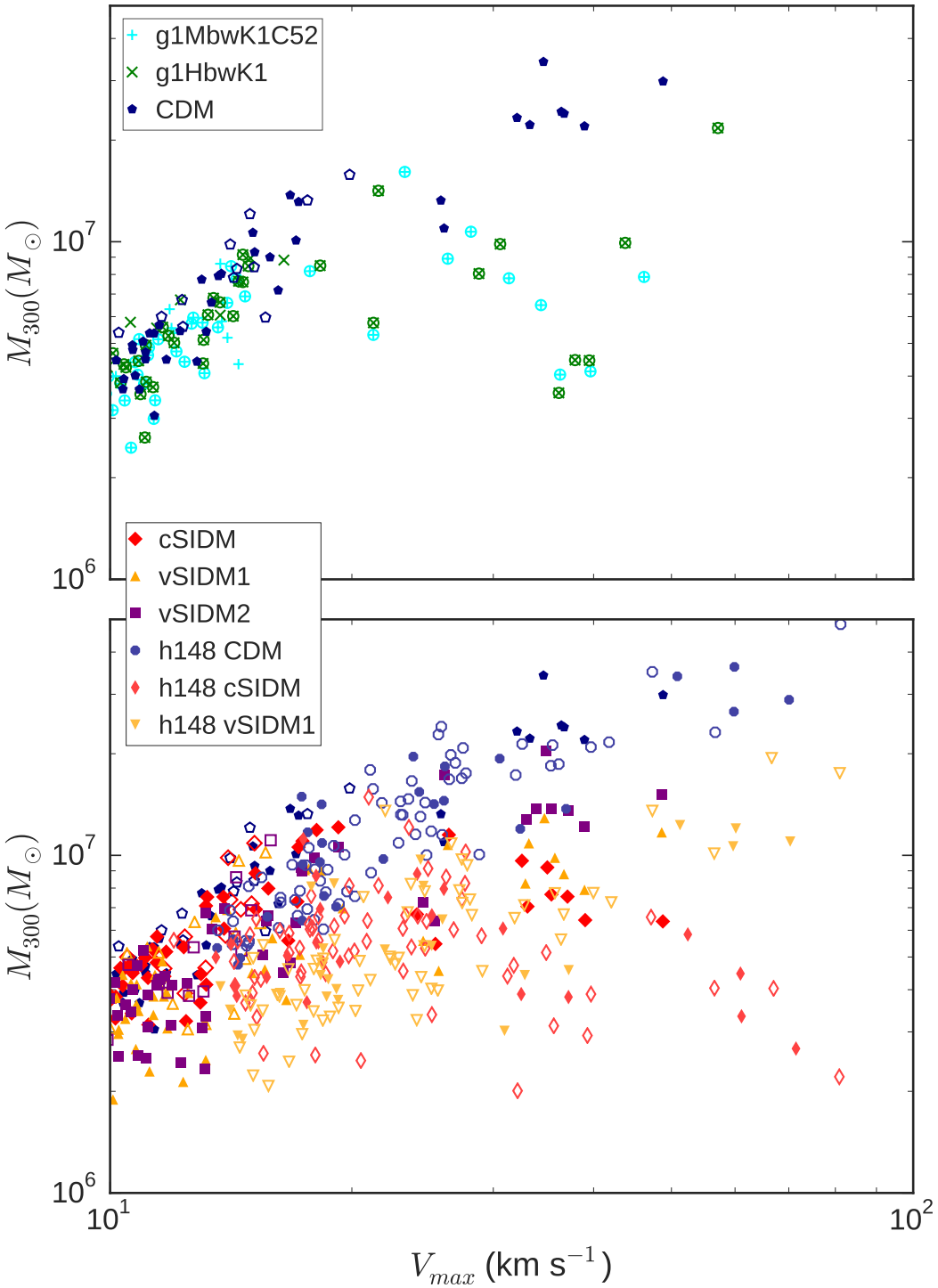

Figure 4.35: The mass enclosed inside 300 pc for halos from h937 and h148 simulations down to halos with 2^{13} particles. The top panel shows a DM only CDM run compared to CDM+baryon runs; at $V_{max} \approx 20$ km s^{-1} and below the CDM+baryon runs have less than 10^3 star particles and thus do not have stellar feedback and converge to CDM. The bottom panel shows DM only runs. The open or un-circled points are satellites and the filled or circled points are field halos.

Chapter 5

SUMMARY, OUTLOOK AND CONCLUSIONS

5.1 Summary

Self-Interacting Dark Matter is a viable alternative to CDM. The impetus for this work is the behavior of the smallest galaxies (though evidence for SIDM also comes on larger scales (Dawson et al., 2013; Massey et al., 2015) from observations of the spatial separation between the luminous galaxies and their gravitating centers in clusters). Dwarf galaxies are the smallest yet most abundant galaxies in the Universe. Small galaxies are important in understanding cosmology because they contribute to a range of astrophysics: they are likely the majority dominant source of UV photons during reionization, they are the building blocks of larger systems, they enrich the intergalactic medium, and they trace the predicted population of dark matter halos. The careful spectroscopic and astrometry observation of stars in dwarf galaxies is one of the keys to understanding and constraining collisional dark matter.

This work highlights how simulations that include realistic SF and feedback processes are necessary to take advantage of astrophysical constraints on DM models. Velocity independent cross section SIDM models cannot simultaneously explain cluster scale and dwarf scale physics. The SIDM cross section that would be necessary to alter dwarfs (observably, beyond what SF and feedback already do) would make clusters (with relative velocities during merging of several thousands of km s^{-1}) too spherical compared to observed elliptical distribution of clusters, and these large velocities would result in substructure evaporation even at cluster scales.

- Once SF and resulting feedback is introduced galaxies will become as cored as the strongest coring mechanism present will allow whether that mechanism is stars or SIDM. For our constant cross section model with 2 cm^2 g^{-1} and for galaxies with circular velocity of 30 to 70 km s^{-1} the central DM mass distribution and velocity

dispersion becomes similar for CDM and SIDM galaxies with stellar masses in the 10^6 to 10^8 $M_\odot$ range and total matter content is in good agreement with observational estimates of Local Group dwarfs.

- SIDM forms constant density central cores in halos. Below a few $\times 10^8$ $M_\odot$ variable cross section models with the parameters $\sigma_0 = 16$, $v_{max} = 18$ km s^{-1} or $\sigma_0 = 35$, $v_{max} = 10$ km s^{-1} can form cores, but for the constant cross section regime probed here (2 cm^2 g^{-1}) cores are not formed for halos less than a few $\times 10^9$ $M_\odot$ which is consistent with analytical predictions.

- The central density of constant cross section SIDM halos scales as $\rho_0 \propto 1/V_{max}$. This finding is consistent with previous results and which may explain why dwarf galaxies may span a factor of 10000 in luminosity while maintaining nearly the same density (Elbert et al., 2014; Strigari et al., 2008a). The central core size of constant cross section SIDM scales as a nearly fixed fraction of the would be NFW scale radius.

- Cores begin to form early, $\sim$3 Gyr, for CDM+baryons and all SIDM models, if the cores are going to form at all.

- SIDM can alleviate the too big too fail problem by reducing the densities of subhalos. The central density of a halo with a given V_{max} is less in SIDM models. In constant cross section models the most massive halos are least dense. In CDM or velocity dependent SIDM the least massive halos are also the least dense.

- SIDM alone cannot solve the missing satellites problem. SIDM does not reduce the absolute number of DM satellite halos for constant cross sections of 2 cm^2 g^{-1} and below. Self-interacting dark matter models that are cosmologically consistent will not significantly reduce the number of DM satellite halos we would expect to exist in the Local Group (D'Onghia & Burkert, 2003) because the SIDM power spectrum is similar to CDM at small scales and subhalos survive evaporation (Zavala et al., 2013).

- There is an small relative environmental difference at the center ($.1R_{vir}$ to $.2R_{vir}$) of very small satellites compared to their field counterparts. We interpret this as due to their rapid orbital velocities in the dense halos of a massive host. This relative difference offers the potential of using faint galaxies to constrain the cross section of SIDM as a function of the DM velocity: the enhanced interaction rate is much stronger for constant cross section SIDM.

- SIDM makes halos more spherical at all radii and the effect is strongest at the smallest radii where DM interactions are more abundant. Our constant cross section model would be inconsistent with clusters shapes if we extrapolated to higher masses (Peter et al., 2013).

- Galaxies in the V_{max} range of 30 to 70 km s^{-1}, once regulated by feedback, do not differ substantially in CDM versus our constant cross section SIDM model with respect to the SFHs, stellar and gas content and spatial distribution. They both form gas rich galaxies with bulgeless disks which resemble real ones.

- At large radii beyond $\sim R_{vir}/2$ SIDM and CDM halos are identical. At small radii $r \simeq .5$ kpc our constant cross section SIDM halos are under-dense by a factor of a few, but only if they have circular velocities greater than 30 km s^{-1}, for lower velocity halos the difference may be 50% or less.

The motivation for choosing 2 cm^2 g^{-1} as the cross section is that we wanted to see a strong effect of SIDM in order to differentiate from baryonic effects. Previous work has already demonstrated that for smaller galaxies the effects of SIDM can be minor (Vogelsberger et al., 2014). We in fact find that the differences between SIDM and baryons+SIDM are still small even with this relatively large cross section that has been ruled out by other observations. The motivation for choosing the vSIDM1 model ($\sigma_0 = 16$, $v_{max} = 18$ km s^{-1}) was to be able to reproduce the core sizes and central densities observed in dark matter halos at all scales with a significant interaction at low velocity that would create substantial effects for the smallest mass halos. At large scales velocity independent SIDM creates larger

and larger effects that violate observations; work that finds that a constant cross section SIDM model is viable is not being earnest if dissociative galaxy cluster observations and analysis are accurate (we humorously note that Zavala et al. (2013) originally titled their paper *The downfall of velocity-dependent Self-Interacting Dark Matter* before scaling back the claim in the title, but we think this is a more than reasonable title). Velocity dependent models are naturally consistent with all scales when the interaction cross section is very low, if for no other reason than being a weak effect at the scales where we have the most well resolved halos and tightest observational constraints. Unfortunately, choosing a SIDM model with particular parameters makes general conclusions difficult. We caution the reader that the conclusions made above were for the particular models tested here.

It is reasonable to conclude that SIDM must be combined with additional effects to explain the properties of observed Local Group galaxies. The common mass scale of dark matter on small scales in dwarf galaxies (Gilmore et al., 2007; Hayashi & Chiba, 2015) is a clue to the formation of dwarf galaxies. Strigari et al. (2008a) finds that Milky Way dwarf satellites from Segue I with a luminosity of $\sim 3 \times 10^2$ $L_\odot$ all the way to Fornax with a luminosity of $\sim 2 \times 10^7$ $L_\odot$ all contain $\sim 10^7$ $M_\odot$ within their central 300 pc. The constancy at the center of dwarfs can also be viewed as a common density or surface density and as a function of halo mass or V_{max} (Hayashi & Chiba, 2015). Local group dwarf galaxies have been observed with a characteristic density of $\sim 10^8$ $M_\odot$ kpc^{-3} at their center and a characteristic central mass within .3 kpc of $\sim 10^7$ $M_\odot$. The inferred size of DM cores derived from self-consistent models of the DM distribution in these galaxies suggests the cores are small ($r_s < 1.5$ kpc). For example in the case of Fornax, irrespective of the origin of the core, reasonable dynamical limits on the mass of its halo constrain its core radius to be no larger than $\sim$700 pc (Strigari et al., 2006; Jardel & Gebhardt, 2012).

SIDM models that are velocity independent create lower density cores, have flatter slopes, and contain less mass as V_{max} (or halo mass) increases. We find that SIDM models that are velocity dependent create constant density cores at V_{max} increases and they have less mass and have lower density as V_{max} (or halo mass) increases, but these quantities scale with the CDM halo (or concentration thereof). At 300 pc the few most massive halos of h937 (which have V_{max} values of 49, 36, and 37 km s^{-1}) in our CDM model contain a few $\times 10^7$

$M_\odot$ and the SIDM halos contain ∼0.3, ∼0.4, and ∼0.5 times that amount for the cSIDM, vSIDM1, and vSIDM2 models (see figure 4.19 or 4.35). At 300 pc these same halos have a density of $\sim 2 \times 10^8$ in the case of CDM, $\sim 9 \times 10^7$ for vSIDM1, and $\sim 3 \times 10^7$ for cSIDM1 (see figrure 4.34). Given how tight the common mass scale of dwarfs is these results already disfavor that constant cross section model. In Rocha et al. (2013) for example they found the only constant cross section models that could match dwarf to cluster scales had cross sections of .1 cm^2 g^{-1} or less. The common mass scale of dark matter on small scales in dwarf galaxies seems to be associated with the formation of the halos. The central density of dark matter halos is proportional to the density of matter in the universe when the galaxy formed according to theories of hierarchal structure formation (Cole & Lacey, 1996). For dense dwarfs this implies these halos collapsed much less than a billion years after the big bang and during the epoch of reionization (Planck Collaboration et al., 2014). The mass within the central regions of dark matter halos today is related to the depth of the gravitational potential well at formation (Bullock et al., 2001a). Processes such as supernova feedback have long been proposed as a mass scale bias in galaxy formation (Dekel & Silk, 1986), but this doesn't satisfactorily explain how the smallest halos, which are still quite dense, could have ever had sufficient baryonic feedback to suppress their luminosity and create constant density cores equivalent to objects 10000 times more luminous. Velocity dependent dark matter could be involved, but a complete view of galaxy formation in hierarchal structure formation and cosmology offers more answers. Cosmic reionization suppresses star formation in dwarf galaxies (Bullock et al., 2000; Wyithe & Loeb, 2006; Milosavljević & Bromm, 2014; Bullock et al., 2001b). Early photoionization can explain the common mass scale relation that begins at $V_{circ} = 30$ km s^{-1} and reproduce the empirical luminosity-size/metallicity relations because gas accretion in low-mass halos is suppressed after the epoch of reionization: the observed dwarf satellites correspond to the small fraction of halos (among the myriad of dark halos) that accreted substantial amounts of gas before reionization.

Indeed, as stated before, there really isn't a simple model of SIDM that destroys DM halos, but it is possible. A large enough cross section will cause subhalo evaporation: the elastic collisions between a small subhalo and a host halo transfer enough energy to unbind

the DM particles of a small halo as was seen in Vogelsberger et al. (2012) where halos below $\sim 10^8\ M_\odot$ were reduced by a factor of ~ 2 for a constant 10 cm^2 g^{-1} cross section; however these large constant cross sections are easily ruled out. On the other hand for velocity dependent models most scatterings occur in low mass halos at high redshift (for example halos of mass $10^{10}\ M_\odot$ have interaction rates that peak at $z \approx 20$) that would not be resolved in typical cosmological simulations. These interactions would be qualitivetly similar to WDM and would have suppression effects on small growth of structure (Robertson et al., 2015).

A velocity dependent SIDM model combined with strong local cosmic reionization could explain the common mass scale of dark matter on small scales, the missing satellites problem, the too big to fail problem, and the core/cusp problem even in the absence of strong stellar feedback. The fact that the luminosity of observed local dwarfs vary so much while their central mass and density properties do not is evidence in favor of SIDM models.

On the other hand the literature continues to find that the minimum stellar mass required to create cores is lower than expected. Di Cintio et al. (2014a) finds galaxies with galaxies with $M_* < 5 \times 10^6\ M_\odot$ or $(M_*/M_{halo} < 10^{-4})$ can create cores. Most recently in Oñorbe et al. (2015) they simulate dwarf galaxies with a stellar masses of 10^4 to $10^6\ M_\odot$ in halos with $M_{vir} \simeq 10^{9.5}\ M_\odot$ and find that it is possible to form $\sim$1 kpc dark cores using bursty feedback all while remaining within local group observational bounds of half-light radii, metallicities, star formation histories, and stellar mass function. The dark matter cores sizes they find are largest in systems that form their stars late ($z < 2$) or after the early epoch of cusp building mergers has ended; early star formation leads to cuspy dark matter halos. The inclusion of SF and baryonic feedback processes erase the differences for reasonable cross section SIDM models at the scale of dwarf galaxies with V_{max}=30 to 70 km s^{-1} where SN couple energy to DM efficiently.

5.2 Outlook

Dark matter is effectively non-self-interacting for most of astronomy. It has negligible dissipation (or annihilation) on the largest scales, yet this effect has not yet been proven to be negligible on the smallest scales. It not the mere fact that such interactions are

possible though that motivates this work: the discrepancies between CDM and observations motivate this work. Observations that find missing satellites or simulations which show that cores may be formed secularly through stellar feedback even for faints dwarfs diminish the theoretical motivation for studying SIDM. We can readily find such recent work. There was a recent discovery of at least 9 ultra-faint dwarf satellites of the Milky Way with data from the first year of the Dark Energy Survey (The DES Collaboration et al., 2015; Koposov et al., 2015); these detections could secularly explain the missing satellites problem. These surveys identify new dwarf galaxies by finding statistically significant over-densities of individual stars consistent with the expected isochrone and luminosity function of an old and metal-poor stellar population. As telescopes become more powerful, we will be able to sample more stars, examine lower luminosity galaxies, and accurately probe dwarfs around our neighbor M31. It is the observational constraint from an ensemble of dwarf galaxy observations (and therefore individual stars) that will truly constrain SIDM. On the theoretical front we must determine if feeble star formation can still create cores. In Oñorbe et al. (2015) they simulate dwarf galaxies with stellar masses down to 10^4 in halos with $M_{vir} \simeq 10^{9.5}\ M_\odot$ and find that it is possible to form $\sim$1 kpc dark cores using bursty feedback all while remaining within local group observational bounds of half-light radii, metallicities, star formation histories, and stellar mass function.

There are is also recent interesting observational results that corroborate the existence of new DM physics. The new satellites found by the Dark Energy Survey also offer new targets for detection of DM annihilation. Indeed, excess source counts of γ rays from the newly discovered Reticulum II have been observed (Geringer-Sameth et al., 2015) and the galactic center remains intriguing. This may be dark matter annihilation. Additionally, direct evidence for a dark matter drag force generated by SIDM has been seen in clusters with large angular separation between luminous and gravitating centers (Dawson et al., 2013). Most recently in Massey et al. (2015) they find an offset of stellar and DM distribution (reconstructed from background lensed sources) of 1.62 kpc in the Galaxy cluster Abell 3827 which, if interpreted as the result of SIDM gives the result that SIDM has a cross section of $\sigma_{DM} = 1.7 \times 10^{-4}\ \mathrm{cm}^2\ \mathrm{g}^{-1} \times (t_{infall}/10^9\ \mathrm{yr})^{-2}$ where t_{infall} is the time the galaxy took in-falling into the dense cluster center. This is an uncertainty that is bounded

by if nothing else the age of the Universe. This observation may be evidence of dark matter interacting.

A theory of DM that solves the problems that baryons cannot is the most compelling. For example, a well motivated particle physics theories predict the existence of particles, such as sterile neutrinos, which acquire non-negligible thermal velocities in the early universe. These particles could behave as warm dark matter (WDM) and generate a small-scale cutoff in the linear density power spectrum which scales approximately inversely with the particle mass. Thus, in WDM models the abundance of satellites that orbit in the halo of the Milky Way depends on the mass of the warm particle (which would need to be of order a KeV to cutoff on the scale of dwarf galaxies). Paradoxically, if WDM solves the missing satellites problem, then it cannot simultaneously create cores in those satellites — those galaxies would have been prevented from forming in the first place (Macciò et al., 2012a; Nierenberg et al., 2013). The addition of self interactions to sterile neutrino WDM models can modulate DM thermalization in the early universe to further make the theory compatible with precision cosmological observations of structure formation (Hannestad et al., 2014). The frontier of dark matter models with self interactions are models with excited states. If dark matter has an internal structure with bound atomic like states and dark photons then DM could dissipate and form dark disks or other collapsed structures, but generally such states or the percent of dark matter that has such interactions is limited. It is also theorized that a nearly-degenerate states could exist with a spectrum of decay initiated by collisional excitation or de-excitation; such a mechanism could explain the 3.5 KeV line observed in galaxy clusters (Schutz & Slatyer, 2015).

In the next few decades if DM is not detected it would leave a theoretical vacuum that could be filled by dark sector ideas. The final limit of direct detection experiments will occur from the neutrino background; solar pp-neutrinos will generate an electron recoil background that could in principle be discriminated from nuclear recoils inside the detector, but the higher energy supernova neutrino background would generate nuclear recoils that may not be discriminated (Baudis, 2012). The final limit of indirect detection of DM annihilation signals is a combination of γ-ray generating backgrounds including cosmic isotropic backgrounds, inverse Compton scattering, Bremsstahlung, resolved sources, and diffuse galactic emission

that together place fundamental uncertainty on the origin of γ-ray flux from any object.

There are observations that can constrain the parameter space of SIDM. These observations would likely require such resources as space based missions (such as the Space Interferometry Mission), repeated observation over decades, telescopes of greater than thirty meters in diameter, or large survey areas. To understand the nature of dark matter we must understand its exact distribution on the smallest scales in the smallest galaxies nearly devoid of stars. There are many observational approaches to this problem, including for example, precision astrometry which offers several ways to illuminate dark matter:

- Astrometric measurements of dwarfs (or subhalos in cluster environments) could reveal a physical offset between dark matter and stellar content (Harvey et al., 2013).

- Astrometric measurements of the proper motion of stars in dwarfs in addition to spectroscopic line-of-sight velocity dispersion measurements could measure dark matter profiles inside dwarf galaxies stellar cores (Strigari et al., 2007a).

- Astrometric microlensing measurements could be capable of detecting intermediate-mass DM subhalos depending on the steepness of their density profile and ultimately reveal whether dark halos are simply devoid of stars or non-existent (Erickcek & Law, 2011).

5.3 Conclusions

Self-interacting dark matter is a theoretically consistent and observationally motivated refinement of the standard cosmological model. However, constrains on the interaction strength of DM mean that any observable effects will be subtle for the most luminous objects. Velocity dependent SIDM predicts that the central slope of very dim yet dark matter rich galaxies will remain cored (dSPH galaxies will be under dense compared to CDM models). SIDM predicts that DM dominated halos will be more spherical at small radii, in opposition to CDM models. SIDM predicts that even the least massive halos can have cores. These observations are testable against the current ΛCDM model. The current

model is not an especially beautiful theory; it is just that no other consistent, predictively successful alternative exists. DM really is a great unsolved problem in physics.

Some theorists have began to argue that we need to broaden our search for dark matter. In particular we may have to consider the unsatisfying prospect that DM is a combination of things such as warm DM, axions, WIMPS, and MACHOS (Bertone et al., 2005). And it may be that the traditional probes of dark matter in large scale structure or galaxies are insufficient. Strange compact objects that aggregate dark matter over long time scales such as neutron stars or white dwarfs may hold clues to dark matter that are unique.

Non-detections have placed relatively interesting constraints on dark matter. The prospect of the dark sector remains. We find that SIDM is quite viable, yet we also find that DM+baryon simulations replicate galaxies well. We can not firmly state what SIDM cross sections are viable without also stating what velocity dependence the given model has. Summarily, simulations without stellar feedback do not match observations. On the largest scales, where cosmology has made firm predictions, our SIDM modification does nothing, but on small scales, where the theory of dark matter shows signs of faltering, it helps with several issues.

A robust theory of dark matter that naturally predicts or excludes self interactions which is predictively successful would be very exciting. We may never know for certain whether dark matter has self-interactions because it could always be posited that an interaction just below our observational limit exists. At best, we might put an upper limit on how strong such interactions could be.

BIBLIOGRAPHY

Ackermann, M., Ajello, M., Atwood, W. B., et al. 2012, ApJ, 761, 91

Adams, J. J., Simon, J. D., Fabricius, M. H., et al. 2014, ApJ, 789, 63

Agertz, O., & Kravtsov, A. V. 2015, ApJ, 804, 18

Agnese, R., Ahmed, Z., Anderson, A. J., et al. 2013, Physical Review Letters, 111, 251301

Aguilar, M., Aisa, D., Alpat, B., et al. 2014, Physical Review Letters, 113, 221102

Amorisco, N. C., & Evans, N. W. 2012, MNRAS, 419, 184

Anderson, L., Aubourg, E., Bailey, S., et al. 2012, MNRAS, 427, 3435

Anderson, L., Aubourg, É., Bailey, S., et al. 2014, MNRAS, 441, 24

Arkani-Hamed, N., Finkbeiner, D. P., Slatyer, T. R., & Weiner, N. 2009, Phys. Rev. D, 79, 015014

Auriere, M. 1982, A&A, 109, 301

Bailin, J., Kawata, D., Gibson, B. K., et al. 2005, ApJ, 627, L17

Balberg, S., Shapiro, S. L., & Inagaki, S. 2002, ApJ, 568, 475

Bastidas Fry, A., Governato, F., Pontzen, A., et al. 2015, ArXiv e-prints

Baudis, L. 2012, Physics of the Dark Universe, 1, 94

Benson, A. J. 2012, New A, 17, 175

Bertone, G., Hooper, D., & Silk, J. 2005, Physics Reports, 405, 279

Bett, P. 2012, MNRAS, 420, 3303

Bett, P., Eke, V., Frenk, C. S., et al. 2007, MNRAS, 376, 215

Binney, J., Gerhard, O., & Silk, J. 2001, MNRAS, 321, 471

Bird, C. M. 1994, AJ, 107, 1637

Boylan-Kolchin, M., Bullock, J. S., & Kaplinghat, M. 2011, MNRAS, 415, L40

—. 2012, MNRAS, 422, 1203

Bradač, M., Allen, S. W., Treu, T., et al. 2008, ApJ, 687, 959

Brook, C. 2015, ArXiv e-prints

Brook, C. B., Di Cintio, A., Knebe, A., et al. 2014, ApJ, 784, L14

Brook, C. B., Governato, F., Roškar, R., et al. 2011, MNRAS, 415, 1051

Brooks, A. M., & Zolotov, A. 2014, ApJ, 786, 87

Buckley, M. R., Charles, E., Gaskins, J. M., et al. 2015, Phys. Rev. D, 91, 102001

Buckley, M. R., Zavala, J., Cyr-Racine, F.-Y., Sigurdson, K., & Vogelsberger, M. 2014, Phys. Rev. D, 90, 043524

Bullock, J. S., Kolatt, T. S., Sigad, Y., et al. 2001a, MNRAS, 321, 559

Bullock, J. S., Kravtsov, A. V., & Weinberg, D. H. 2000, ApJ, 539, 517

—. 2001b, ApJ, 548, 33

Burkert, A. 2000, ApJ, 534, L143

Charbonnier, A., Combet, C., Daniel, M., et al. 2011, MNRAS, 418, 1526

Chen, C.-S., Lee, F.-F., Lin, G.-L., & Lin, Y.-H. 2014, ArXiv e-prints

Christensen, C., Quinn, T., Governato, F., et al. 2012, MNRAS, 425, 3058

Christensen, C. R., Brooks, A. M., Fisher, D. B., et al. 2014a, MNRAS, 440, L51

Christensen, C. R., Governato, F., Quinn, T., et al. 2014b, MNRAS, 440, 2843

Clowe, D., Bradač, M., Gonzalez, A. H., et al. 2006, ApJ, 648, L109

Cole, S., & Lacey, C. 1996, MNRAS, 281, 716

Colín, P., Avila-Reese, V., Valenzuela, O., & Firmani, C. 2002, ApJ, 581, 777

Cyr-Racine, F.-Y., de Putter, R., Raccanelli, A., & Sigurdson, K. 2014, Phys. Rev. D, 89, 063517

Davé, R., Spergel, D. N., Steinhardt, P. J., & Wandelt, B. D. 2001, ApJ, 547, 574

Dawson, W., Wittman, D. M., Jee, M. J., et al. 2013, in American Astronomical Society Abstracts, Vol. 221, American Astronomical Society Meeting Abstracts 221, 125.04

Dawson, W. A., Wittman, D., Jee, M. J., et al. 2012, ApJ, 747, L42

Debattista, V. P., Moore, B., Quinn, T., et al. 2008, ApJ, 681, 1076

Dekel, A., & Silk, J. 1986, ApJ, 303, 39

Del Popolo, A. 2009, ApJ, 698, 2093

Di Cintio, A., Brook, C. B., Dutton, A. A., et al. 2014a, MNRAS, 441, 2986

Di Cintio, A., Brook, C. B., Macciò, A. V., et al. 2014b, MNRAS, 437, 415

Domínguez, A., Siana, B., Brooks, A. M., et al. 2014, ArXiv e-prints

D'Onghia, E., & Burkert, A. 2003, ApJ, 586, 12

Eisenstein, D. J., Zehavi, I., Hogg, D. W., et al. 2005, ApJ, 633, 560

Elbert, O. D., Bullock, J. S., Garrison-Kimmel, S., et al. 2014, ArXiv e-prints

Erickcek, A. L., & Law, N. M. 2011, ApJ, 729, 49

Evans, A. K. D., & Bridle, S. 2009, ApJ, 695, 1446

Evans, N. W., An, J., & Walker, M. G. 2009, MNRAS, 393, L50

Feng, J. L. 2010, ARA&A, 48, 495

Feng, J. L., Kaplinghat, M., & Yu, H.-B. 2010, Phys. Rev. D, 82, 083525

Ferrero, I., Abadi, M. G., Navarro, J. F., Sales, L. V., & Gurovich, S. 2012, MNRAS, 425, 2817

Franx, M., Illingworth, G., & de Zeeuw, T. 1991, ApJ, 383, 112

Garrison-Kimmel, S., Boylan-Kolchin, M., Bullock, J. S., & Kirby, E. N. 2014, MNRAS, 444, 222

Geringer-Sameth, A., & Koushiappas, S. M. 2011, Physical Review Letters, 107, 241303

Geringer-Sameth, A., Walker, M. G., Koushiappas, S. M., et al. 2015, ArXiv e-prints

Ghigna, S., Moore, B., Governato, F., et al. 1999, in Astronomical Society of the Pacific Conference Series, Vol. 176, Observational Cosmology: The Development of Galaxy Systems, ed. G. Giuricin, M. Mezzetti, & P. Salucci, 140

Gill, S. P. D., Knebe, A., & Gibson, B. K. 2004, MNRAS, 351, 399

Gilmore, G., Wilkinson, M. I., Wyse, R. F. G., et al. 2007, ApJ, 663, 948

Gnedin, O. Y., & Ostriker, J. P. 2001, ApJ, 561, 61

Governato, F., Mayer, L., Wadsley, J., et al. 2004, ApJ, 607, 688

Governato, F., Brook, C., Mayer, L., et al. 2010, Nature, 463, 203

Governato, F., Zolotov, A., Pontzen, A., et al. 2012, MNRAS, 422, 1231

Governato, F., Weisz, D., Pontzen, A., et al. 2015, MNRAS, 448, 792

Griest, K., Cieplak, A. M., & Lehner, M. J. 2013, Physical Review Letters, 111, 181302

Haardt, F., & Madau, P. 1996, ApJ, 461, 20

Hannestad, S., Hansen, R. S., & Tram, T. 2014, Physical Review Letters, 112, 031802

Hanyu, C., & Habe, A. 2001, ApJ, 554, 1268

Harvey, D., Massey, R., Kitching, T., et al. 2013, MNRAS, 433, 1517

Hayashi, K., & Chiba, M. 2015, ApJ, 803, L11

Hernquist, L. 1990, ApJ, 356, 359

Hooper, D., & Baltz, E. A. 2008, Annual Review of Nuclear and Particle Science, 58, 293

Hopkins, P. F., Kereš, D., Oñorbe, J., et al. 2014, MNRAS, 445, 581

Jardel, J. R., & Gebhardt, K. 2012, ApJ, 746, 89

Jetley, P., Gioachin, F., Mendes, C., Kale, L., & Quinn, T. 2008, in Parallel and Distributed Processing, 2008. IPDPS 2008. IEEE International Symposium on, 1–12

Jetley, P., Wesolowski, L., Gioachin, F., Kale, L., & Quinn, T. 2010, 1

Jing, Y. P., & Suto, Y. 2002, ApJ, 574, 538

Jungman, G., Kamionkowski, M., & Griest, K. 1996, Phys. Rep., 267, 195

Kaplinghat, M., Keeley, R. E., Linden, T., & Yu, H.-B. 2014, Physical Review Letters, 113, 021302

Katz, N. 1992, ApJ, 391, 502

Kauffmann, G. 2014, MNRAS, 441, 2717

Kazantzidis, S., Kravtsov, A. V., Zentner, A. R., et al. 2004a, ApJ, 611, L73

Kazantzidis, S., Mayer, L., Mastropietro, C., et al. 2004b, ApJ, 608, 663

Kesden, M., & Kamionkowski, M. 2006, Phys. Rev. D, 74, 083007

Klypin, A., Kravtsov, A. V., Valenzuela, O., & Prada, F. 1999, ApJ, 522, 82

Knollmann, S. R., & Knebe, A. 2009, ApJS, 182, 608

Koda, J., & Shapiro, P. R. 2011, MNRAS, 415, 1125

Komatsu, E., Smith, K. M., Dunkley, J., et al. 2011, ApJS, 192, 18

Koposov, S. E., Belokurov, V., Torrealba, G., & Evans, N. W. 2015, ApJ, 805, 130

Koposov, S. E., Yoo, J., Rix, H.-W., et al. 2009, ApJ, 696, 2179

Kravtsov, A. V., Gnedin, O. Y., & Klypin, A. A. 2004, ApJ, 609, 482

Kroupa, P. 2001, MNRAS, 322, 231

Li, B., Barrow, J. D., Mota, D. F., & Zhao, H. 2008, Phys. Rev. D, 78, 064021

Loeb, A., & Weiner, N. 2011, Physical Review Letters, 106, 171302

Lynden-Bell, D., & Eggleton, P. P. 1980, MNRAS, 191, 483

Macciò, A. V., Dutton, A. A., van den Bosch, F. C., et al. 2007, MNRAS, 378, 55

Macciò, A. V., Paduroiu, S., Anderhalden, D., Schneider, A., & Moore, B. 2012a, MNRAS, 424, 1105

Maccio', A. V., Sideris, I., Miranda, M., Moore, B., & Jesseit, R. 2007, ArXiv e-prints

Macciò, A. V., Stinson, G., Brook, C. B., et al. 2012b, ApJ, 744, L9

Madau, P., Shen, S., & Governato, F. 2014, ApJ, 789, L17

Martin, C. L., Shapley, A. E., Coil, A. L., et al. 2012, ApJ, 760, 127

Martinez, G. D., Bullock, J. S., Kaplinghat, M., Strigari, L. E., & Trotta, R. 2009, J. Cosmology Astropart. Phys., 6, 14

Mashchenko, S., Wadsley, J., & Couchman, H. M. P. 2008, Science, 319, 174

Massey, R., Williams, L., Smit, R., et al. 2015, MNRAS, 449, 3393

Mateo, M. L. 1998, ARA&A, 36, 435

Maxwell, A. J., Wadsley, J., & Couchman, H. M. P. 2015, ArXiv e-prints

McConnachie, A. W. 2012, AJ, 144, 4

Menon, H., Wesolowski, L., Zheng, G., et al. 2015, Computational Astrophysics and Cosmology, 2, 1

Merten, J., Coe, D., Dupke, R., et al. 2011, MNRAS, 417, 333

Milosavljević, M., & Bromm, V. 2014, MNRAS, 440, 50

Minor, Q. E., Martinez, G., Bullock, J., Kaplinghat, M., & Trainor, R. 2010, ApJ, 721, 1142

Miralda-Escudé, J. 2002, ApJ, 564, 60

Moore, B., Gelato, S., Jenkins, A., Pearce, F. R., & Quilis, V. 2000, ApJ, 535, L21

Moore, B., Ghigna, S., Governato, F., et al. 1999, ApJ, 524, L19

Munshi, F., Governato, F., Brooks, A. M., et al. 2013, ApJ, 766, 56

Nanbu, K. 1983, Journal of the Physical Society of Japan, 52, 3382

Navarro, J. F., Eke, V. R., & Frenk, C. S. 1996a, MNRAS, 283, L72

Navarro, J. F., Frenk, C. S., & White, S. D. M. 1996b, ApJ, 462, 563

Navarro, J. F., Ludlow, A., Springel, V., et al. 2010, MNRAS, 402, 21

Neto, A. F., Gao, L., Bett, P., et al. 2007, MNRAS, 381, 1450

Nierenberg, A. M., Treu, T., Menci, N., Lu, Y., & Wang, W. 2013, ApJ, 772, 146

Oñorbe, J., Boylan-Kolchin, M., Bullock, J. S., et al. 2015, ArXiv e-prints

Oh, S.-H., Brook, C., Governato, F., et al. 2011, AJ, 142, 24

Okabe, N., Bourdin, H., Mazzotta, P., & Maurogordato, S. 2011, ApJ, 741, 116

Okabe, N., & Umetsu, K. 2008, PASJ, 60, 345

Papastergis, E., Martin, A. M., Giovanelli, R., & Haynes, M. P. 2011, ApJ, 739, 38

Peñarrubia, J., Benson, A. J., Walker, M. G., et al. 2010, MNRAS, 406, 1290

Peñarrubia, J., Pontzen, A., Walker, M. G., & Koposov, S. E. 2012, ApJ, 759, L42

Peter, A. H. G., Rocha, M., Bullock, J. S., & Kaplinghat, M. 2013, MNRAS, 430, 105

Planck Collaboration, Ade, P. A. R., Aghanim, N., et al. 2014, A&A, 571, A16

Pontzen, A., & Governato, F. 2012, MNRAS, 421, 3464

—. 2014, Nature, 506, 171

Pontzen, A., Read, J., Teyssier, R., et al. 2015, ArXiv e-prints

Pontzen, A., Roškar, R., Stinson, G., & Woods, R. 2013, pynbody: N-Body/SPH analysis for python, Astrophysics Source Code Library

Porter, T. A., Johnson, R. P., & Graham, P. W. 2011, ARA&A, 49, 155

Power, C., Navarro, J. F., Jenkins, A., et al. 2003, MNRAS, 338, 14

Ragozzine, B., Clowe, D., Markevitch, M., Gonzalez, A. H., & Bradač, M. 2012, ApJ, 744, 94

Read, J. I., & Gilmore, G. 2005, MNRAS, 356, 107

Riddle, R., Langsford, A., Bowen, P., & Cox, G. 1965, Nuclear Physics, 61, 457

Robertson, A., Massey, R., Eke, V., & Bower, R. 2015, ArXiv e-prints

Rocha, M., Peter, A. H. G., Bullock, J. S., et al. 2013, MNRAS, 430, 81

Roškar, R., Teyssier, R., Agertz, O., Wetzstein, M., & Moore, B. 2014, MNRAS, 444, 2837

Schneider, M. D., Frenk, C. S., & Cole, S. 2012, J. Cosmology Astropart. Phys., 5, 30

Schutz, K., & Slatyer, T. R. 2015, J. Cosmology Astropart. Phys., 1, 21

Shen, S., Madau, P., Conroy, C., Governato, F., & Mayer, L. 2014, ApJ, 792, 99

Shen, S., Wadsley, J., & Stinson, G. 2010, MNRAS, 407, 1581

Spergel, D. N., & Steinhardt, P. J. 2000, Physical Review Letters, 84, 3760

Springel, V., White, S. D. M., & Hernquist, L. 2004, in IAU Symposium, Vol. 220, Dark Matter in Galaxies, ed. S. Ryder, D. Pisano, M. Walker, & K. Freeman, 421

Stinson, G., Seth, A., Katz, N., et al. 2006, MNRAS, 373, 1074

Strigari, L. E., Bullock, J. S., & Kaplinghat, M. 2007a, ApJ, 657, L1

Strigari, L. E., Bullock, J. S., Kaplinghat, M., et al. 2006, ApJ, 652, 306

—. 2008a, Nature, 454, 1096

Strigari, L. E., Frenk, C. S., & White, S. D. M. 2010, MNRAS, 408, 2364

Strigari, L. E., Koushiappas, S. M., Bullock, J. S., & Kaplinghat, M. 2007b, Phys. Rev. D, 75, 083526

Strigari, L. E., Koushiappas, S. M., Bullock, J. S., et al. 2008b, ApJ, 678, 614

Teyssier, R., Pontzen, A., Dubois, Y., & Read, J. I. 2013, MNRAS, 429, 3068

The DES Collaboration, Bechtol, K., Drlica-Wagner, A., et al. 2015, ArXiv e-prints

Tollerud, E. J., Barton, E. J., Bullock, J. S., & Trinh, C. 2011, in EAS Publications Series, Vol. 48, EAS Publications Series, ed. M. Koleva, P. Prugniel, & I. Vauglin, 455–457

Tollerud, E. J., Boylan-Kolchin, M., & Bullock, J. S. 2014, MNRAS, 440, 3511

Tollerud, E. J., Bullock, J. S., Strigari, L. E., & Willman, B. 2008, ApJ, 688, 277

Tolstoy, E., Hill, V., & Tosi, M. 2009, ARA&A, 47, 371

Trujillo-Gomez, S., Klypin, A., Primack, J., & Romanowsky, A. J. 2011, ApJ, 742, 16

Tulin, S., Yu, H.-B., & Zurek, K. M. 2013, Phys. Rev. D, 87, 115007

van den Aarssen, L. G., Bringmann, T., & Pfrommer, C. 2012, Physical Review Letters, 109, 231301

van den Bosch, F. C., Burkert, A., & Swaters, R. A. 2001, MNRAS, 326, 1205

Velliscig, M., van Daalen, M. P., Schaye, J., et al. 2014, MNRAS, 442, 2641

Vogelsberger, M., & Zavala, J. 2013, MNRAS, 430, 1722

Vogelsberger, M., Zavala, J., & Loeb, A. 2012, MNRAS, 423, 3740

Vogelsberger, M., Zavala, J., Simpson, C., & Jenkins, A. 2014, MNRAS, 444, 3684

Wadsley, J. W., Stadel, J., & Quinn, T. 2004, New A, 9, 137

Wadsley, J. W., Veeravalli, G., & Couchman, H. M. P. 2008, MNRAS, 387, 427

Walch, S. K., & Naab, T. 2014, ArXiv e-prints

Walker, M. G., Mateo, M., Olszewski, E. W., et al. 2009, ApJ, 704, 1274

Walker, M. G., McGaugh, S. S., Mateo, M., Olszewski, E. W., & Kuzio de Naray, R. 2010, ApJ, 717, L87

Walker, M. G., & Peñarrubia, J. 2011, ApJ, 742, 20

Warren, M. S., Quinn, P. J., Salmon, J. K., & Zurek, W. H. 1992, ApJ, 399, 405

Weisz, D. R., Dolphin, A. E., Dalcanton, J. J., et al. 2011, ApJ, 743, 8

Willman, B., Blanton, M. R., West, A. A., et al. 2005, AJ, 129, 2692

Wolf, J., Martinez, G. D., Bullock, J. S., et al. 2010, MNRAS, 406, 1220

Wyithe, J. S. B., & Loeb, A. 2006, Nature, 441, 322

Yoshida, N., Springel, V., White, S. D. M., & Tormen, G. 2000, ApJ, 544, L87

Zavala, J., Vogelsberger, M., & Walker, M. G. 2013, MNRAS, 431, L20

Zolotov, A., Brooks, A. M., Willman, B., et al. 2012, ApJ, 761, 71